Surface Acoustic Wave Nebulization as a Mass Spectrometry Ionization Source, Characterization and Application

Yue Huang

A dissertation

submitted in partial fulfillment of the

requirements for the degree of

Doctor of Philosophy

University of Washington

2013

Reading Committee:

Frantisek Tureček, Chair

David R. Goodlett

Matthew F. Bush

Program Authorized to Offer Degree:

Department of Chemistry

University of Washington

Abstract

Surface Acoustic Wave Nebulization as a Mass Spectrometry Ionization Source,

Characterization and Application

Yue Huang

Chair of the Supervisory Committee:

Professor Frantisek Tureček

Department of Chemistry

This dissertation describes a novel method to generate ions for mass spectrometers that simplifies the operation and decreases the internal energy distribution of ions. The surface acoustic wave nebulization (SAWN) is a nebulization method generating both positive and negative ions from liquid phase. We have validated this method by successfully ionizing protein, peptide, lipid and other small molecules. The measured internal energy distribution of SAWN is lower compare to electrospray ionization (ESI). To improve the SAWN performance, a standing wave SAWN chip was designed and fabricated. The droplet size of standing wave SAWN was measured and is in general smaller than progressive wave SAWN. The standing wave SAWN design enhanced SAWN performance and kept its low internal energy distribution. After the characterization and improvement, we combined SAWN with digital microfluidics (DMF) for sample preparation before MS detection. DMF-SAWN platform was applied to the analysis of phosphorylated protein mixture. Peptides from all three proteins of the mixture were identified with DMF-SAWN.

Dedicated to my parents, Zhongxiang Huang and Leya Zheng,

and my husband, Bingchuan Wei.

Acknowledgement

It has been my fortune to be guided and helped by excellent people through my five years in University of Washington. I would never have been able to graduate without the suggestions from my committee and co-workers and the support from my family and friends. I would like to thank my research advisor, Prof. Frank Tureček for the expert guidance, constructive criticism and patience. I would also like to thank Prof. David Goodlett for his valuable suggestions and enthusiasm for science. He provided an excellent atmosphere for research and always encouraged me whenever I face difficulties in the project.

I would also like to thank the group members I worked with on the SAWN project. I would like to thank Dr. Scott Heron and Dr. Scott Edgar for helping me from the very beginning of the project teaching me so many things about fluidics and micro fabrication. I also share my credits with Dr. Sunghwan Yoon and Dr. Michael Volny, for the instructions on mass spectrometry instrumentation. This work will not be completed without the help from mass spectrometry centers and micro fabrication centers in and around the campus. I wish to thank Dr. Martin Sadilek, Dr. Dale Whittington, Dr. Priska Von Haller and Prof. Karl Böhringer.

My education has been guided by wonderful teachers and researchers. I would like to express my special thanks to Jiarong Li, my undergraduate advisor, for leading me to the path of chemistry. I would also like to thank Prof. Norman Dovichi for the mentoring of the first two years in University of Washington.

My parents, Zhongxiang Huang and Leya Zheng, both biological scientists, were the first to inspire my interest in science. It is impossible to complete the education without their support and understanding for their daughter. I gave special thanks to Bingchuan Wei, who joined the journey as my husband and supported me with his patience, humor and love.

Table of Contents

List of Figures

List of Tables

Chapter 1 Introduction

1.1 Mass Spectrometry Overview and Bio-analytical Applications

1.1.1 Mass Spectrometry in Recent Decade

Mass spectrometry was introduced more than 100 years ago when the first mass spectrometer was invented. The history of mass spectrometry dates back to Sir J.J. Thomson of University of Cambridge[1]. After the investigations on the conduction of electricity by gases, J.J. Thomson went on to develop a "parabola spectrograph", in which ions were separated by their parabola trajectories in an electromagnetic field. The generated spectrum was recorded on a photographic plate as a figure[2]. This was the prototype of what is now recognized as a mass spectrometer. After these first experiments, scientists have made efforts to make mass spectrometers that allow more accurate mass measurements, achieve higher resolution, and are easier to operate and capable of being applied to a broader range of substrates[3]. To pursue the above goals, several different mass analyzers such as magnetic sector double focusing, time of flight (TOF), quadruple and ion cyclotron resonance (ICR) were invented over the century[4, 5]. Various kinds of ionization sources have also been developed. The advances in mass spectrometers have allowed for the detection of polar and nonpolar compounds with masses ranging in size from single atoms to intact viruses[4, 5].

There has been a growing interest in mass spectrometry applications throughout the past decade. Over 10,000 research papers on mass spectrometry are published every year and the number is steadily increasing. Mass spectrometry have been applied to various areas, including newborn

screening[6], food and drug safety, plant and agriculture as well as biological studies such as proteomics and lipidomics[7-9]. Mass spectrometry is routinely coupled to liquid chromatography, gas chromatography capillary electrophoresis and other bioassays as a detection method. These combinations improve the ability of mass spectrometry to analyze complex mixtures[10].

1.1.2 Mass Spectrometry Instrumentation Development

Since the first demonstration of mass spectrometry by Sir J.J. Thomson, various modifications have been made to mass spectrometers to improve performance. The performance of mass spectrometers is characterized by figures of merit, such as accuracy, resolution, mass range, scan speed as well as the ability to perform tandem mass analysis. For example, resolution[4] is the ability to distinguish between ions with a different mass-to-charge ratio. The IUPAC definition for mass spectrometer resolution is $R=M/\Delta M$, where ΔM is the full width at half maximum and M is mass to charge ratio (m/z). Certain FTICR instruments can reach a resolution of over 100,000, making it possible to distinguish different isotopes of multiply charged ions. The mass range, defined as the range of m/z amenable to analysis by a given analyzer, is another example. With TOF instruments, the theoretical mass range is unlimited[5]. In addition to the technological advancement of mass spectrometers, software to control the instrument and analyze data has also improved with the development of computer technology. Libraries of mass spectra and elemental analysis have made it a routine matter to identify functional groups or substrates by accurate mass, eliminating the need for manual spectra analysis in many instances. Improvements in mass spectrometry hardware have made it possible to obtain accurate and detailed information of complex samples, while new computer algorithms made it possible to quickly identify large

quantities of molecules. These advancements have led to the widespread adoption of mass spectrometry in bio-analytical applications.

1.1.3 Applications of Mass Spectrometry in Bio-analytical Chemistry

Over the last decade, bio-analytical applications have received the most attention from the mass spectrometry community. A biological sample usually contains several categories of molecules, including DNA/RNA, proteins, lipids and other small molecules. Although mass spectrometry was used to analyze peptides as early as 1966, mass spectrometry did not become widely adopted until it was combined with soft ionization methods such as electrospray ionization (ESI) and matrix assisted laser desorption ionization (MALDI). Soft ionization methods preserve most of the precursor ion information, making it possible to ionize large bio-molecules without breaking the chemical bonds. Therefore ESI and MALDI have become a standard method for analyzing complex biological samples. Relevant bio-analytical applications related to this dissertation are briefly reviewed below.

Mass spectrometry has become the *de facto* method for the study of proteins due to its high sensitivity, rapid detection time, and ability to couple downstream to chromatographic methods. Proteins are often referred to as the functional unit inside living cells. They function as molecular transporters, enzymes, ion gates and so on. While the genome of a patient with a serious disease may be the same as a healthy person, protein expression often varies. For example, a disease related protein level might be either increased or decreased; other might even not exist despite the similarities in genomic profiles. Studying the protein expression of biological samples helps

understand how diseases function and finding protein biomarkers. These are all important factors in finding cures for disease. The large-scale study of proteins, particularly their structure and function, is defined as proteomics. In proteomics studies two types of mass spectrometry experiments are commonly performed[11]. Proteins or peptides are ionized and the mass recorded. This is referred to as an MS^1 scan. The structural information can then be obtained by fragmenting the precursor ions and analyzing the subsequent fragment ions. This is referred to as an MS^2 scan and the combination of MS^1 and MS^2 scans is often referred to as a tandem mass scan. Mass spectrometry based proteomics can identify the sequence of amino acids in a protein through fragmentation, detect post translation modifications, and provide information about tertiary structure of proteins when combined with crosslinking[12] or HD exchange[13].

In addition to proteins, lipids are also a class of biomolecules that is widely studied by mass spectrometry. Since lipids are the majority component of cell membranes, they have received significant attention from scientists. Interestingly, it has recently been shown that identification of lipids from bacteria could help with identifying the species and allow for appropriate treatment[14]. Unlike DNA and proteins, lipids do not fragment in an easily predictable manner, making structural elucidation challenging. The study of lipids using mass spectrometry often requires multiple layers of fragmentation to determine the structure of the lipid.

For biological samples, researchers are interested in the spatial distribution of molecules in tissues. Mass spectrometers with MALDI ionization source have become imaging tools with the ability to ionize molecules in a specific area[15]. In MALDI imaging experiments tissue samples are coved with matrix. A laser is scanned methodically over an area of interest in the tissue

sample and the resulting mass spectra are recorded. The scans are compiled to provide both spatial and chemical information about the distribution of molecules in the tissue sample. Compared to traditional microscopy, mass spectrometry imaging provides information at the molecular level.

In addition to the applications described above, there are still other applications of mass spectrometry, such as study of post-translational modifications of proteins and non-covalent interactions. Due to the complexity and diversity of biological samples, there have been many efforts aimed at faster sample preparation, simple ionization methods and improved data analysis software. Among these improvements, one important aspect is the development of ambient ionization techniques.

1.2 Ambient Ionization Techniques

1.2.1 Basic Components of Mass Spectrometer

Mass spectrometers are usually composed of three main components, the ionization source, mass analyzer and ion detector[7], as shown in Figure 1.1. Molecules are first ionized in the ion source, and then reach the mass analyzer where they are separated in space or in time according to their mass-to-charge ratios. Ions reach the detector and after signal processing generate the spectra. Different instruments have characteristic functions to satisfy various requirements, leading to different designs.

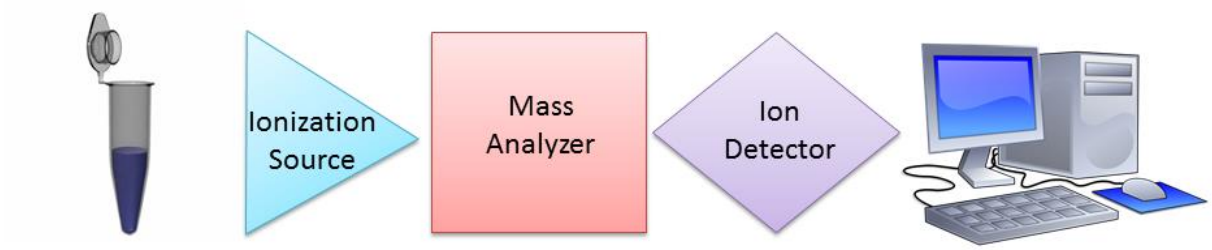

Figure 1.1 Three components of mass spectrometry. Ionization source could be EI, ESI, MALDI etc., Mass analyers could be sectors, quadrupole, iontrap, time of flight etc. or a combination of different mass analyzers. Ion detectors could be faraday cup, electron multipliers etc..

1.2.2 Ionization Methods and "Soft" Ionization Sources

Since mass analyzers could only separate ions, it is important that molecules are ionized before entering. Ionization sources ionize molecules with various methods. The commonly seen ones are listed below. 1) Electron capture ionization generating negative ions or electron ejection generating positive ions. Both methods are seen in electron ionization, one of the earliest ionization methods. Using these methods, one can usually get information on both fragment ions and molecular ions. However it is hard to control the amount of fragmentation and therefore in

some cases it is difficult to identify the molecular ion peak. 2) Charged molecules can be transferred into the gas phase directly and become ions. This happens in a variety of ionization sources. 3) Removing protons from compounds that contain acidic groups provides negative ions. However both methods work only for certain type of compounds. 4) Many compounds can be ionized through accepting a proton or a cation such as Na+ or K+. This is referred to as protonization or cationization. Most ionization sources contain more than one ionization method[7], shown in table 1.1.

Ionization Source	Acronym	Description	Ionization method
Electron Ionization	EI	Electron beam/Electron Transfer	Electron ejection/ Electron capture
Chemical Ionization	CI	Proton Transfer	Protonation/ Deprotonation
Electrospray Ionization (Nanospray Ionization)	ESI (nanoESI)	Evaporation of charged aerosol droplet in electric field	Protonation/Cationization/ Deprotonation/Transfer of charged aerosol droplets directly
Matrix Assisted Laser Desorption Ionization	MALDI	Photon absorption/proton transfer	Protonation/Cationization/ Deprotonation

Table 1.1. Common Ionization Sources and a description of the ionization method.

Electron ionization (EI), also called electron impact ionization, is an ionization method in which gas phase molecules interact with energetic electrons to produce ions. It was among the first ionization methods and was the main ionization method before the 1980s. Electron ionization causes fragmentation, therefore it is often referred to as a "hard" ionization technique. The

limitations of EI have encouraged research of other ionization technologies. However EI is still commonly used as an ionization method for gases and small organic molecules.

Chemical ionization (CI) was developed as an analytically useful technique in the 1960s. CI shares rather close similarity with EI in some aspects, however it is among the first of the soft ionization methods. In CI, gas phase molecules interact with ions and form new ion species. The process may include transfer of an electron, proton or other charged species between the analyte molecule and ions generated from the reagent gas (e.g. methane). Since CI still requires thermal desorption of the analyte, it is limited to molecules that are thermally stable. Currently, CI is still been used and has developed to have negative CI (NCI) and atmospheric pressure chemical ionization (APCI).

MALDI[16] and ESI[17] both offer excellent mass range and sensitivity. They are now the two most widely used ionization sources in Bioanalytical applications of mass spectrometry. Although these ionization methods are quite different, both methods are considered "soft ionization" sources which preserve the molecule ion.

Electrospray ionization (ESI) was first introduced in the late 1960s, shortly after the application of CI. In ESI, a liquid passes through a needle to which a high DC voltage (usually 1-3kV) is applied. The voltage produces an electrical gradient on the liquid passing through the needle, causing the charges to spread on the surface and forcing the liquid exiting the needle to form a Taylor cone. At the tip of the Taylor cone, the liquid reaches the Rayleigh limit. Surface tension and electrostatic repulsion reach a balance and a highly charged droplet is formed. The charged

droplets are attracted to the mass spectrometer due to the electric field formed between the needle and the entrance of the mass analyzer. During this process, liquid constantly evaporates from the surface of the droplet, decreasing the droplet volume and thereby increasing the surface charge density. When the mutual Columbic repulsion between the same charges on the surface exceeds the forces of surface tension of the droplet, a smaller portion of the droplet will be ejected from the parent droplet. This process is repeated several times until finally gas-phase ions are formed. To help promote evaporation, heat and drying gas are often present in ESI configurations.

The relative softness of ESI allows for the preservation of intact molecular ions and sometimes even non-covalent complexes during ionization. Therefore, it has been widely used in peptide and protein analysis. Since ESI requires a constant flow of liquid, it is amenable to coupling with liquid chromatography. ESI can also generate multiply-charged ions, which is useful for analyzing large molecules by decreasing the mass-to-charge ratio into the observable mass range of the mass analyzer. ESI has a low tolerance to salts and is affected by a carryover from sample to sample, so it is important to have a pure sample without contamination to get clean mass spectra. A commonly used variation of ESI was low flow electrospray, often called nanospray (NSI or NanoESI)[18]. In NSI, the orifice of the needle is reduced to around 5 μm, the flow rate has been lowered to hundreds of nL/min resulting in increased sensitivity.

MALDI was invented by Tanaka in 1988. In MALDI, samples are prepared by premixing an analyte and a matrix compound that allows co-crystallization. Irradiation of this analyte-matrix mixture was irradiated with a laser and results in the vaporization of the matrix, which

subsequently carries the analyte with it. The matrix plays a key role in the generation of ions. Commonly used matrices are UV absorbing, non-volatile, weak organic acids. Although there have been several theories developed, the mechanism of desorption by MALDI is still under debate.

MALDI is capable of generating ions with mass ranges up to 300 kDa and has a very low detection limit. The use of matrix however makes analysis of masses under 700 Da challenging. The selection of matrix is very important in MALDI since background interference is highly dependent on the matrix material. Since MALDI requires the sample plate to be under vacuum when operating, it is not considered an atmospheric on-line detection method.

1.2.3 Recent Development of Ambient Ionization Sources

Although ESI and MALDI have been applied widely in analytical and bio-analytical area, there are still some limitations of these ionization methods and therefore development of new ionization techniques continues[19]. Along with the introduction of the Direct Analysis in Real Time (DART) method by JEOL, desorption electrospray ionization (DESI) was introduced by the Cooks group. Since then more than 30 ambient ionization methods for mass spectrometry have been reported[20, 21]. A selection of ambient ionization techniques with their abbreviations are listed in table 1.2. The research in refining these techniques and their associated applications is still ongoing and new methods are continually being introduced.

Acronym	Method Name	Sample State	Year
DESI	Desorption electrospray ionization[22, 23,24]	Solid, Liquid Polar	2004
ASAP	Atmospheric pressure solids analysis probe[25]	Solid, Liquid Polar/nonpolar	2005
DAPCI	Desorption atmospheric pressure chemical ionization[26]	Solid, Liquid Polar	2005
DART	Direct analysis in real time[27]	Solid, Liquid, Gas Polar/nonpolar	2005
ELDI	Electrospray laser desorption ionization[28]	Solid, Liquid Polar	2005
EESI	Extractive electrospray ionization[29]	Liquid, Gas Polar	2006
LDTD	Laser diode thermal desorption[30]	Solid, Liquid Polar/nonpolar	2006
DAPPI	Desorption atmospheric pressure photoionization[31]	Liquid Polar/nonpolar	2007
DBDI	Dielectric barrier discharge ionization[32]	Solid, Liquid Polar/non-polar	2007
MALDESI	Matrix-assisted laser desorption electrospray ionization[33]	Solid, Liquid Polar	2007
PADI	Plasma-assisted desorption ionization[34]	Solid, Liquid Polar/non-polar	2007
APGDI	Atmospheric glow discharge ionization[35]	Solid, Liquid Polar/non-polar	2008
EASI	Easy ambient sonic spray ionization[36]	Solid, Liquid Polar	2008
IR-LADESI	Infrared laser-assisted desorption electrospray ionization[37]	Solid, Liquid Polar	2008
LSI	Laser spray ionization	Liquid Polar	2008
LTP	Low temperature plasma probe[21]	Solid, Liquid, Gas Polar/non-polar	2008
DEMI	Desorption electrospray metastable-induce Ionization[38]	Solid, Liquid. Polar	2009
PSI	Paper spray ionization[39]	Liquid. Polar	2009
DCBI	Desorption corona beam ionization[40]	Solid, Liquid Polar/non-polar	2010
FIDI	Field-induced droplet ionization[41]	Liquid. Polar	2010
LDSPI	Laser desorption spray post-ionization[42]	Solid, Liquid. Polar	2010
TDAMS	Thermal desorption-based ambient mass spectrometry[43]	Liquid. Polar	2010
USI	Ultrasound ionization[44]	Liquid. Polar	2010

Table 1.2. Ambient Ionization Sources.

New ambient ionization methods usually have one or more of the following aspects that result in improvements over previous methods:

1) Straightforward setup: Some new ambient ionization methods have a simplified setup (e.g. a spray technique that removed DC voltage or desorption methods under atmospheric pressure).

2) Simplified sample preparation: In DESI, sampling is performed directly from the surface of a solid sample. With simplified sample preparation, large amounts of labor are saved and the efficiency of sample analysis is improved.

3) Soft ionization. Most new ambient ionization techniques are soft ionization methods. Some of them have the ability to analyze fragile compounds and preserve more biologically interesting information.

4) Improved ionization efficiency: Some new ambient ionization methods have proved to be able to generate ions from carbon hydrates, providing the possibility to analysis molecules that were previously challenging to ionize.

5) High salt/matrix tolerance or molecular specificity: ESI is sensitive to salts or other contaminants and thus it requires a salt content below 100 mM. MALDI has a higher tolerance to salts, but also have significant interference from matrix in low m/z ranges. New ambient ionization techniques with high salt tolerance and no matrix interference can help with impure samples.

6) Ability to perform high throughput experiments: DART has a higher throughput than ESI direct infusion over a set period of time. The simplified sample injection of DART does not require sample change, rinsing and pumping as in ESI.

Refinement of experiments and mechanism study follows the report of new ambient ionization techniques. Both types of study will be useful to improve the performance of new ionization techniques. In fact, some ambient ionization techniques generate complex ion clusters without the time-resolved nature from conventional analysis (LCMS), making the application of complex sample difficult. For example, a study on coupling DESI with ion mobility have shown the advantages of gas phase separations[45]. However, overall downstream analysis of the ions generated by these new techniques has received relatively low attention.

1.3 Surface Acoustic Wave

1.3.1 Mechanism and properties

A surface acoustic wave (SAW) is an acoustic wave traveling along the surface of a material. The amplitude typically decays exponentially with depth into the substrate. Surface acoustic mode of propagation was first explained in 1885 by Lord Rayleigh who also predicted its properties. Named after their discoverer, Rayleigh waves have a longitudinal and a vertical shear component that can couple with any media in contact with the surface. This coupling strongly affects the amplitude and velocity of the wave, allowing SAW sensors to directly sense mass and mechanical properties. In nature elephants communicate with each other using surface acoustic

waves generated by stomping their feet. In electronics, SAW devices are widely used as filters, oscillators and transformers.

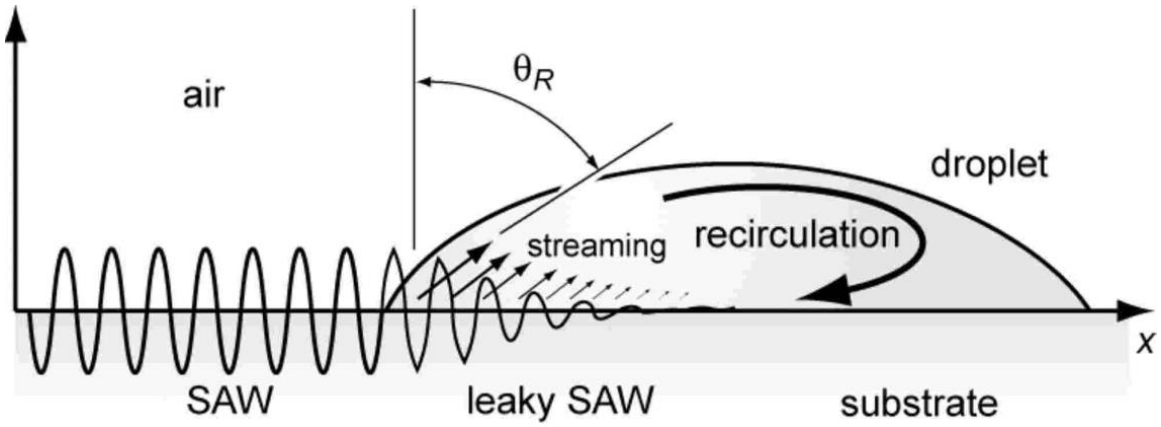

Figure 1.2 Surface Acoustic Wave. A typical process for photolithography is shown as above A.

As shown in Figure 1.2, when SAW travels and reaches something on the surface (*e.g.* a liquid droplet), the energy will be transferred into the droplet. Usually when the sample is a liquid, SAW energy will induce a circuit movement and cause the liquid to shake[46]. As the amplitude increases, the liquid droplet might move, jet or nebulize depending on the applied power. Nebulization is also referred to as "atomization" in certain literature (especially engineering literature)[47]. Atomization is not an accurate term here since the generated plume is not composed of single atoms. In our research it is shown that this plume contains molecular ions, therefore we avoided using the term "atomization"; and use "nebulization" instead[48].

The convenience of energy transfer made SAW technology useful within the field of microfluidics[49- 50]. Importantly, and unlike other microfluidic methods for sample manipulation, it does not require pressure driven pumps, interconnects, nor the integration of electrodes and

micro channels[51-52].The removal of the need for pumps and interconnects eliminate many problems commonly associated with dead volumes, which are particularly disadvantageous when using small volumes of rare, low abundance samples.

SAW devices have already been incorporated into microfluidic workflows to enable mixing using SAW micro centrifugation in channels, heating, liquid droplet movement and delivery to or from a microfluidic port[48 - 53]. SAW is also known to be able to nebulize protein samples for array writing with masks[54, 55]. More recently SAW nebulization has been used to generate aerosol droplet with diameters of between 5 to 10nm to assist with the synthesis of polymeric nanoparticles and to generate protein aerosols and nanoparticles for drug delivery[56, 57].

1.3.2 Surface Acoustic Wave Nebulization

When the amplitude of the SAW is high enough, large amounts of energy will be transferred to the liquid sample on the surface. As the applied energy overcomes the surface tension, droplets will nebulize into aerosols. This phenomenon has been investigated by the Yeo group and applied to develop medical devices[56] that delivered medicine to patients in the form of an aerosol[57, 58]. Despite this, nebulization, compared to other SAW driven droplet movements, has received little attention especially from the microfluidics or electronics community[55, 59].This is because nebulization is not a useful way to transfer a signal or to carry out SAW related mass transfer.

In 2010, surface acoustic wave nebulization (SAWN) was introduced as an ionization method by Scott Heron et al[48, 60]. A SAWN chip was constructed from lithium niobate ($LiNbO_3$) wafers and placed next to the heated transfer capillary of a Thermo LTQ instrument. The plume generated from SAWN was attracted to the mass spectrometer through a pressure differential. Angiotensin I was used as an analyte to test the ability of SAWN. The results showed that SAWN was capable of generating ions without applying a high DC voltage as in ESI. Tandem spectra were also obtained to verify the molecular structure. SAWN has since proven to be a soft ionization method imparting less internal energy to the nebulized ions than ESI[61]. This indicated SAWN could potentially be applied to the investigation of fragile compounds and non-covalently bonded compounds. In 2011, the Go group used paper to deliver sample directly to SAWN and created a paper based microfluidics system[62]. In 2012, the Goodlett group reported the use of SAWN and hierarchical tandem mass spectrometry (HiTMS) algorithm to define lipid structures[63]. While numerous applications of SAWN-MS have been reported, the mechanism of SAWN remains under investigation. The Goodlett group suggested the mechanism of fast vibration tearing apart liquid into both positive and negative aerosol droplet. In 2012, the Go group run a simulation of the piezoelectric surface and discussed the possible origin of charges.

1.4 Digital Micro Fluidics

Digital microfluidics (DMF) is an alternative technology for lab-on-a-chip systems based upon micromanipulation of discrete liquid droplets. It is based on electrowetting, a phenomenon that results in the wetting, or changing of contact angle, of a droplet placed on the surface of a substrate containing electrodes and a dielectric layer. The surface charge of the substrate changes

when an electric field is applied or removed allowing for the preferential wetting of the droplet[64]. Microfluidic processing is performed on unit-sized packets of fluid which are transported, stored, mixed, reacted, or analyzed using a standard set of basic instructions.

The mechanism of electrowetting was discovered in the early 20th century. However bio-analytical applications did not start to emerge until after 2000[65]. With DMF, a controlled amount of liquid could be separated, moved, stirred and merged with other liquids. When DMF is combined with other techniques, it is possible to incubate, centrifuge, separate different phases and crystalize. Recently DMF has been applied to immunoassays[66], micro scale chemical/enzymatical reactions[67], DNA based reactions[68,69,70] (*e.g.* sequencing) and cell dividing and concentrating[68, 71]. Detection methods for DMF have primarily been optical methods. Mass spectrometry has also been used for DMF detection in the recent years[72].

1.5 Micro Fabrication Basic Techniques

Micro fabrication is the design and manufacture of devices with dimensions measured in micron range. A variety of techniques have been utilized for the research presented in this thesis. Although chip design and selected fabrication is different for each experiment, most fabrications follow the same standard procedure. Here a summery on the chip material, fabrication process, and surface modification will be provided.

The most commonly used wafer material in micro fabrication is silicon or glass. To generate SAW, a piezoelectric substrate is required. The selected material here is Lithium Niobate

($LiNbO_3$). $LiNbO_3$ is a transparent colorless solid insoluble in water, with a trigonal crystal system. The $LiNbO_3$ wafers used here are either 3 or 4 inch diameter 0.5mm thick 128 °Y-cut X-propagating. Before any fabrication or modifications the wafers must be thoroughly cleaned. The process usually starts with sonication in acetone, then before acetone dries wash the wafer is sequentially washed with isopropyl alcohol and DI water. The remaining water droplets are then blown off with nitrogen gas.

Photolithography is a process used in micro fabrication to pattern parts of a thin film or the bulk of a substrate. It uses light to transfer a geometric pattern from a photo-mask to a light-sensitive chemical "photoresist" on the substrate. A series of chemical treatments then either engraves the exposure pattern into, or enables deposition of a new material in the desired pattern upon, the material underneath the photo resist. In our experiments, the wafer is covered with an adhesion promoter and then a photoresist (AZ 1512). After baking, there are two ways to create the pattern on the chip. Laser writing is often used for small batches of SAWN, while mask alignment is used for production of larger amounts. The wafer was developed after exposure. After baking again, the wafer was metallized with a layer of 20nm Cr following 60nm Au. The chip is finally washed with acetone to remove all the excess gold and photoresist.

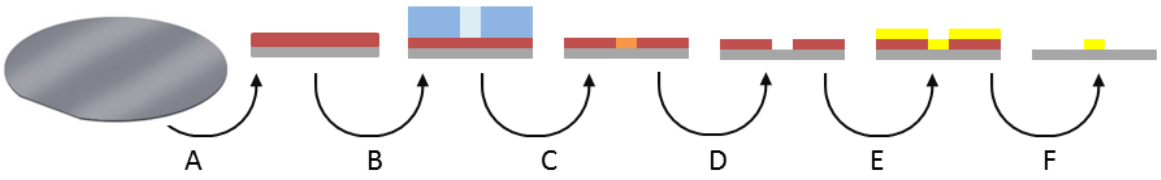

Figure 1.3 Photolithography process. A typical process for photolithography is shown as above A. Wafer is cleaned with standard processes and baked for 90 sec at 110 ℃. After the wafer is

cooled down to room temperature it is spincoated with positive photoresist (P20 and A1512), the chip is baked at 110 ℃ for 90 sec again to allow the photoresist to solidify. B&C. The wafer from process A will be covered with a mask with features, UV light is allowed to expose certain areas that is not coverd by the mask for a specific time related to spin coating thickness (4.5 sec). D. Remove from exposure and soke in developer solution (AZ developer) for 60 sec. The exposed area will be washed off, showing the wafer surface.The wafer is then soaked in DI water to stop the developing process and then baked at 110 ℃ againg to evaporate any remaining liquid. E. The wafer is places in a metal evaporation instrument and coated with selected thickness of metal (20nm Cr and 60nm Au). F. The wafer is sonicated in Acetone to remove remaining photoresist and excess metal, then washed with the standard process.

Several chip modifications have been done to the wafer after production, including chemical evaporation, spin coating, plasma enhanced chemical vapor deposition (PECVD) and dry etching. The wafer is then divided into chips after the fabrication is complete, through hand cutting with a diamond pen or through a dicing saw. Cutting with a dicing saw gives a cleaner edge and has better control when the target piece is small, while hand cutting fits better if the design is of a larger area. The process for these methods can be found on the website of micro fabrication facilities (https://coral-prod.engr.washington.edu/upload/manuals/).

Chapter 2 Internal Energy Distribution of Surface Acoustic Wave Nebulization with Survival Yield Method

2.1 Survival Yield Method to Determine Internal Energy

The "softness" of an ionization source is usually evaluated by the ability to preserve molecular ions. The internal energy distribution of ions can be measured with the survival yield method[73]. The internal energy distribution of "soft" ionization sources such as ESI, MALDI[74,75,76] has been investigated with the survival yield method. After the development of a new ambient ionization method, the internal energy distribution is routinely characterized. The effect of the parameters of the new ambient ionization source (voltage, temperature, etc.) on the internal energy distribution is studied to optimize the performance. Therefore internal energy distribution can contribute to designing and modifying of the ionization source.

In 1998, E. De Pauw et al used the survival yield method to study the internal energy distribution of ions generated by ESI[73]. The effect of voltage settings and solvent composition in ESI was also discussed. In 2003, the method was modified to investigate MALDI[75]. In 2008 Nefliu et al used the survival yield method to study the internal energy distribution of DESI[77]. Touboul et al investigated the internal energy distribution of two new ambient ionization sources (EESI and SSI), the result was compared with ESI[78]. In 2009 SPALDI was analyzed and compared with other two desorption ionization methods (LDI and DIOS)[79]. In 2010 DART was studied and compared to ESI[80]. New ambient ionization methods were commonly compared to a standard spray method (ESI) or desorption method (MALDI). This made it possible to cross-compare different ionization methods with a the standard method such as ESI or MALDI.

2.2 Method and Instrumentation

2.2.1 Calculation of Survival Yield Method

Survival yield is defined as the molar fraction molecular ions remaining after ionization. The molar fraction is usually calculated from the peak height or peak area in the obtained spectrum. The selected ions for the measurement are usually benzylpyridinium cations. There are two reasons for the selection: 1) under conditions of typical ESI and MALDI they fragment by single bond dissociation between pyridine and the benzyl group. This allows for a simple calculation of the process energetics. 2) Benzylpyridinium cations are relatively small species to allow for calculations of the physical quantities. Since SAWN uses pure liquid without matrix, clean spectra could be obtained in the mass region of *m/z* 50 - 250) without matrix effect. Survival yield methods measure the fraction of molecular ions having an internal energy below the dissociation threshold. Under the assumption that the time for the dissociation is long enough to exclude a kinetic shift (kt 991 for E9Eb), it can be shown that this value also corresponds to the integral of the internal energy distribution function from zero to the energy barrier Eb (Equation 1). In the following equation, SY represents the survival yield and P(E) is the internal energy distribution.

$$SY = \int_0^{E_b} P(E)dE \qquad \text{Eq. 1}$$

The survival yield is obtained experimentally by measuring the ratio of the residual molecular ion intensity to the sum of intensities of the molecular ion and its fragment (Equation 2).

$$SY = \frac{I(M^+)}{I(M^+) + I(F^+)}$$ Eq. 2

An S-shaped curve, SY(E), is fitted to the data and its first derivative is taken as the internal energy distribution function P(E). $I(M^+)$ and $I(F^+)$ represent the intensity of the ions of interest. In addition to the data acquired for the synthetic BzPy derivatives used here, four other data points were used as boundary conditions for curve fitting, with –1 eV, 0 eV, 0.1 eV corresponding to 0 % survival a yield and 5 eV corresponding to 100 % survival yield. When using the survival yield method, it is important to account for the contribution of all possible fragmentation channels. While BzPy ions mainly fragment by loss of pyridine, it has been reported that under certain conditions, a mass spectrum might contain other fragments. To mitigate the effect in our calculations from non-pyridine fragmentation pathways, a sum of all detected fragment ion intensities was used.

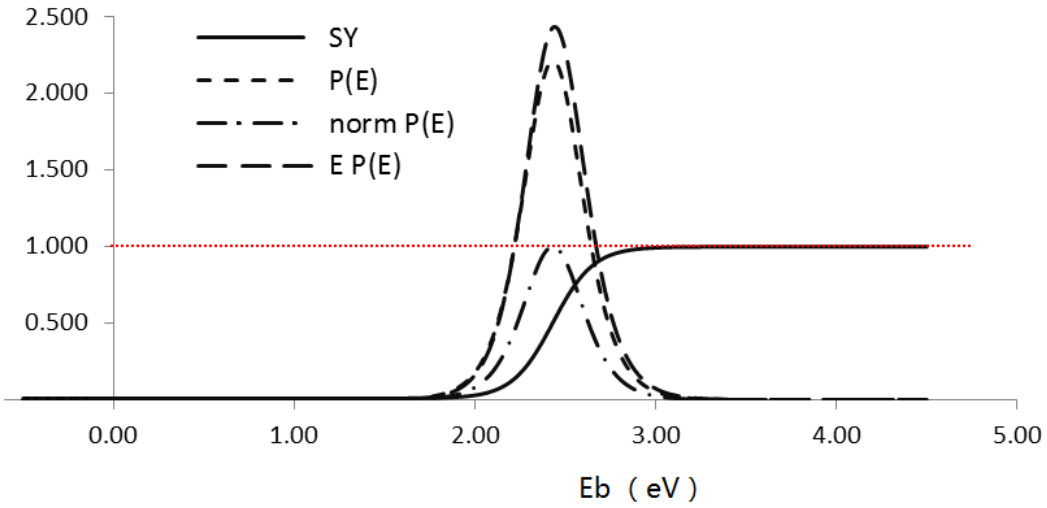

*Figure 2.1 Calculation of internal energy distribution.SY (survival yield) is measured for four different ions, a shaped curve is fitted as the SY line. P(E) is calculated based on SY and normalized for easier comparison. E*P(E) is calculated based on P(E).*

Specifically, the fragment ions included for MeO-BzPy were at m/z 121, 106, 91, and 77, those for Me-BzPy were at m/z 105, 103, 79, and 77, those for Cl-BzPy were at m/z 125, 99, and 89, and those for NO_2-BzPy were at m/z 136, 169, 106, 90, and 78. The corresponding survival yield of the four substituted BzPy ions were plotted versus their respective dissociation energies and the curve was fit to a sigmoidal function. With the assumption that the intake of internal energy per vibrational mode is the same for all reactant ions under given experimental conditions, the derivative of the sigmoidal curve becomes an approximate internal energy distribution function of all precursor ions.

2.2.2 Synthesis of Thermometer ions

Four substituted benzylpyridinium (BzPy) salts were prepared, which were 4-methoxy (MeO), 4-methyl (Me), 4-chloro (Cl), and 4-nitro (NO_2). The substituted BzPy salts were synthesized

following the reaction depicted in Scheme 1. All reagents and solvents used were obtained from Sigma-Aldrich Co. (St. Louis, MO, USA). Various benzyl chloride derivatives were mixed with a slight excess (1.2 molar equivalents) of pyridine in dry acetonitrile and stirred using a magnetic bar. Reactions were performed at room temperature overnight, except for 4-Cl BzPy where the reaction was carried out at 80 °C for 3 h. At the end of the reaction time, diethyl ether was added to precipitate the BzPy salts. Solids were collected by filtration and dissolved in a water methanol mixture (1:1 vol/vol) at 2 mg/L.

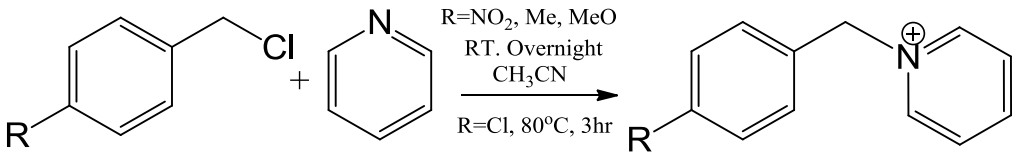

Figure 2.2 Synthesis of benzylpyridinium ions. Four different coumpound is synthesised.

2.2.3 Instrumentation

The fabrication and operation of SAWN chips have been reported in detail elsewhere[48]. Each device was made up of 20 pairs of 100 μM interdigitated (IDT) electrodes (40 in total) with 100 μM spacing and 10 mm aperture. Additionally, an electrode was patterned in the SAWN transducer activation area to allow the application of an external voltage to liquid droplet or to ground the sample. The operating frequency of the transducer used in this study was 9.56 MHz. A MXG analog signal generator (Agilent N5181A, Santa Clara, CA) and a Mini Circuits ZHL-5W-1, 5-500 MHz amplifier (GwInstek GPS-2303, New York, NY) were used to activate the SAWN chip. Experiments were carried out on an LTQ instrument (Thermo Scientific, San Jose, CA).

Both ESI and SAWN sources were mounted on the same instrument with identical mass spectrometer settings. The atmospheric pressure ionization (API) inlet capillary voltage was maintained at 20 V and the tube lens was set to 110 V for all experiments. A Thermo Scientific IonMax source (Thermo Scientific) was used for all ESI experiments. Figure 2.3 shows how the SAWN chip was interfaced to the mass spectrometer inlet. The area of the chip supporting the droplet was positioned 4-6 millimeters in front and under the capillary inlet and a droplet was deposited on the surface of the wafer (Figure 2.3B). To aerosolize the sample in the liquid droplet a waveform was applied to the IDT. The plume of aerosols formed was pulled into the mass spectrometer heated capillary inlet (Figure 2.3C) by local gas flow. For some experiments a silica capillary was placed right above the chip surface in front of the mass spectrometer inlet and the solution containing the sample was continuously supplied to the SAWN chip by means of a syringe pump. Electrode 3 was always grounded in this experiment as in Figure 1A.

For the comparison experiments of ESI and SAWN, 3 μL/min flow rate was applied and three different API inlet capillary temperatures of 150 ℃, 225 ℃, and 300 ℃ were used. For the SAWN flow rate experiments, an 8 μL/min flow rate which is the highest flow rate sustainable under SAWN operation conditions was used to compare with the 3 μL/min results. To mitigate the effect of instantaneous signal fluctuations, the data were averaged for one minute for both the SAWN and ESI experiments. At least three replicates for each of the BzPy compounds was acquired and survival yield determined by averaging across all three replicates.

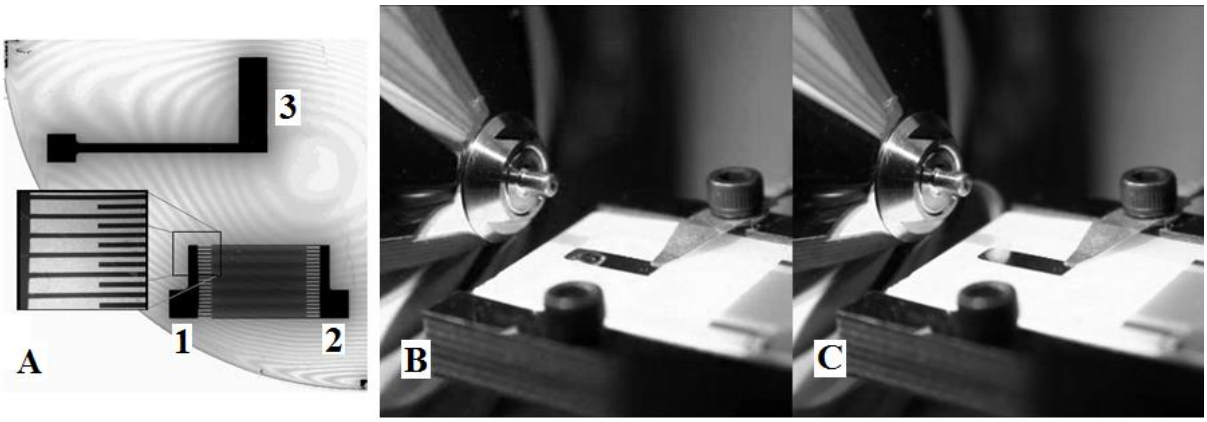

Figure 2.3 A surface acoustic wave nebulization (SAWN) chip and process. Configuration of electrodes on the SAWN chip where electrode 1 and 2 of the interdigitated transducer (IDT) are connected to a signal generator to produce a SAW and electrode 3 which is used to ground the chip surface and sample containing droplet (A); Coupling SAWN with an atmospheric pressure ionization (API) inlet mass spectrometer where a drop of liquid is visible prior to SAW activation (B); and plume of nebulized liquid shown entering the API MS instrument post SAW activation (C).

2.3 Results and Discussion

2.3.1 Mass Spectra of Thermometer Ions.

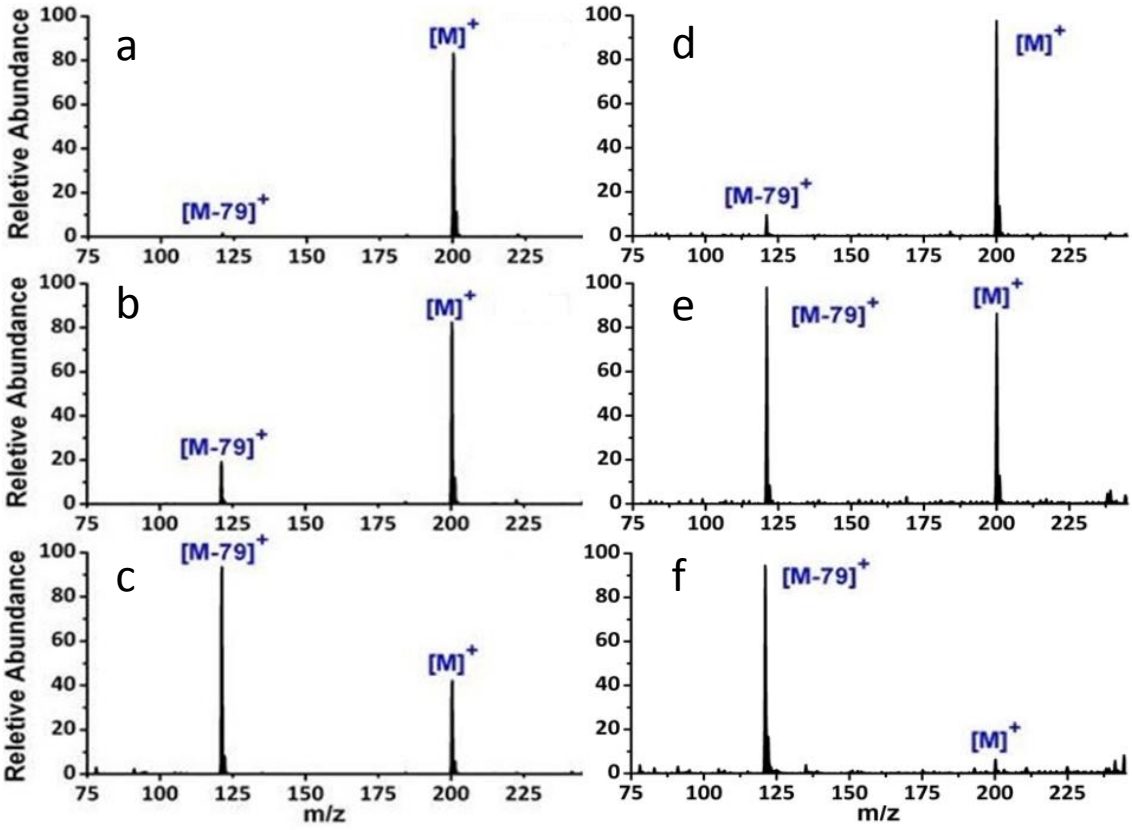

Figure 2.4 Mass spectra of 4-MeO benzylpyridinium ion and loss of pyridine. The molecular ion and a fragment ion are shown in each panel for the loss of pyridine as a neutral compound obtained by electrospray ionization (d, e, f) and surface acoustic wave nebulization (a, b, c) at increasing temperatures measured on the same capillary of an atmospheric pressure ionization inlet mass spectrometer at 150 ℃ (a,d), 225 ℃ (b,e) and 300 ℃ (c,f).

Figure 2.4 shows the spectra of the 4-MeO BzPy derivatives obtained by SAWN and ESI at increasing temperatures in the mass spectrometer inlet capillary used to aid desolvation. At an inlet temperature of 150 ℃ (Figure 2.4 a, b), 4-MeO BzPy (m/z 200) was the dominant peak with very little dissociation into 4-methoxybenzyl (m/z 121). The average survival yield for the

molecular ion was 95.3 % for SAWN and 90.6% for ESI. However, increasing the temperature to 225 ℃ resulted in a noticeable increase of the 4-methoxybenzyl ion relative intensity, and the survival yield was reduced to 65.8 % for SAWN and 45.3% for ESI (Figure 2.4 c, d). Upon increasing the capillary inlet temperature to 300 ℃, the relative abundance of the molecular ion was further reduced, and the survival yield dropped to 21.1 % for SAWN and 5.7% for ESI (Figure 2.4 e, f). The survival yield was therefore easily determined for each thermometer ion using Eq. 2. Measurements on the series of BzPy derivatives were extrapolated to determine the ion deposition energy. Not surprisingly, the data show that the temperature of the mass spectrometer inlet capillary used to aid desolvation played a large role in the internal energy deposition during the ionization process regardless of the ionization method used. Analysis of the temperature affects for 4-Me BzPy, 4-Cl BzPy and 4-NO_2 BzPy yielded similar spectra and results.

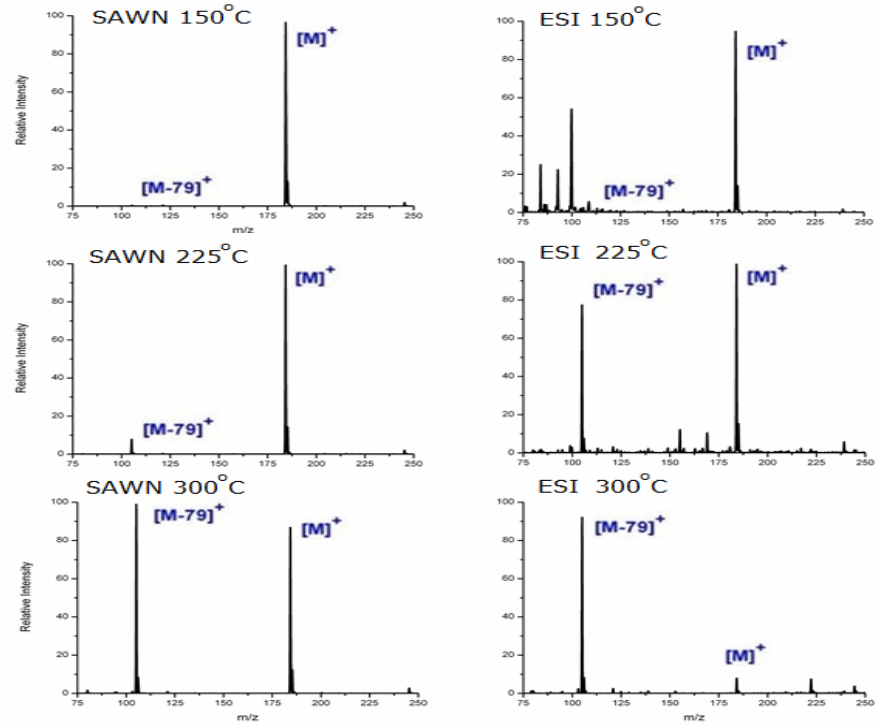

Figure 2.5 Mass spectra of 4-Me benzylpyridinium ion and loss of pyridine.

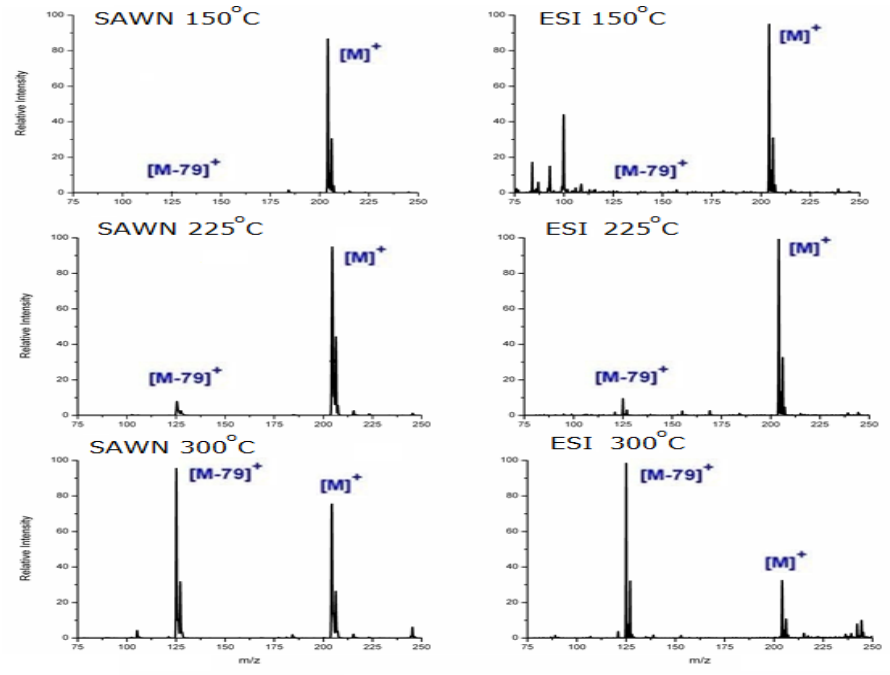

Figure 2.6 Mass spectra of 4-Cl benzylpyridinium ion and loss of pyridine.

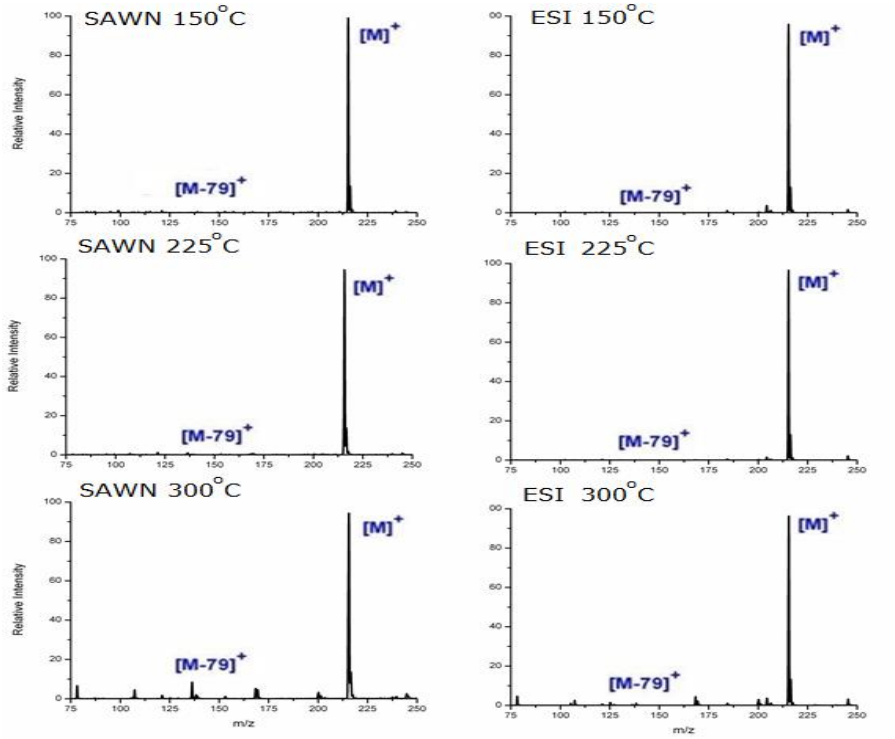

Figure 2.7 Mass spectra of 4-NO_2 benzylpyridinium ion and loss of pyridine.

2.3.2 Dissociation energy calculations

The fragmentations of substituted BzPy ions are known to proceed via the mechanism described in Figure 2.8. The precursor ion dissociates into a fragment ion (benzylium ion A or tropylium ion B) and a neutral pyridine molecule[81,82,83].

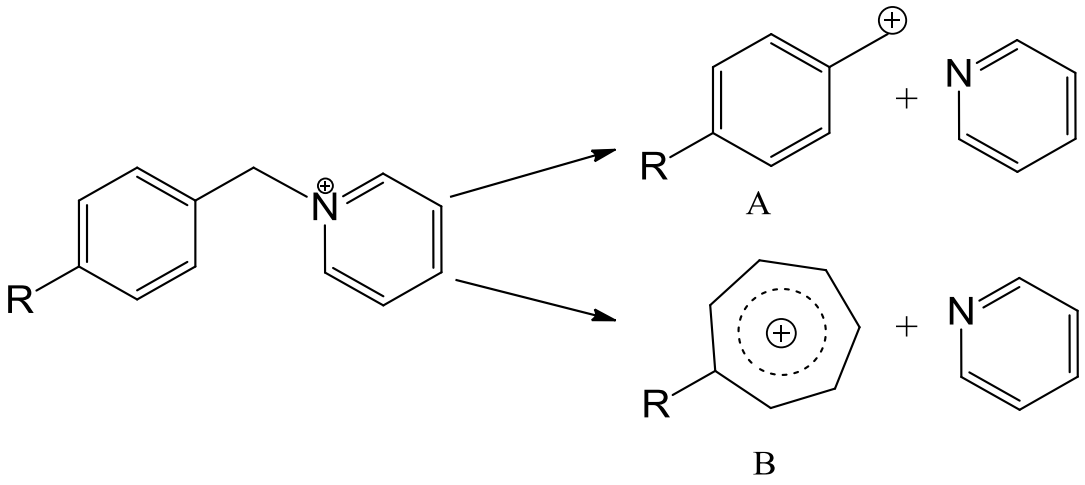

Figure 2.8 Fragmentation of benzylpyridinium ions. BzPy ion fragment in to A benzylium ion or B tropylium ion.

In order to derive ion internal energies from the measurements of ion survival yields, the dissociation energies for each BzPy ion are required. Several methods to calculate dissociation energies have been reported in the literature that gave different results, mainly due to the low level of theory used previously[76,82, 84,]. We reasoned that higher-level calculations at the "chemical accuracy limit"[85] should provide more accurate bond energies to be used as benchmarks for the evaluation of the experimental data, therefore also providing more accurate data fitting. Here we employed high-level computational methods including electron correlation as implemented in the Gaussian 03 suite of programs[86]. Optimized geometries were obtained by

density functional theory calculations using Becke's hybrid functional (B3LYP)[87, 88] and the 6-31+G(d,p) basis set. Stationary points were characterized by harmonic frequency calculations with B3LYP/6-31+G(d,p) as local minima with all real frequencies. The calculated frequencies were scaled with 0.963 and used to obtain zero-point energy corrections for the dissociation energies. Improved energies were obtained by single-point calculations that were carried out with B3LYP and MP2(frozen core) using split-valence triple-basis sets of increasing size furnished with polarization and diffuse functions; e.g, 6-311++G(2d,p), and 6-311++G(3df,2p). Single point energies were also calculated with coupled-cluster theory[89] including single, double, and disconnected triple excitations (CCSD(T))[90] and the 6-311G(d,p) basis set. These were then expanded to effective CCSD(T)/6-311++G(3df,2p) energies using the standard linear formula (Eq. 3):

E[CCSD(T)/large basis set] =

E[CCSD(T)/small basis set] + E[MP2/large basis set] – E[MP2/small basis set] Eq. 3

The dissociation energies calculated as described above for 4-MeO, 4-Me, 4-Cl and 4-NO_2 BzPy ions are summarized in Table 1. The CCSD(T) data showed dissociation energies for all benzylpyridinium ions that were 0.4-0.5 eV higher than those from B3LYP calculations (Table 1). Hence, the energy scale using these ions was recalibrated to comply with the high-level data. Benzylium and tropylium ions have the same m/z values, but different enthalpies of formation, which implies different threshold dissociation energies for the pertinent fragmentations. For the Me, Cl, and NO_2 substituents, the tropylium ions were slightly more stable than their benzyl counterparts. The MeO-substituted benzyl and tropylium had comparable energies (Table 2.1).

We used the lower of the calculated dissociation endothermicities to assess the energy thresholds in our internal energy calculations[73,74,77,80].

-R	*B3LYP/6-31+G(d,p) (eV)*		*CCSD(T)/6-311++G(3df,2p) (eV)*	
	Benzylium	***Tropylium***	***Benzylium***	***Tropylium***
MeO	1.457	1.382	1.870*	1.916
Me	1.808	1.575	2.303	2.139*
Cl	1.947	1.756	2.407	2.301*
NO_2	2.471	2.101	2.911	2.623*

Table 2.1 Calculated bond dissociation energies for substituted benzylpyridinium compounds. stands for lowest calculated energy path.*

Survival yields and internal ion energies in ESI vs. SAWN. Figure 3a shows the survival yields obtained for SAWN and ESI produced ions under identical source conditions as a function of calculated dissociation energy. Data points correspond to the four BzPy derivatives: 4-MeO, 4-Me, 4-Cl and 4-NO_2 BzPy in order of increasing dissociation energy. Survival yield was plotted versus calculated bond dissociation energies in electron volts derived from Eq. 3 for each substituted BzPy compound. The corresponding ion internal energy distributions were estimated by fitting a sigmoidal SY(E) function to the experimental data and taking the first derivative. Mean ion internal energies determined in two independent series of measurements are summarized in Table 2. As can be seen from Figure 2.9 a, ions produced by SAWN clearly displayed higher survival yield, and hence lower internal energy than their ESI formed counterparts, regardless of the substituent carried by the benzene ring. In fact, the mean internal energy deposited by ESI under these atmospheric ionization source conditions was over 30% higher than that of SAWN.

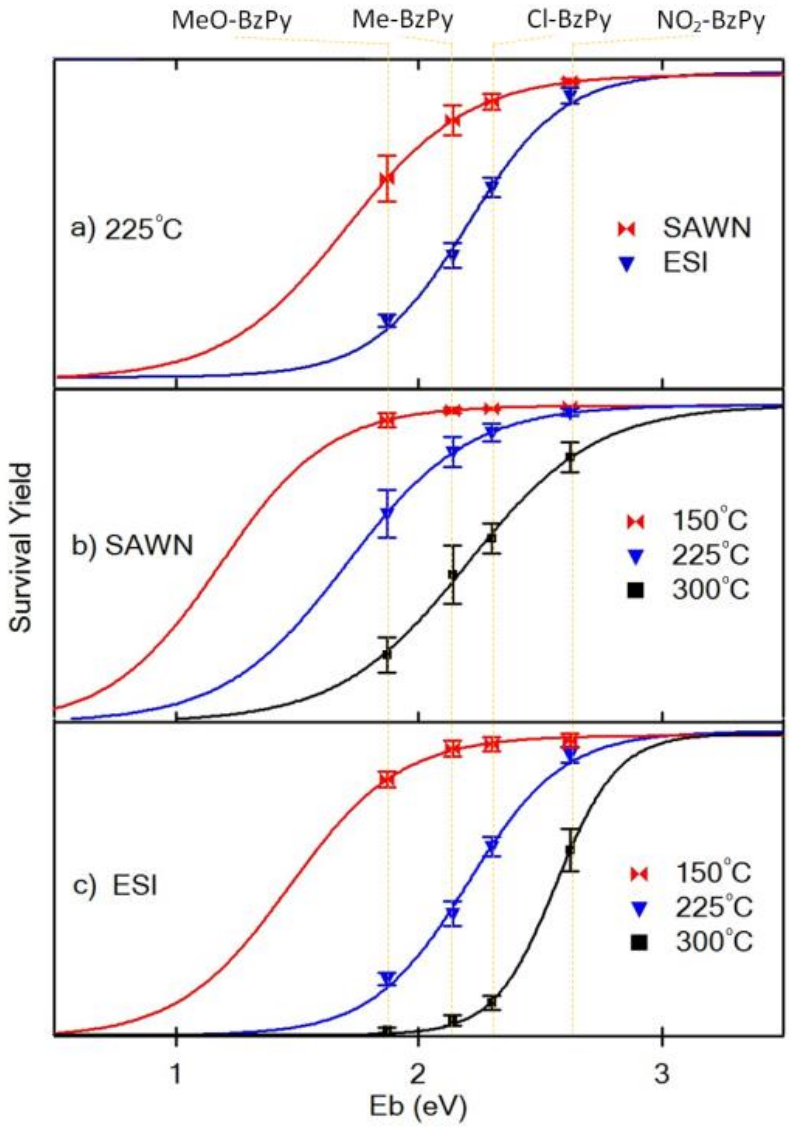

Figure 2.9 Comparison of SAWN and ESI internal energy distribution. a) Survival yield versus bond energy for four benzylpyridinium compounds obtained under identical atmospheric pressure ionization source conditions (i.e. inlet temperature 225 ℃). b) and c). Effect of increasing the atmospheric pressure ionization inlet capillary temperatures on survival yields of substituted BzPy ions for surface acoustic wave nebulization (SAWN; b) and electrospray ionization (ESI; c).

Two factors could be invoked to explain this difference. One explanation could be a difference in solvation between ions formed by both methods. Since the energy provided by the heated inlet capillary was the same for both ionization methods, more solvated ions would experience more evaporative cooling. Consequently, less energy would be transferred to the analyte, preserving more of the precursor ion. For ESI, previous studies had indicated the droplet size to be in the range of 1 to 20μm[91,92]. In support of this explanation, pilot experiments using the same solvent conditions and SAWN chips as used here (Langridge-Smith personal communication) have indicated that, depending on the SAWN experimental parameters (i.e. frequency, amplitude), aerosol droplets produced by SAWN range from 1-1000 μM with most being similar to ESI. However, there is also a substantial contribution from aerosol droplets that are 10-100 times larger than ESI produced aerosol droplets, which has been observed under different experimental conditions[56, 57]. A more detailed study about the distribution of aerosol droplet size will be discussed in chapter three.

Another reason for the lower internal energies of SAWN-produced ions may be related to the absence of high electric field in the SAWN process and the low charge density of the SAWN aerosols. Regarding the charge density, our preliminary measurements with model analytes indicated lower ion currents generated by SAWN than by electrospray. Combined with larger aerosol droplets, the lower total charge indicates that the SAWN-produced aerosol droplet have lower charge densities than those formed by electrospray. Thus, the SAWN aerosol droplets undergo more solvent evaporation before reaching the Rayleigh limit for fission and ion desorption on the gas phase, forming cooler ions. Additionally, in the high voltage gradient between the ESI tip and the inlet capillary, the ESI formed aerosol droplets experience

acceleration and many collisions with the ambient gas. In ESI the speed of the droplet would be a combination of the acceleration from the electric field and the thermal velocity. While the thermal velocity of a common ESI droplet[93], is relatively low (10 mm/s), the ESI electric field provides substantial acceleration. Comparison of the typical travel time of an ESI droplet (<1 ms)[94] with that of a SAWN droplet (50-100 ms) clearly indicates that the latter move more slowly and thus the kinetic energy of aerosol droplets entering the capillary inlet is likely to be lower from SAWN than ESI, which contributes to the observed ion internal energy effect. Therefore, it is likely that a combination of larger SAWN aerosol droplets, lower charge density, and less kinetic energy contributes to higher ion survival yields in SAWN compared to ESI. While the exact mechanism is still unclear, these results suggest that SAWN could be an attractive alternative to ESI for the analysis of thermally or chemically labile molecules.

2.3.3 Effect of inlet capillary temperature on survival yield

Temperature	E_{int} SAWN (eV)	E_{int} ESI (eV)
150 ℃	1.23 ±0.02	1.29 ±0.01
225 ℃	1.49 ±0.05	1.96 ±0.02
300 ℃	2.17 ±0.04	2.44 ±0.01

Table 2.2. Mean internal energy deposited during surface acoustic wave nebulization (SAWN) and electrospray ionization (ESI) at increasing capillary inlet temperatures.

When estimating bond dissociation energies from atmospheric pressure ionization (API) using an empirical method such as survival yield method, several API parameters have been shown to influence ion dissociation[73]. In the API configuration used here, aerosol droplets entered a heated

inlet capillary that assisted solvent vaporization and ion desolvation. The surviving, solvent-free ions were then detected by the mass analyzer. In the present study, to avoid introduction of artificial differences in measured ion survival yields between ESI and SAWN, all mass spectrometer parameters were nominally identical for both API methods. To further investigate the effect of desolvation on internal energies, three inlet capillary temperatures were examined. As shown in Figure 2.9 b, c and Table 2, the temperature of the inlet capillary of the mass spectrometer had a dramatic effect on the survival yield and the calculated mean ion internal energy from both SAWN and ESI. At the lowest temperature tested (150 ℃), the internal energy difference between SAWN and ESI was quite modest (0.06 eV). As the temperature increased, the difference in deposited energy between ESI and SAWN became much more significant. Overall, SAWN displayed higher survival yields than ESI over the whole range of temperatures tested, and the greatest difference (0.47 eV) was observed at 225 ℃.

The internal energy the ions receive depends on the heat input from the hot desolvation gas and the heat loss by solvent evaporation from the droplet and ion desolvation after droplet fission. Therefore, presuming that the last stages of ion desolvation are similar for ESI and SAWN-produced aerosol droplets, one would expect that ions originating from larger aerosol droplets would receive less energy during the API process than ions originating from smaller aerosol droplets. Our experimental results are therefore consistent with the hypothesis that SAWN produced aerosol droplets are larger than those produced by ESI and thus produce ions of a relatively lower internal energy.

2.3.4 Effect of Flow Rate on Survival Yield

In the same way as direct infusion by ESI, SAWN experiments were conducted using a continuous deposition of liquid on the chip. This allowed the relationship between internal energy distribution and flow rate to be studied under varying inlet capillary temperatures. Results from a series of such measurements are summarized in Table 2.2. We observed an increase in the survival yield for all four BzPy ions when increasing the flow rate from 3 μL/min to 8 μL/min, the highest flow rate that could be used while still maintaining the nebulization process. However, this effect was less pronounced than the temperature effect, or the difference between SAWN and ESI. Overall, under all tested temperatures, less fragmentation occurred during the ionization process when the sample flow rate was set at 8 μL/min. This could be explained by the fact that the larger quantity of liquid brought onto the surface of the chip per unit time influenced the size distribution of the nebulized aerosol droplets or possibly increased the number of aerosol droplets formed in a certain period of time. Regardless, this increase in flow rate resulted in a requirement of more energy to evaporate the solvent and generate ions, which in turn led to higher survival yield. Thus, the increase in precursor ion survival yield for all four BzPy ions resulted in an even lower internal energy distribution at the higher flow rate. Again, these results are consistent with the hypothesis that larger aerosol droplet (or more droplet) affect the energy distribution of SAWN.

Temperature	E_{int} (eV) 3 μL/min	E_{int} (eV) 8 μL/min
150 ℃	1.23±0.01	1.18±0.02
225 ℃	1.49±0.05	1.32±0.06
300 ℃	2.17±0.04	2.06±0.03

Table 2.3. Calculated internal energies (E_{int}) for surface acoustic wave nebulization at different flow rates and temperatures

2.3.5 Effect of Concentration on Survival Yield

In order to prove the assumption that solvent evaporation is important in the internal energy distribution of the ionization method, another experiment is performed with different instrument settings and a series of different concentration BzPy ions. The concentration of BzPy ions used in this experiment is 0.01 μg/mL, 0.1 μg/mL, 1 μg/mL and 10 μg/mL. Instrument conditions are kept the same during the experiment, with 3 μL/min sample injection rate and 300 ℃ inlet capillary temperature. The survival yield of same substrate was observed to be increasing as the concentration decreased. For example, MeO-BzPy had a survival yield of 20% at 1 μg/mL, compared to 50% at 0.01 μg/mL. The mean internal energy distribution for these four concentrations is 1.90, 2.07, 2.17 and 2.16 eV from lowest to highest concentration respectively, as shown in table 2.3. This supported the assumption of solvent evaporation been an important factor during fragmentation.

Concentration	0.01 μg/mL	0.1 μg/mL	1 μg/mL	10 μg/mL
E_{int} (eV)	1.90	2.07	2.17	2.16

Table 2.4. Calculated internal energies (E_{int}) for surface acoustic wave nebulization at different sample concentration.

2.4 Conclusions

We have investigated the energetics of SAWN generated precursor ions and compared these results to ESI under identical API source conditions using a common ion survival yield method with a series of four substituted BzPy ions. The results clearly showed that the survival yield of SAWN generated ions was indeed higher than those of ESI, suggesting SAWN is a "softer" ionization process. In fact, under all conditions tested, SAWN generated ions had a higher survival yield than those formed by ESI. We also noted that the difference between SAWN and ESI was more pronounced at higher inlet capillary temperature. This suggests that either the SAWN generated aerosol droplet required more energy for desolvation or that the ESI generated droplet experienced a higher rate of desolvation due to the additional voltage differential they experience from the voltage applied for ESI. Another parameter that could contribute to the difference is droplet size because it is likely that the SAWN generated aerosol droplets presented a larger average diameter compared to ESI generated droplets. The internal energy distribution of BzPy ions was also affected by sample flow rate, but to a lesser extent. This could be explained by the difference in the amount of droplet entering the inlet capillary or by an increase in droplet size resulting from the use of higher flow rates. Finally, and interestingly for those studying ions susceptible to fragmentation by currently available methods, we can estimate that SAWN may

impart the least energy of all commercially available API methods. For example, while a direct comparison of internal energy distribution of SAWN with other ambient ionization source has not been conducted here, previous results have been reported for DART and DESI using the same BzPy ions series. From these studies it was shown that DESI produced similar ion internal energy distributions to ESI and the mean internal energy of DESI was 10% higher than ESI[77]. Additionally, DART[80] was compared to ESI and shown to produce slightly lower ion survival yields (between 25 % to 36 % depending on conditions). Given our results showing that SAWN, depending on the conditions used, deposits around 4 % to 23 % less internal energy than ESI, we can conservatively estimate that SAWN is "softer" than both DESI and DART. Due to the many operational parameters of SAWN that are just beginning to be understood, such as sample flow rate, amplitude and frequency of the acoustic wave, these encouraging results require further investigation.

Chapter 3 Improving the Performance of SAWN

3.1 Introduction

In the previous chapter，the internal energy distribution of SAWN was discussed and compared with ESI. The SAWN chip described there contained a single interdigitated transducer (IDT) electrode design that is referred to as a progressive wave (PW) design. In this setup, SAWN was placed in front of the open inlet of a mass spectrometer with continuous flow or discrete liquid drops placed on the surface. Activation of a SAW resulted in nebulization of the liquid on chip and subsequent transfer to the heated capillary of the atmospheric pressure inlet (API) by the pressure difference between atmosphere and the API. This PW SAWN design, while simple, lacked the sensitivity required to make SAWN a routinely useful device for transferring compounds to a mass spectrometer. In this chapter, experiments are described that resulted in performance improvements to that original PW SAWN device. Performance of PW SAWN was studied using polar and nonpolar compounds with different molecular weights in commonly used liquid solvents. Several parameters were selected and modifications were made to the original SAWN design with an aim toward providing higher sensitivity while maintaining the low internal energy distribution. Several methods, including applying DC voltage, raising capillary temperature and modifying SAWN chip design were evaluated to increase SAWN signal intensity. These optimization experiments resulted in development of a standing wave (SW) SAWN design.

3.2 The Performance of PW SAWN

3.2.1 Peptide and Protein

The first PW SAWN report contained a mass spectral characterization of Angiotensin I[48]. The resulting mass spectra were compared to Angiotensin I produced by ESI revealing a striking difference in charge state distribution. It was noted that PW SAWN produced mass spectra where the $[M + H]^+$ ion was around 90% of the base peak whereas they were only about 10% when produced by ESI. This difference was explained based on the lack of DC voltage. To verify that such a shift of charge state distribution centered at lower m/z is a common feature among mass spectra produced by SAWN, additional peptide and protein mass spectra were acquired. The selected spectra are shown in Figure 3.1 (peptide), 3.2 (protein) and 3.3 (comparison with ESI).

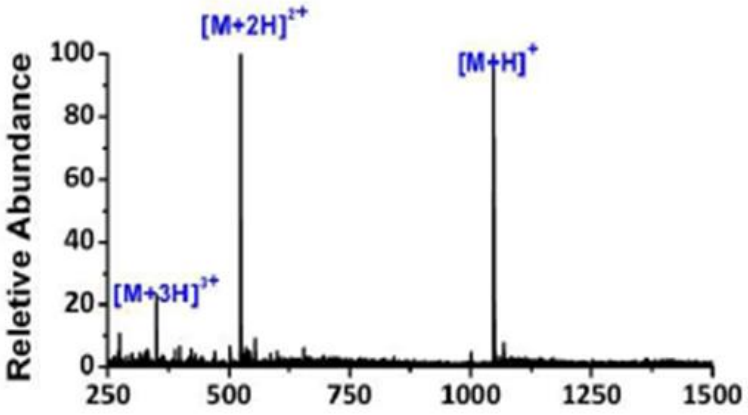

Figure 3.1 PW SAWN spectrum of Angiotensin II. m/z=1046. $[M+H]^+$ peak is of a larger portion compared to ESI spectrum of the same mass spectrometer configuration.

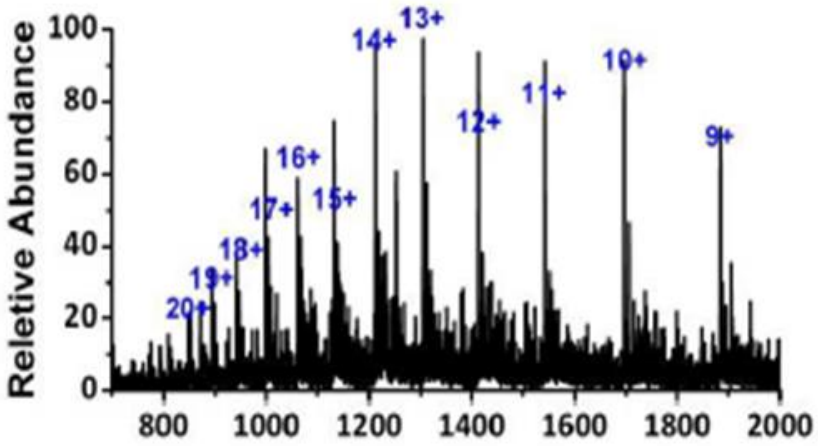

Figure 3.2 PW SAWN spectrum of beta casein.

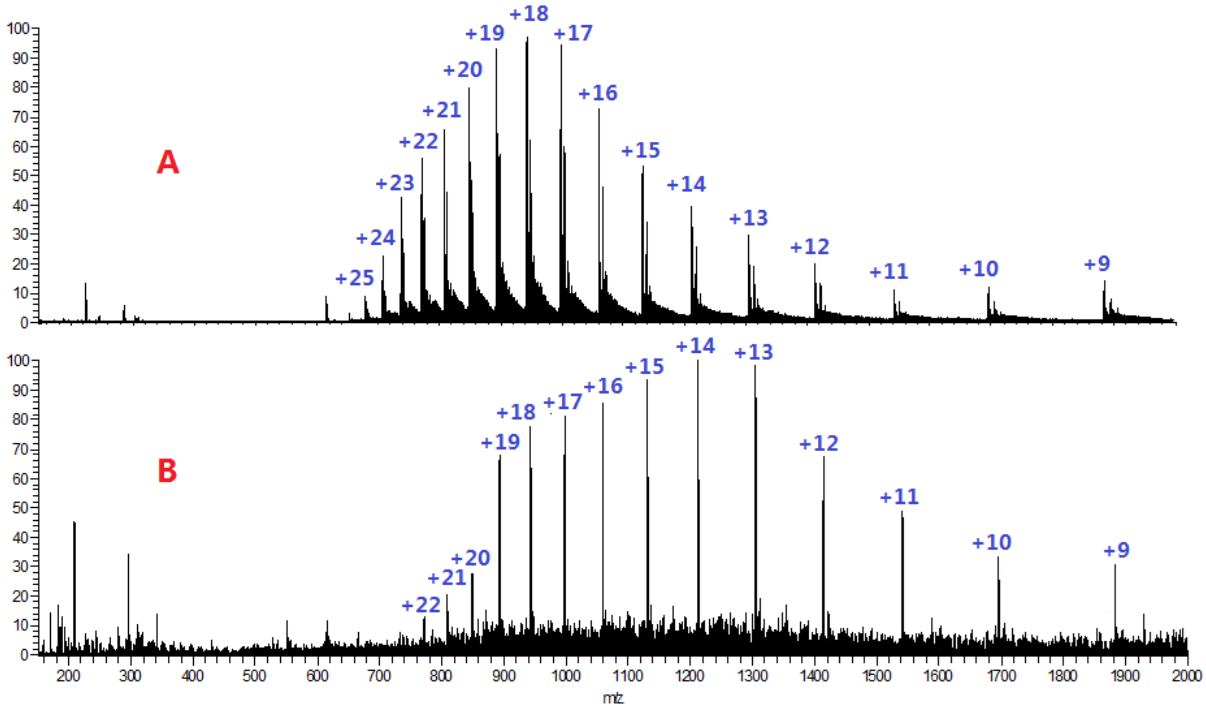

Figure 3.3 Comparison of ESI (A) and PW SAWN (B) spectra of Myoglobin (horse heart) . ESI (1.5 kV) produced ions with more charges then PW SAWN (0 kV).

In the above spectra, PW SAWN demonstrated the ability to ionize molecules with a molecular weight above 20kD such as beta casein (Figure 3.2, MW=25kD). As observed in the PW SAWN mass spectra of Angiotensin II, beta casein mass spectra produced by PW SAWN also showed a shift in the charge state distribution to ions of lower charge states relative to the same by ESI. Specifically, in the Angiotensin II mass spectrum (Figure 3.1) the dominant ion produced by ESI (not provided here) is usually the triply charged molecular ion, but in PW SAWN mass spectrum the $[M+3H]^{3+}$ ion is only 20% of the $[M+2H]^{2+}$ base peak with the $[M+H]^{+}$ ion being ~ 98% of the base peak. Figure 3.3 shows Myoglobin (Sigma Aldrich, horse heart, MW=17kD) mass spectra produced by ESI and PW SAWN under identical mass spectrometer configurations. As seen by ESI, the highest charge state in the spectrum is +25 with the +18 ion being the base peak, while by PW SAWN the highest charge state is the +22 ion and the +14 ion is the base peak. Finally, we note that heme – protein adduct is not observed by either method.

Angiotensin II prepared in an aqueous 0.1% formic acid solution was also used to test the linear dynamic range of PW SAWN by dispensing discrete 5 μL droplets on chip. The data were collected on a Thermo LTQ instrument with an ion funnel with a transfer capillary temperature of 300 ℃ and a SAW amplitude of –8 dBm. The total peak areas of $[M+H]^{+}$ (1046) and $[M+2H]^{2+}$ (523) are plotted for different concentration samples. As shown in Figure 3.4, PW SAWN presents an approximately linear log-log response from 10 nmol/mL to 10 μmol/mL.

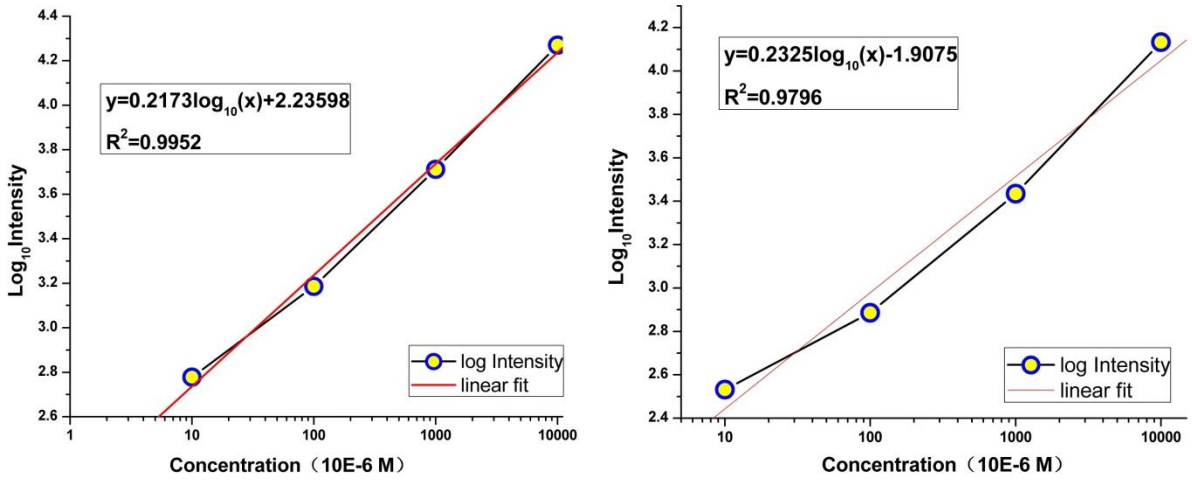

Figure 3.4 Dynamic range of SAWN with Angiotensin II (MW=1046) from 10 nmol/mL to 10 μmol/mL.

3.2.2 Small Molecules and Lipids

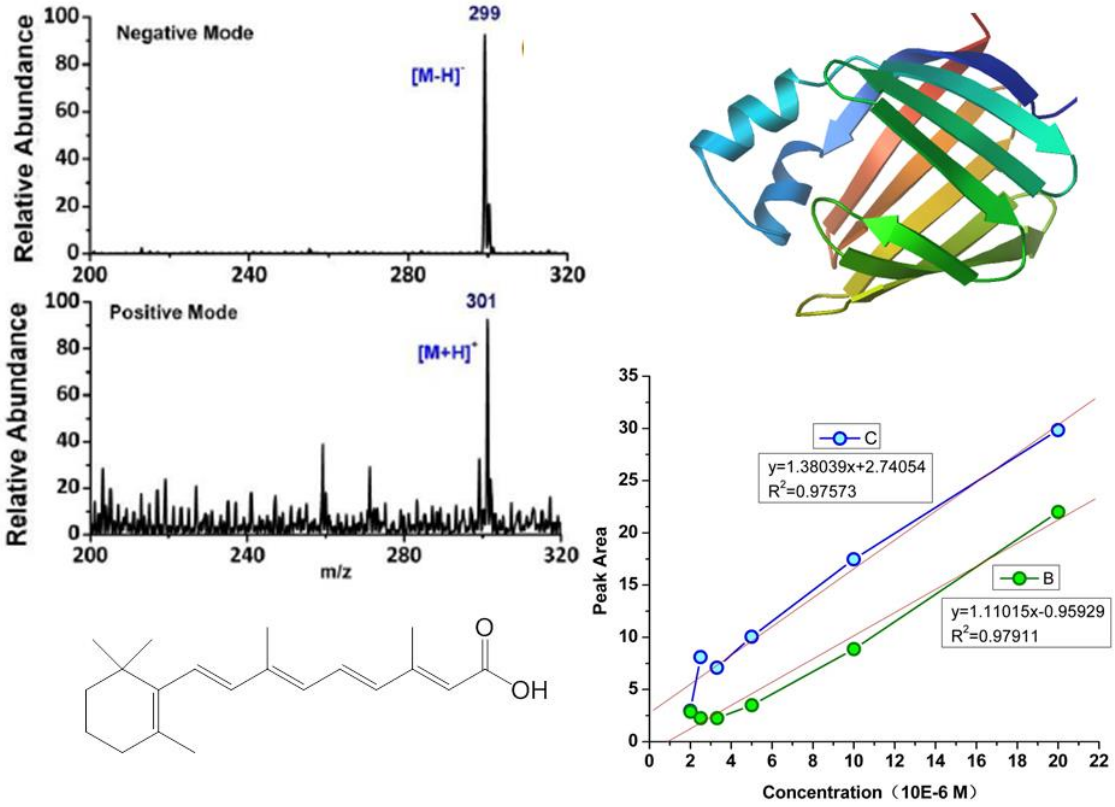

Figure 3.5 PW SAWN mass spectra of all-trans retinoic acid (at-RA, M=300 D) in both positive and negative ion mode. The protein CRABP II (top right) binds all-trans retinoic acid as observed by addition of increasing amounts of at-RA to a static amount of CRABP II.

PW SAWN was also applied to the studies of small molecules and lipids. *all-trans* Retinoic acid (MW=300, provided by our collaborator Prof. Isoherranen of the University of Washington, Seattle, WA) is a metabolite related to vitamin A metabolism. It mediates the functions of vitamin A required for growth and development[9, 95]. Retinoic acid is highly reactive with UV light and easily oxidized when exposed to atmospheric concentrations of oxygen. Under native PW SAWN, both positive and negative ions were generated and detected by mass spectrometry without excess fragmentation and no detectable oxidation (Figure 3.5). Retinoic acid occurs in

both *cis* and *trans* isomers that are difficult to separate chromatographically. However, the protein CRABP II, is known to bind only the *trans* isomeric form and thus was used to conduct a drug depletion assay[96]. The base peak of *all-trans* retinoic acid was the $[M–H]^-$ ion at 300 m/z, which showed a linear dynamic range of detection from 1 to 22 μM in negative ion mode.

Traditional study of lipid A by mass spectrometry uses either matrix assisted laser desorption ionization (MALDI) or electrospray ionization (ESI)[14,97]. While both produce useful mass spectra, each presents challenges for analysis of small molecules. For example, with MALDI it is challenging to generate a mass spectrum under 700 Da that does contain excess ions produced by the matrix and with ESI precipitation of lipids often clogs the narrow capillaries used. For these reasons we investigated use of PW SAWN to ionize lipids. Additionally, we investigated the degree to which the negative lipid ions generated by PW SAWN could be used for tandem mass spectral structure characterization[98].

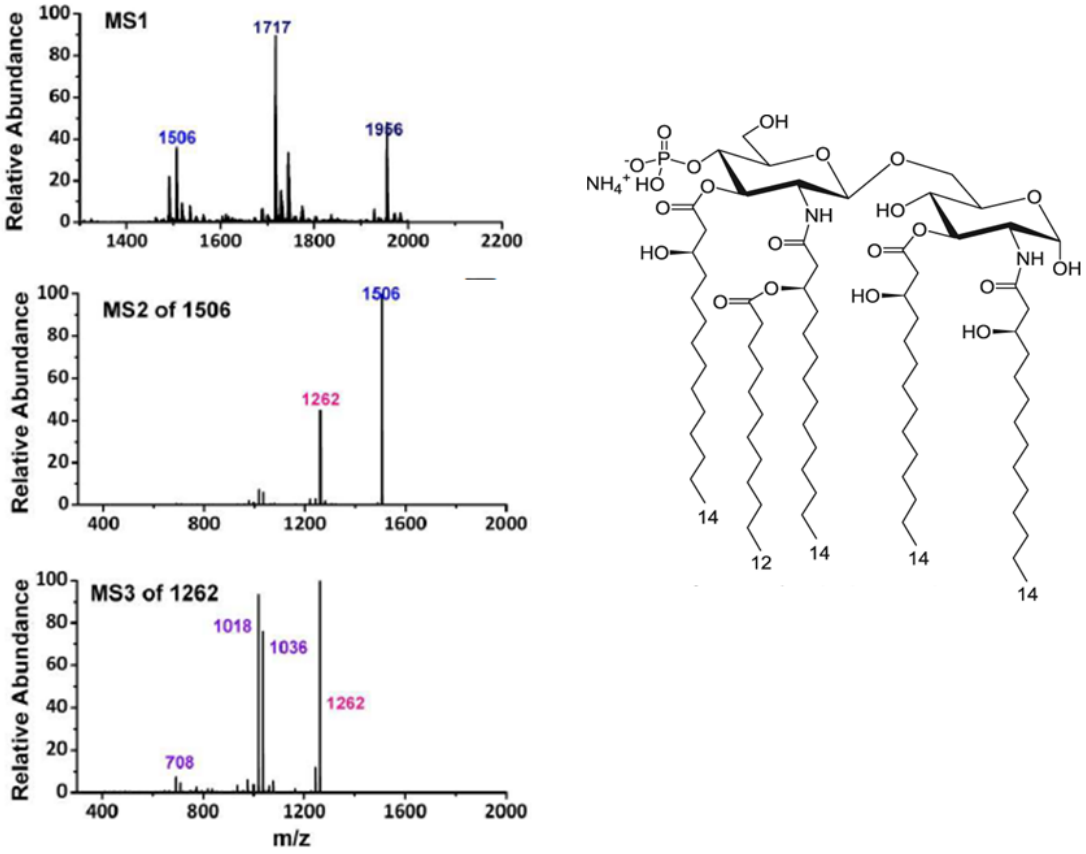

Figure 3.6 PW SAWN mass spectral charactrization of lipid A. The commercially available lipid A (Avanti Polar Lipids, Alabaster, Alabama) is a mixture of different lipid A molecules. The majority of which is represented by the structure shown to the right. The tandem mass spectrum (MS2 of 1506) contains a primary fragment peak at 1262 m/z from the loss of side chain fatty acids, while the tandem mass spectrum of 1262 (MS3 of 1262) produces additional fragment ions at 708, 1018 and 1036.

Phosphorylated lipids[99,100,101] are a category of often studied small molecules with importance in all organisms that are especially difficult to study by ESI because they are labile. In addition to ease of use, PW SAWN was shown to impart less energy during nebulization than ESI, and therefore to produce less fragmentation than ESI. This fact is an important consideration when analyzing chemical compounds of an unknown composition because more of the precursor ions

are likely to survive during the transition from the ionization source to the mass analyzer. Here we analyzed a mixture of phosphatidylglycerol (PG (16:0/18:1)) and phosphorylated ethanolamine (PE (16:0/18:1) by SAWN. Tandem MS of the following free fatty acids ((16:0), *m/z* 255 and (18:1), *m/z* 281) were observed and also for the fatty acid losses (*m/z* 483, 465, 478, and 452). The characteristic peak of PG (*m/z* 391), generated by loss of the glycerol, was easily observed.

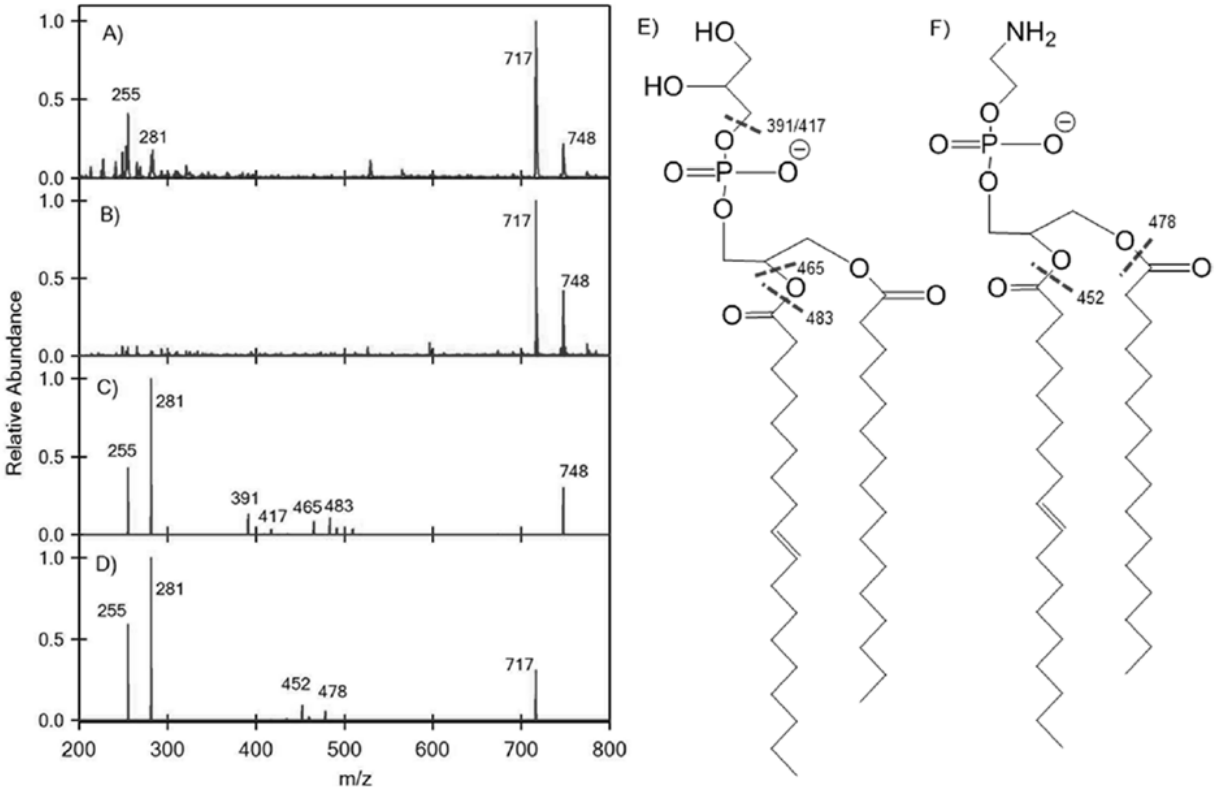

Figure 3.7 PW SAWN MS spectra of two different phosphorylated lipids. A) SAWN mass spectrum for stucture in E). B) SAWN mass spectrum for structure in F). The tamdem mass spectra for E) and F) are shown in C) and D).

PW SAWN was also applied to the analysis of natural plant oil[102], a triglyceride mixture. In these experiments the PW SAWN chip was diced into small pieces (1 cm x 3 cm). The chip was dipped into the oil to be analyzed and nebulized directly with a solvent line supplying methanol

to help nebulization. In Figure 3.8 shows the PW SAWN spectra of three kinds of different kinds of plant oil mixtures in positive ion mode.

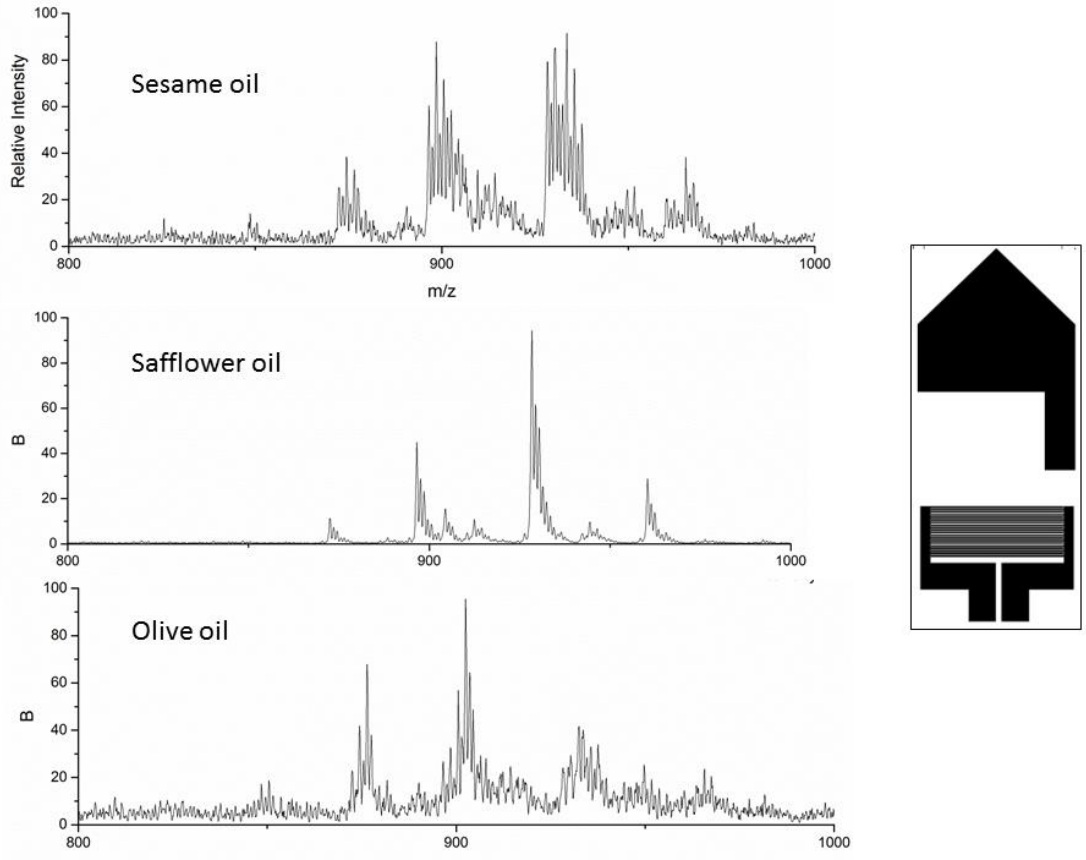

Figure 3.8. SAWN-MS spectra of three plant oil samples. Mixtures of different triglycerides are shown in each mass spectrum. From top to bottom the oils investiagetd were from the following plant materials: seasame, safflower, and oilve.

3.3. Improving the Ionization Efficiency of PW SAWN

While PW SAWN produces ions of lower energy than ESI (i.e. provides softer ionization), which can preserve the original state of ions, it suffers from lower relative signal intensity. A number of modifications have been made to the PW SAWN ionization source to enhance the performance, such as adding a voltage through a gold electrode on the chip, or adding a

hydrophobic coating to increase the contact angle of the liquid thus limiting the movement of the droplet on the surface. Despite these improvements, an ESI produced mass spectrum of angiotensin II usually has 10^2-10^3 higher relative signal intensity than the same produced by PW SAWN. From previous research, sample loss was observed during the PW SAWN process most often due to aerosol droplets that fail to enter the mass spectrometer API inlet. Some large aerosol droplets are too heavy to enter the mass spectrometer. These droplets either fall back onto the chip or stick to the ion transfer capillary, causing sample loss. Secondly, while using an ion funnel we observed that the jet disrupter used to capture neutrals was more thoroughly covered during the SAWN experiments, which indicates that although the droplets have passed through the heated inlet capillary, there was still quite a lot of neutral droplets persisting.

3.3.1 Effect of Transfer Capillary Temperature on Signal Intensity for PW SAWN

It has been observed that under the same operational conditions signal intensity of SAWN increases with a higher transfer capillary temperature. This was not observed in either ESI or NSI. A possible explanation is that the large size of SAWN generated aerosol droplets evaporate more efficiently when transfer capillary temperature is raised.

3.3.2 Adjusting the Amplitude

The SAW amplitude determines the energy transferred to the liquid droplet. Since changing the operation frequency requires a new chip design, changing the amplitude is the most straight forward way to adjust the SAW produced on the lithium niobate surface. From SAW theory it is known that a higher amplitude will cause a larger shape change on the surface and take a longer

distance to decay. Adjusting the amplitude within the proper range has multiple effects on the nebulization process. At the lower limit is the threshold to nebulization of the droplet, whereas at the upper limit damage occurs to the chip in the form of cracking. Additionally the amplitude necessary to achieve the highest signal intensity during nebulization is dependent on the kind of liquid present.

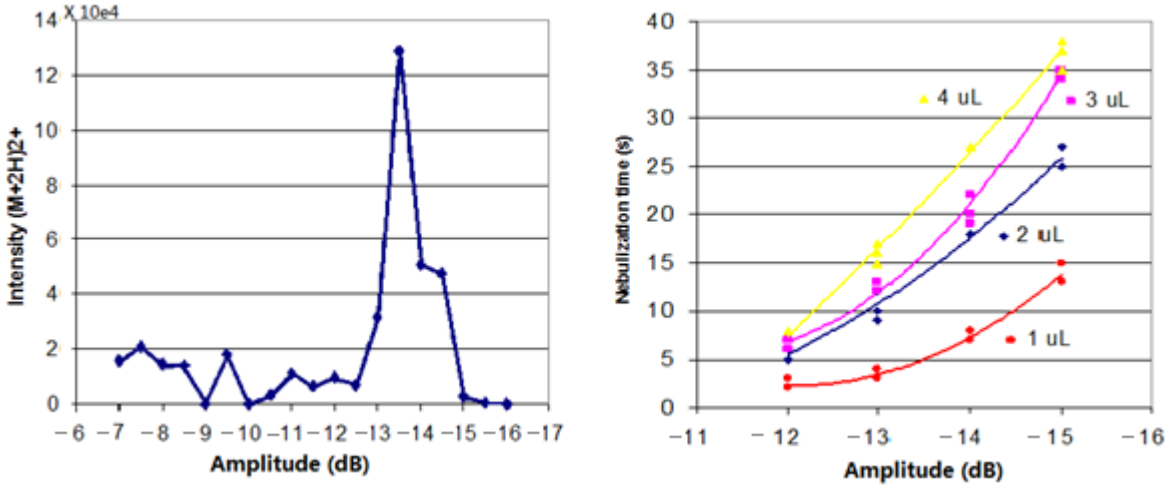

Figure 3.9 Effect of amplitude on signal intensity and nebulization time for SAWN-MS. Left: the amplitude from the signal generator has an optimal point for nebulizaiton of a certain liquid (in spectrum methanol:water 50:50 mix). Right, the higher the amplitude (lower dBm) the smaller the nebulization time will be.

1) Nebulization time. Under normal nebulization settings, the nebulization time of the liquid droplet placed on chip will be longer if the amplitude is lower. Figure 3.8B shows the relationship between nebulization time and amplitude. From these data it is clear that the nebulization time is related more to the amplitude than the amount of liquid placed on chip. As seen in the same figure, nebulization time is not linearly related to the amount of liquid on chip.

2) Plume shape. Under the condition where no droplet is moving and is present at a certain distance from mass spectrometer inlet, a higher amplitude will provide more energy and raise the plume higher from the chip surface. Thus, amplitude must be empirically adjusted according to the distance from the API inlet because if the plume is too high, then it will pass the mass spectrometer inlet capillary and detection will not occur.

3) Aerosol size distribution. Research from the Yeo group shows that the average aerosol droplet size does not have a linear relationship with the amplitude[56]. At higher amplitudes, it is more likely to generate aerosol droplets with greater diameter. This phenomenon might be explained by a higher amplitude providing more energy, making it possible to elevate more mass off the chip surface. In PW SAWN MS, these large aerosol droplets were not efficiently desolvated by the heat from transfer capillary, therefore the signal intensity is decreased.

3.3.3 Applying DC Voltage on Chip Surface

One possible explanation for the lower signal intensity of PW SAWN relative to ESI might be from the lack of DC voltage. The fact that both positive and negative ions are generated at the same time indicates the charges are generated from the high frequency mechanical wave breaking the liquid apart into positively and negatively charged aerosol droplets. The ion current from PW SAWN spray was measured to test this assumption. A vacuum chamber with a metal transfer capillary was built to simulate the environment of the mass spectrometer. To effectively collect ions, a copper plate was placed after the heated transfer capillary with a 2 mm distance. The SAWN device was placed in front of the transfer capillary. The SAWN nebulized plume was guided into the vacuum chamber through a pressure gradient, as shown in Figures 3.9 A, B,

C and D. A typical measurement result for a single liquid droplet nebulization is shown in Figure 3.9 E.

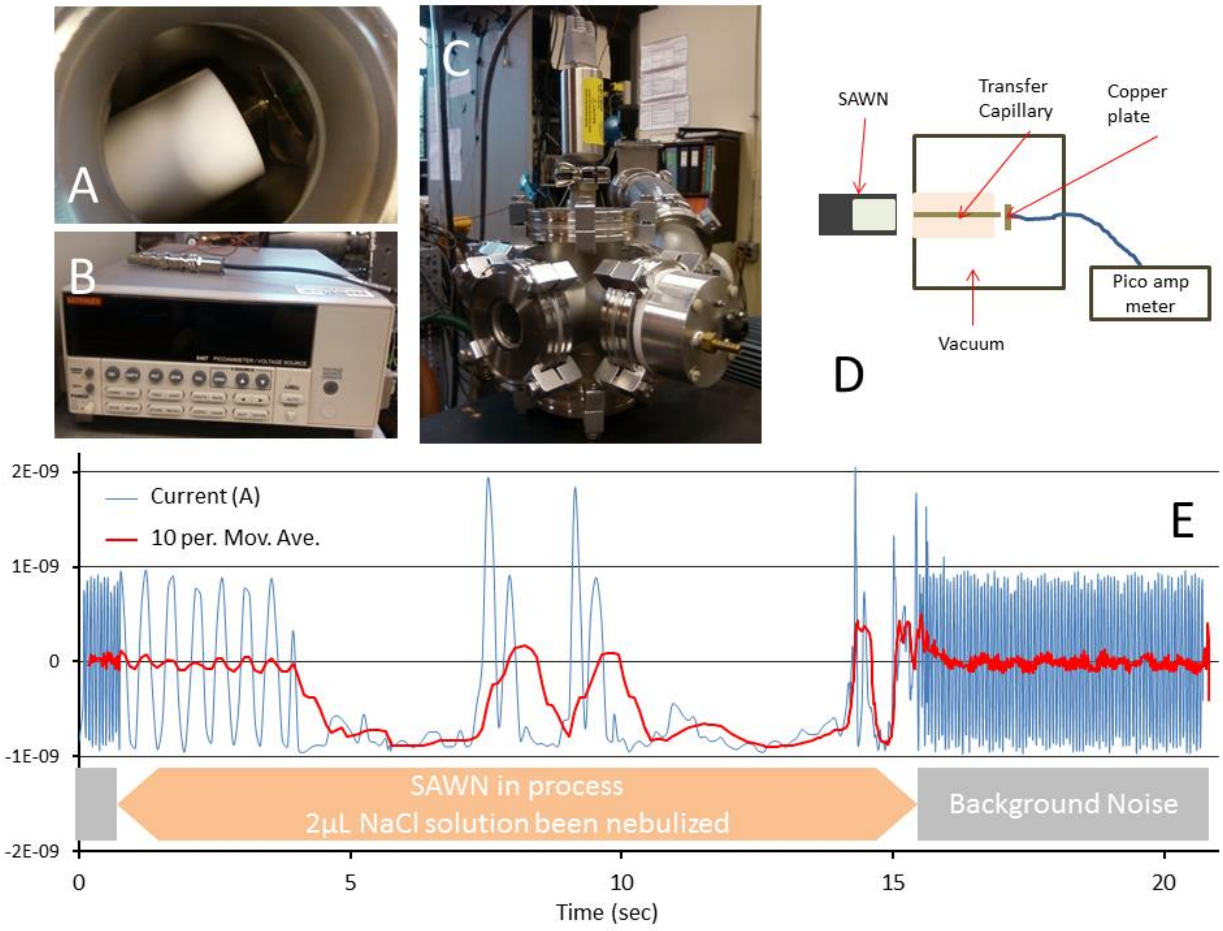

Figure 3.10 Pico ammeter measurement experiment of PW SAWN. A) a copper collector is placed close to the end of the transfer capillary. B) frontview of the pico ammeter. C) sideview of the entire set up. D) the filament is settled in a vacumm system with transfer capillary in front to bring in ions and is connected to the pico ammeter through the back end of the vacumm chamber. E) measured result for PW SAWN nebulization of one aqueous NaCl droplet.

It has been observed from the al-trans-retinoic acid spectra that PW SAWN under native conditions generates both positive and negative ions. From the pico ammeter measurement, the PW SAWN generates both positive and negative ions with relatively equal amounts. The total

current fluctuates around zero. Figure 3.10 shows the effect of applying a DC voltage to the chip through the DC electrode, where the liquid droplet is placed. The calculated peak area shows that the applied DC voltage will increase the signal intensity. This phenomenon can be explained by: 1) liquid on the surface being affected by the biased surface charges, which generates more positive aerosol droplets; and 2) an electric field is formed in between the chip surface and the inlet capillary, providing guidance to the aerosol droplets and increasing the droplet's momentum. In this instance, the friction between the liquid droplets and the surrounding gas molecule enhances the desolvation process.

Applying DC voltage on PW SAWN is referred to as electro SAWN. It is especially useful when ionizing large molecules. Figure 3.11 shows a comparison between a native PW SAWN and an electro PW SAWN spectrum of myoglobin. The electro PW SAWN produces more high-charge state ions than what is created in native PW SAWN, which behaves similar to ESI. However, the electro PW SAWN setup is not a particularly stable system which further exacerbates the concern that it is not safe to apply high voltage to an open surface.

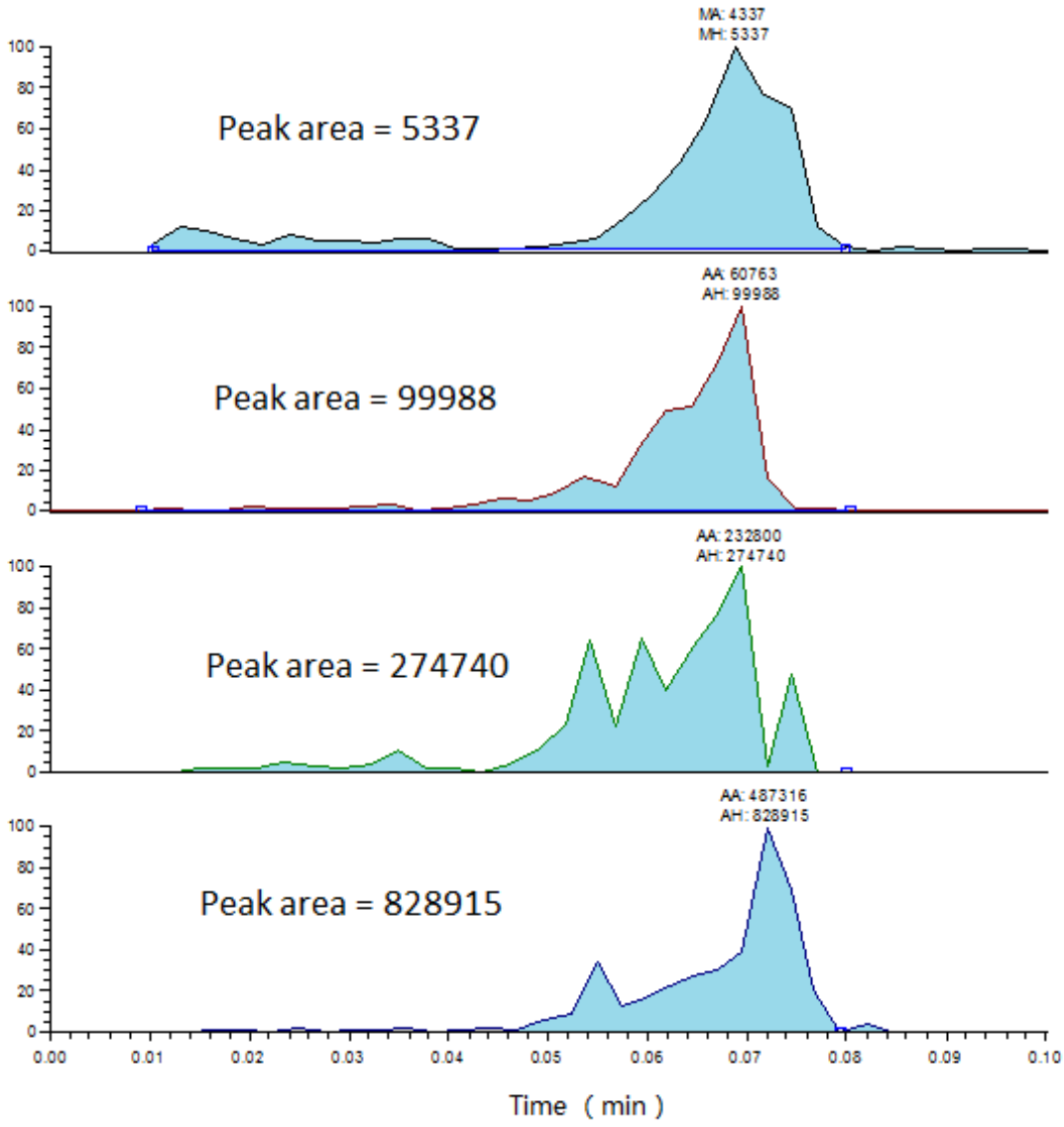

Figure 3.11 Signal intensity of SAWN-MS nebulizing a single droplet under different voltage. From top to bottom, SAWN with 0kV, 1kV, 2kV and 3kV. The signal intensity increased with higher applied voltage.

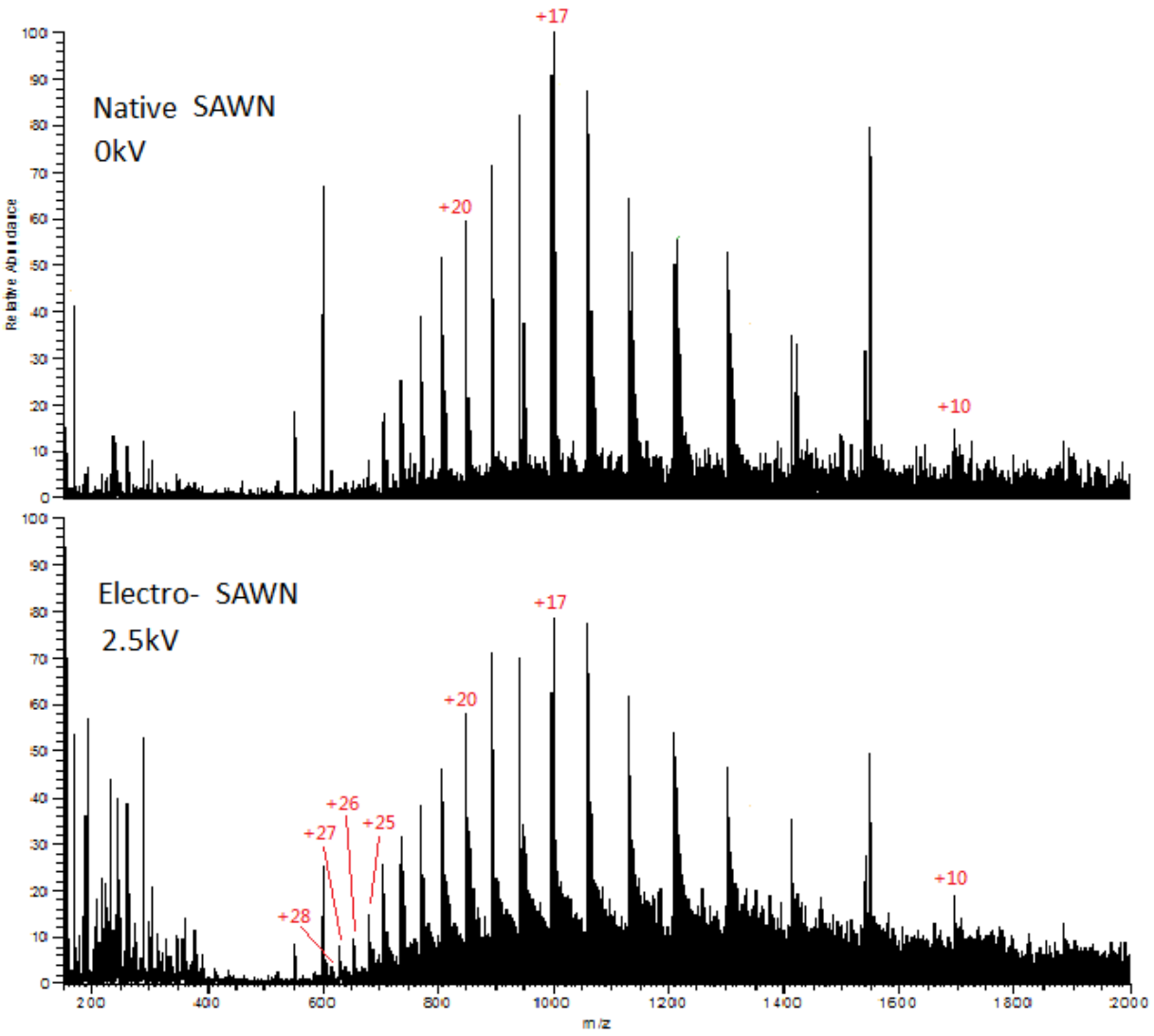

Figure 3.12 Comparison of native SAWN (0kV, above) and electro SAWN (2.5kV, below). With applied DC voltage the peaks in electro SAWN are boosted to a higher signal intensity. The charge state of electro SAWN also showed a difference compared to native SAWN, with more ions in the higher charge state appearing.

3.4. Standing Wave SAWN

Standing wave, also known as a stationary wave, is a wave that remains in a constant position[103]. Such a standing wave can be generated from SAW action by placing two interdigitated electrodes facing each other, with a set distance in between. The so-called standing wave (SW) SAWN chip is designed to have a specific distance between the IDTs to generate a standing wave while two identical waveforms are applied on the two end IDTs. In brief, the distance d between the two IDTs must be at $d = (n+0.5) \times\lambda$, where n is an integral and λ is the wavelength. In our design, λ is 414.4×10^{-6} m and n=15. The droplet is placed in the middle point of the chip, with the same distance to either side IDT.

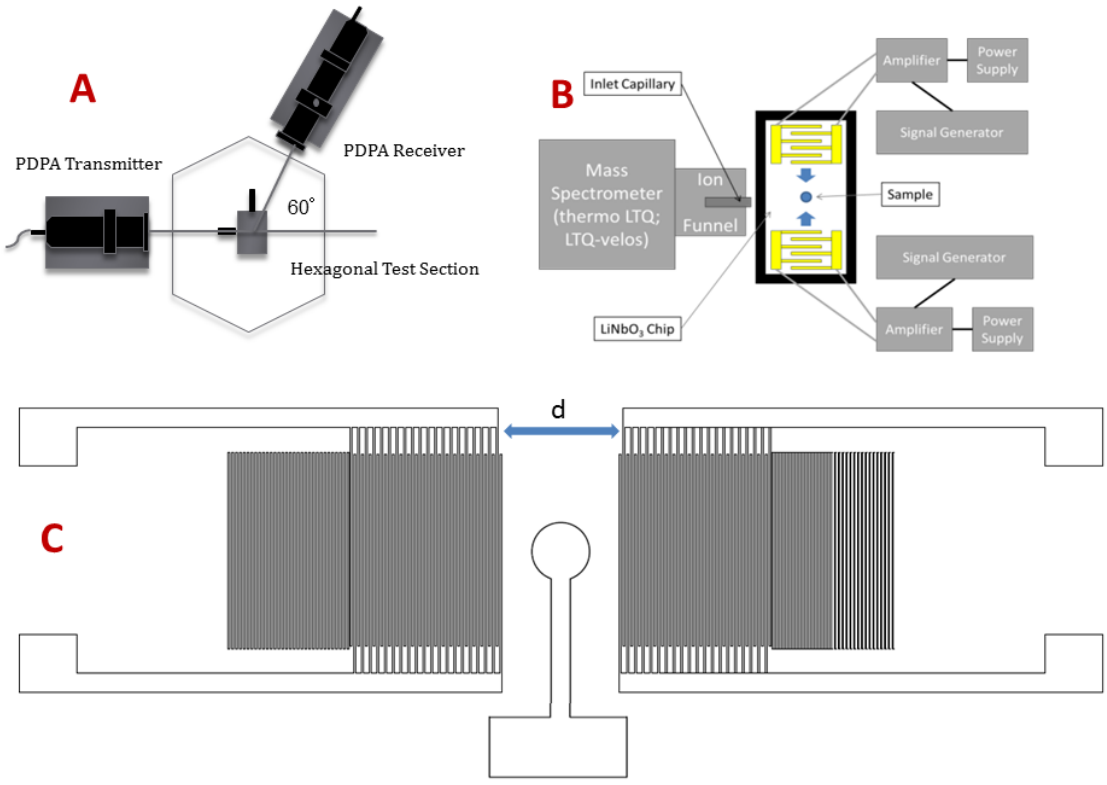

Figure 3.13 Standing wave SAWN. A) PDPA experimental setup. B) SW SAWN electronic control setup. C) SAWN chip design, with dual IDT, reflectors, and a DC electrode.

Based on SAW theory the SW SAWN chips were designed to make the generated aerosol droplets smaller, and thus eliminate or reduce the generation of larger aerosol droplets. As previously discussed, and based in part on our results from the temperature effect of PW SAWN, we believe that smaller aerosol droplets undergo more rapid evaporation and thus should produce a stronger relative signal intensity[61]. Other than the change in IDT design, the SW SAWN chip substrate and applied frequency were the same as for the PW SAWN chips.

3.4.1 Droplet Size Distribution Study of SW SAWN

We conducted high-speed imaging and Phase Doppler Particle Analyzer (PDPA) measurements of the droplet formation process, for both SW SAWN nebulization and PW SAWN nebulization. The results indicate that SW SAWN transferred energy more efficiently and generated smaller aerosol droplets for high and intermediate surface tension values (i.e. for water and 50-50 water-methanol mixtures). In general operation we noted a steadier nebulization process and a plume that rose perpendicular to the chip were created and observed when testing the SW SAWN.

A Phantom high-speed camera (Vision Research Inc., Wayne, NJ) was used to record images at 8000 frames per second during the nebulization process. From these images, it was possible to estimate the aerosol droplet size distribution present in the nebulized plume. The size distribution attained from these images was used to adjust the initial Phase Doppler Particle Analyzer (PDPA, TSI Inc., Shoreview, MN) settings. PDPA measurements of the diameter and velocity were then taken for both PW and SW SAWN devices at the specified operating conditions. The SAWN chips were mounted on a precision micrometer that could adjust the position of the chip in the x-y plane. The height of the chip was adjusted manually by using various sized TSLOTS (Futura

Industries, Clearfield, UT) aluminum base blocks. The x-y position and height of the chip were adjusted until the nebulized plume went through the center of the PDPA measurement volume (Figure 3.12, A). The intersection of two laser beams results in the formation of a fringe pattern. As the droplet moves through the measurement volume, it scatters light as it crosses each fringe. The frequency shift present in this light scattering is proportional to the particle velocity. The phase shift present in the light scattered by the droplet, as measured at three different photodetectors with measurable view angles of the probe volume, allows for a measurement of the droplet size with an assumed spherical shape using Mie scattering theory. The PDPA collects velocity and diameter measurements at a point in the flow (the probe measurement volume) over time. Given the limited duration of the nebulization process, a number of experimental runs were performed for each fluid and operating conditions in the parameter range studied. This was determined by the amount of data points (droplet measurements) collected in each run, and the need for large numbers to converge the statistics. An average of between 5 to 15 experiments was recorded to collectively accumulate 50000 data points. The data for each test condition was averaged to determine the mean diameter and velocity of the aerosol droplets produced. Measurements were exported to text files (FlowSizer, TSI Inc., Shoreview, MN) and later post-processed using MATLAB (MathWorks, Natick, MA).

To verify the assumption that the SW SAWN generates a larger amount of aerosols in a proper diameter range which are thus easier to desolvate for the purpose of generating MS detectable ions[91], SW and PW SAWN devices were tested with three solvent mixtures (DI water, a 50-50 water-methanol mixture, and pure methanol) at two power settings (6.00 and 7.50 W). The intention with testing these three different solvent conditions was to mimic several real world

sample conditions. To minimize any possible bias several liquid droplets were nebulized and recorded. The behavior of the liquid droplets under SW and PW SAWN were also recorded by the high speed camera. The droplet size distribution will be discussed from three aspects: the average diameter, the droplet size distribution and the absolute amount of droplets in a fixed time.

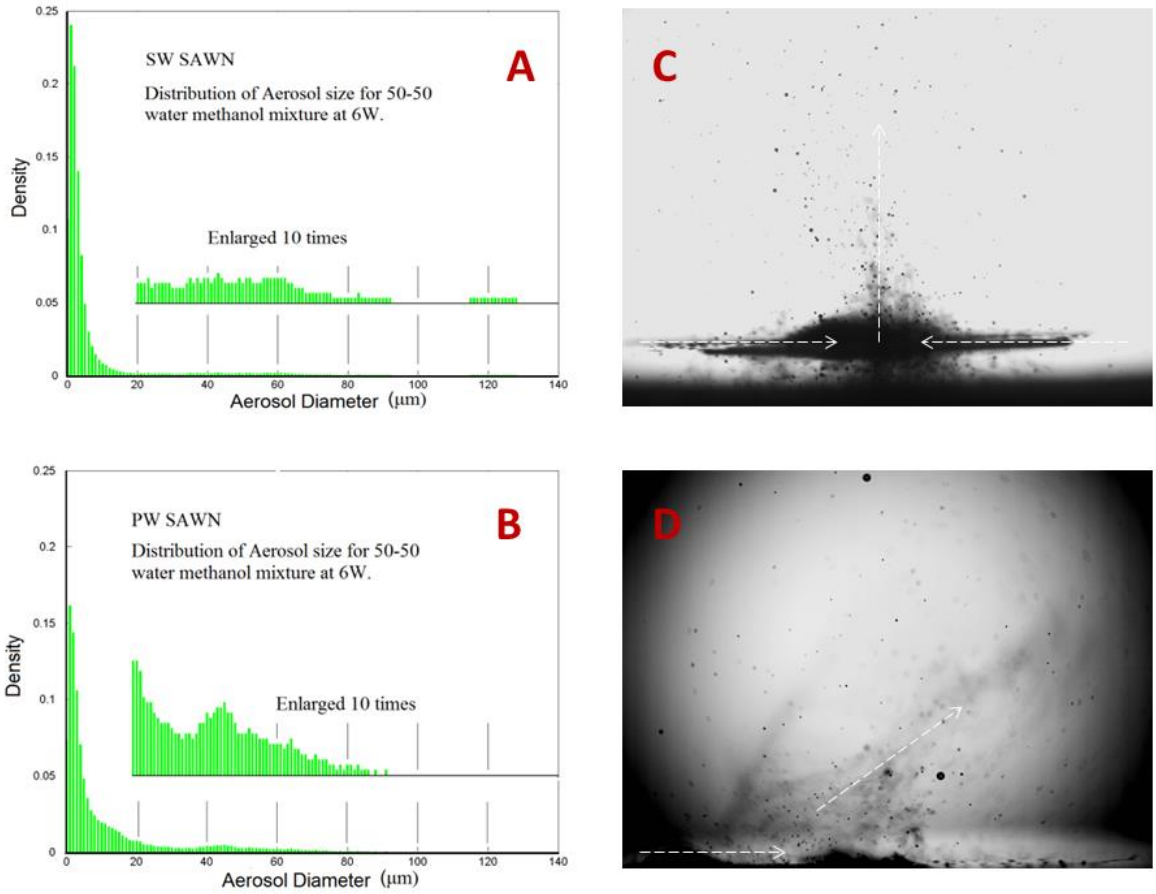

Figure 3.14 Droplet distribution comparison of SW SAWN and PW SAWN. A) Normalized aerosol droplet diameter distribution of SW SAWN. B) Normalized aerosol droplet diameter distribution of PW SAWN. More large aerosol droplets are present. C) High speed camera for SW SAWN (methanol), waves come from both sides and the droplet is forced upwards. D) High speed camera for PW SAWN (methanol) waves come from one side and the droplet nebulization is leaning towards the other side.

The distribution of droplet diameters can indicate the fraction of droplets that are too heavy to efficiently generate ions. As shown in Figure 3.13, the distribution of aerosol droplets can be roughly divided into two categories. Most droplets have a diameter smaller than 20μm, mainly below 10μm. Large aerosol droplets vary from 20-80μm in diameter. A peak is sometimes formed in the diameter range around 40-50μm. Compared to ESI generated droplets, which are usually around 1μm[94], SAWN generated droplets are larger in size and wider in distribution. As hypothesized above having a smaller diameter could help the aerosol droplets to desolvate more efficiently, thus increasing the possibility of ions been detected by MS. Figure 3.13 shows the 50-50 water-methanol mixture under 6.00 W. The PW SAWN generated a greater number of aerosol droplets above the 20μm diameter range than did SW SAWN. For all power settings in SW SAWN, water and water-methanol mixture always showed more droplets below 20μm， but interestingly, methanol showed more droplets above 20μm for SW SAWN than PW SAWN.

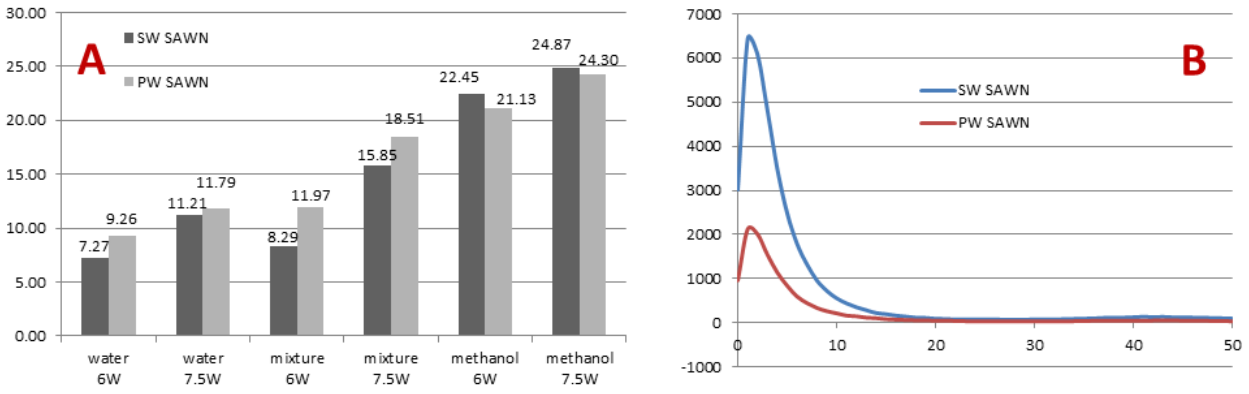

Figure 3.15 Comparison of SW SAWN and PW SAWN. (A) Average diameter of SW SAWN aerosol droplets and PW SAWN aerosol droplets. (B) Absolute amount of aerosol droplets for SW SAWN and PW SAWN.

From the weighted average diameter distribution shown in Figure 3.14, the SW SAWN device produced about the same size or smaller aerosol droplets compared to the PW SAWN device for water and the 50-50 water-methanol mixture at both power settings. However, the PW device produced similar or smaller droplet sizes than the SW device for methanol. This also matches up with the analysis of the droplet size distribution. From the behavior of the different solvent mixtures, we see that SW SAWN generated smaller droplets than PW SAWN for liquids that have a relatively greater surface tension, such as water. From the theory of surface acoustic waves we know that surface tension is one of the most important factors affecting the behavior pattern of the liquid such that liquids with low surface tension (such as methanol) tend to form a flat parent droplet on the chip with a low height/diameter (H/L) value. This structure makes the liquid accept the surface transferred mechanical energy more effectively, therefore making it easier to nebulize, even with a lower amplitude in the surface acoustic wave. In SW SAWN, the energy was above the proper energy to nebulize the droplet therefore generating larger droplets. Interestingly, although the droplet size study showed that all methanol aerosol droplets have a larger diameter than the water aerosol droplets, we did not observe a lower signal intensity in the MS spectra. Considering the low boiling point and low vapor pressure of the liquid, the methanol aerosol droplets still desolvate efficiently although with larger diameter[63].

The signal intensity is not only related to the distribution of the droplet collected over time, it is also related with the absolute number of droplets generated in a fixed time period. During the nebulization process, it was often observed that PW SAWN took a longer time to nebulize the same amount of liquid than SW SAWN. Ten trials of PW SAWN and SW SAWN with water droplets were recorded and the absolute results were averaged (Figure 3.14B). Comparing these

averaged results we see that SW SAWN generated about 2x more total aerosol droplets than PW SAWN from nebulization of one droplet on chip. This might be a result of the: 1) SW SAWN focusing SAW such that the liquid droplet on chip moves less prior to nebulization thus absorbing the SAW energy better and/or 2) maximum energy produced by SW SAWN is greater thus reducing the time for nebulization which in turn reduced evaporation of the liquid on chip.

3.4.2 Comparison of Signal Intensity in SW SAWN and PW SAWN

Although the origin of the charges in SAWN is still under investigation, it is assumed that SAWN aerosols desolvate when they pass the transfer capillary to enter the mass spectrometer. Shown in Figure 3.15 is the signal intensity change with the increasing temperature. SW SAWN spectra have higher signal intensity for all temperatures from 150-400 ℃. This supports our hypothesis that the smaller aerosol droplets generated from SW SAWN for liquid with higher surface tension should desolvate more efficiently and thus allow more analyte to be detected as ions. As observed temperature had less effect on the desolvation process of the smaller aerosol droplets from the SW SAWN chip.

To verify that the production of a larger number of smaller sized droplets would result in increased signal intensity, chips of both designs were compared under the same instrument settings with angiotensin II (1046 m/z). Figure 3.15 A, B shows a comparison of PW SAWN and SW SAWN. The average signal intensity for the PW chip is around 10^5 compared to the average signal intensity of 10^7, for the SW chip with the same amount of angiotensin II placed on chip. Note that the signal intensity used here is an arbitrary scale from Thermo-Fisher software. A serial dilution of angiotensin II was used to test the limit of detection of SAWN. With

measurements capable of a sample volume of 1 μL and concentration of 10^{-3} nmol/mL the detection limit of SW SAWN reached as little as 1 fmol of analyte. The $[M+2H]^{2+}$ peak was used to identify the detection limit, as shown in Figure 3.15 C. For PW SAWN the limit of detection for angiotensin II was around 100 fmol. Thus we can conclude that the SW SAWN chip design improved the limit of detection (LOD) by a factor of 100x compared to PW SAWN design.

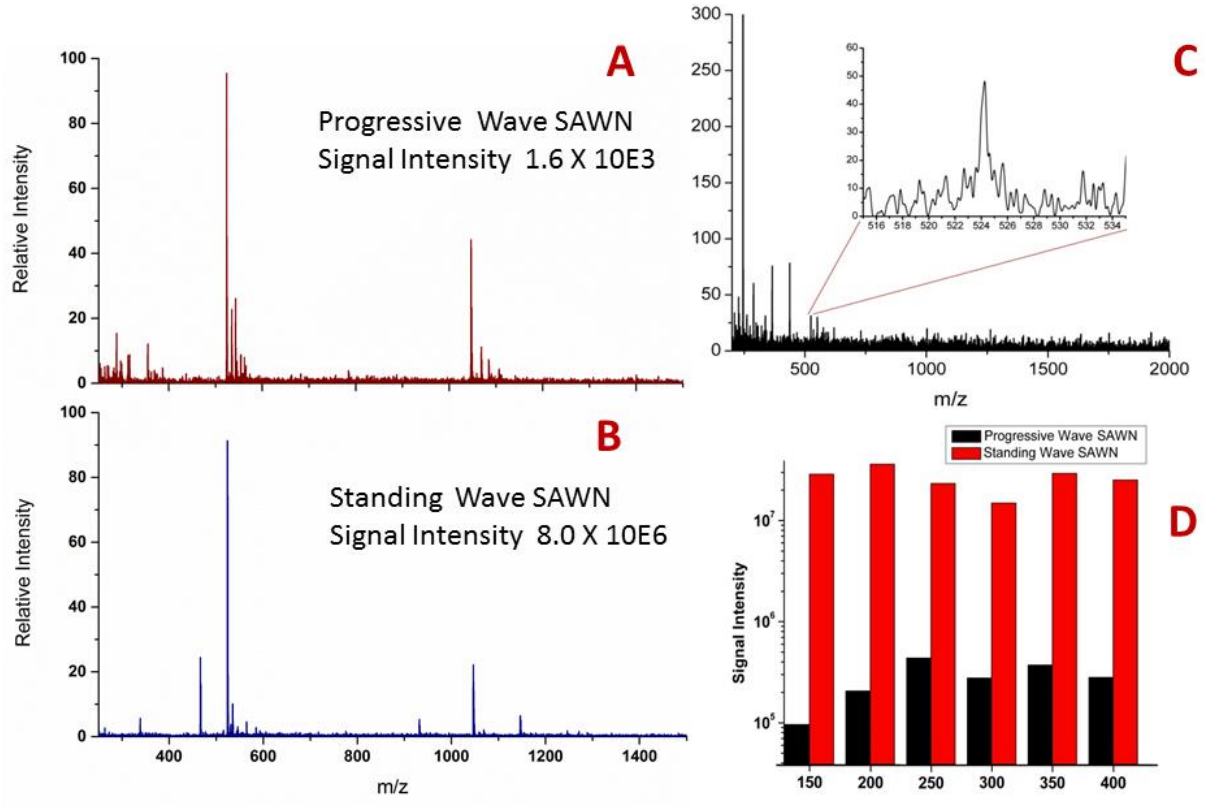

Figure 3.16 Standing wave SAWN spectra of angiotensin II. A and B are comparisons of signal intensity of SW SAWN and PW SAWN. C) Detection limit of SW SAWN on Angiotensin II $[M+2H]^{2+}$ ion reached 1 femtomole. D) The effect of temperature on SW SAWN and PW SAWN.

Since droplet size likely contributes to the lower internal energy of SAWN, decreasing the droplet size might affect the measured "softness" of SAWN. To test the internal energy distribution we compared the survival yield of benzylpyridinium ions of SW SAWN and ESI under exactly the same instrument set up, including the inlet capillary temperature and flow rate. From these experiments we found that the measured average internal energy distribution for SW SAWN under 300 ℃ was 2.25 eV, which is similar to the results for PW SAWN (2.17 eV) and lower than ESI (2.44 eV), indicating SW SAWN was also depositing less energy in to the analyte making it still a "softer ionization" process than ESI. While SW SAWN did not shift all of the droplets to a diameter of 1-20 μm, enough of the larger droplets produced by PW SAWN were eliminated to improve ion detections. A greater percentage of the SW SAWN droplets were in the range below 10 μm, from which ions were efficiently generated while maintaining a low internal ion energy.

3.4.3 Standing Wave SAWN Used for Whole Protein Analysis

Intact whole protein analysis has always been a challenge for mass spectrometry and this is especially a problem for top-down proteomics and native MS studies. PW SAWN was shown to be able to generate intact protein ions. However multiple liquid droplets were needed to average out the noise. Since there was an increase in the signal intensity observed with SW SAWN, this more sensitive method was also investigated for intact protein analysis and the results compared to ESI of the same proteins.

Three different protein solutions were analyzed with SW SAWN and compared to ESI. The proteins used were insulin, cytochrome C and lysozyme, which are all in a 1 μM aqueous

solution with 1% formic acid. For SW SAWN experiments, 2 µL of each protein solution were dispensed on the chip in each run and nebulized without DC voltage. For ESI experiments, the flow rate was set at 3 µL/min.

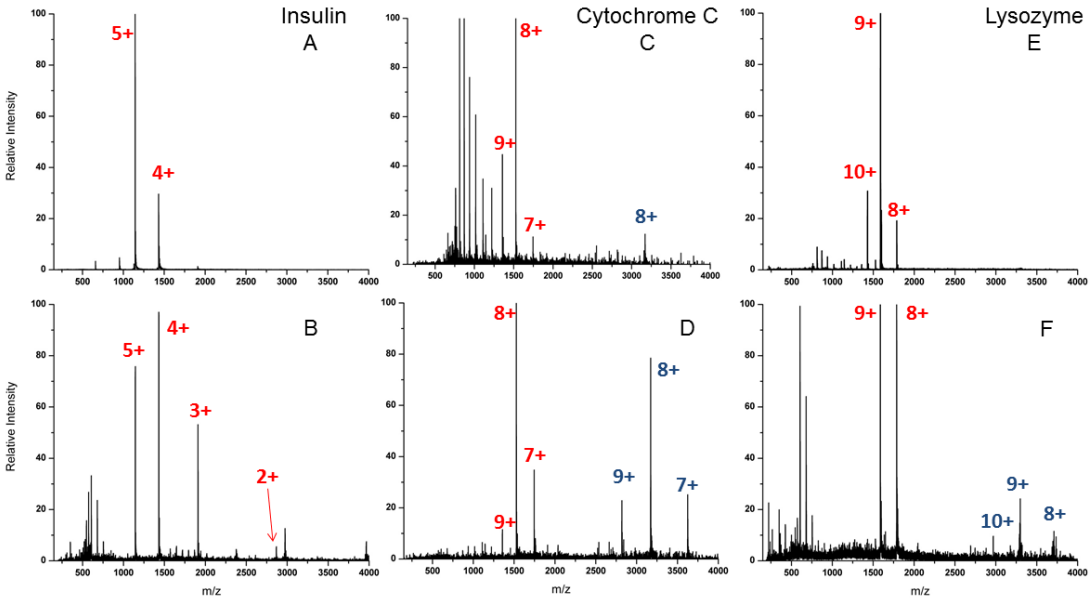

Figure 3.17 Whole protein analysis with SW SAWN. A, C and E are ESI spectra, B, D and F are SAWN spectra.

From the spectra shown in Figure 3.15, the SW SAWN setup generated a useful mass spectrum with high signal intensity in only one scan and these results were comparable to those from ESI. Interestingly we observed a similar charge state distribution difference in SW SAWN. Comparing insulin spectra from ESI (Figure 3.15 A) and SW SAWN (Figure 3.15 B), more low charge state ions (+3 and +2) appeared in the spectra for SW SAWN. The Cytochrome C and Lysozyme, SW SAWN spectra (Figure 3.15 D and F) not only showed a higher amount of low charge state proteins, but also a higher amount of homo-dimers. Since the protein concentration

used in this experiment was fairly high, it is to be expected that these two proteins would form dimers[104]. However, only SAWN generated spectra showed the potential to preserve more protein quaternary structural information.

3.4. Conclusion

In this chapter, PW SAWN was shown to be able to ionize peptides/proteins, lipids/triacylglycerides and other polar molecules. The upper limit of molecular mass detected by PW SAWN was 21kD. Like ESI, SAWN also showed a linear dynamic range over 5 orders of magnitude and thus will likely be useful for quantitative studies. To improve the signal intensity of SAWN spectra, multiple methods were tested based on the assumptions of the SAWN mechanism from Chapter 2. Increasing the temperature and on-chip voltage both increased the signal intensity, while adjusting the amplitude showed a more complicated effect on nebulization time and plume height. The SW SAWN device was fabricated to comparatively study the SAWN mechanism and increase signal intensity. The SW SAWN device focused the droplet in the middle of the chip, eliminating the movements of the droplet and forcing it to absorb more energy from the acoustic wave. Additionally, the distribution of aerosol droplet diameter was investigated. Comparing the SW and PW droplets size distributions, average diameter, and absolute number, a greater number of smaller aerosol droplets were generated in SW SAWN. Experiments with peptides and proteins further supported the conclusion of the size distribution and high signal intensity when SW SAWN was used. Finally, while SW SAWN improved performance over PW SAWN, the mechanism of ion formation from either SAWN device remains unclear.

Chapter 4 DIGITAL MICROFLUIDICS – SAWN PLATFORM FOR SAMPLE PREPARATION AND ANALYSIS

4.1 Introduction

In the previous chapters the SAWN performance was characterized and discussed. As a planar device for ionization, SAWN can be combined conveniently with microfluidic methods. Shortly after the publication of the first paper on SAWN-MS[48], the Go group at University of Notre Dame combined SAWN with a paper based microfluidics system to nebulize samples[62]. Here we present a new combination of digital microfluidics (DMF) with SAWN that allows simple sample preparation all on a single chip before MS analysis. DMF mechanism and general experimental setup were reviewed and several designs for DMF-SAWN will be presented in this chapter. The fabrication process of DMF-SAWN chips and the electronic control devices will be discussed. As an application highlighting the benefits of the DMF-SAWN platform, on-chip digestion of a phosphoprotein was carried out and phosphorylated peptides isolated. Experimental results from the standard phosphorylated peptide mixture and from an on-chip digestion and separation are discussed.

4.2 Digital Microfluidics

Digital microfluidics is an alternative technology for lab-on-a-chip systems based upon micromanipulation of a discrete droplet[105]. Digital microfluidic processing is performed on unit-sized packets of fluid that are transported, stored, mixed, reacted, or analyzed in a discrete manner using a standard set of basic instructions. Unlike traditional microfluidics, since the

control of droplet movement is digitalized, DMF provides the possibility of automatically performing high throughput analysis with a small amount of sample and reduced labor cost[66,106].

4.2.1 Electrowetting on Dielectric Material

Electrowetting was observed very early and probably first explained in 1875 by Gabriel Lippmann[64]. It is the phenomenon of the different wetting properties of a liquid on a solid surface by the application of an electric potential. More specifically, the contact angle of the liquid and the solid surface is changed by the application of an electric field. Different electrowetting configurations were studied in the recent decade and electrowetting on dielectric material (EWOD) became the most interesting one due to its stability[64,65]. In EWOD, the solid surface is patterned with a metal electrode and covered with a dielectric layer and a hydrophobic layer, but sometimes the dielectric layer can also serve as the hydrophobic layer. When voltage is conducted through the metal electrode, liquid sitting on the hydrophobic surface spreads and wets the surface. Electrowetting has been studied in various fields such as applied physics, electrical engineering and physical chemistry where in each case different models have been developed to investigate the phenomenon[64]. Below is a very basic introduction on the theory of EWOD for a homogeneous substrate. The liquid is usually an aqueous solution surrounded by a gas, which is most often simply the surrounding atmosphere. Under these conditions, surface tension is the dominant effect on the droplet[107].

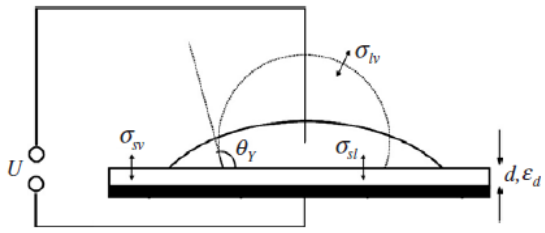

.

Figure 4.1 Electrowetting phenomenon on dielectrode material. Picture shows a liquid droplet on the hydrophobic surface with a metal probe inserted from the top. When there is no voltage present, the droplet will be in the more round format, with a higher H/L. When a proper voltage is applied through the metal probe the liquid will flatten down to the surface.

There are three phases existing in this figure: solid (s), gas (or vapor, v) and liquid (l). Two equations must be fulfilled for any equilibrium liquid morphology.

$$\Delta p = \sigma_{lv}\left(\frac{1}{r_1}+\frac{1}{r_2}\right) = \sigma_{lv}\cdot\kappa \qquad \text{Eq 1}$$

$$\cos\theta_Y = \frac{\sigma_{sv}-\sigma_{sl}}{\sigma_{lv}} \qquad \text{Eq 2}$$

The first is the Laplace equation (Eq 1) where Δp is a constant, independent of the position on the interface. The second is Young's equation (Eq 2), which relates Young's equilibrium contact angle θ_y to the interfacial energies. Here r1 and r2 are the two principal radii of curvature of the surface, κ is the constant mean curvature and σ_{lv} is the liquid-vapor interfacial energy. For homogeneous substrates, the liquid droplet adopts a spherical cap shape in mechanical equilibrium. Under electrowetting conditions, a voltage U is applied. Berge et al derived the basic equation for EWOD[64].

$$\cos\theta = \cos\theta_Y + \frac{\varepsilon_0 \varepsilon_d}{2d\sigma_{lv}} U^2 = \cos\theta_Y + \eta \qquad \text{Eq 3}$$

θ is the contact angel after applying voltage U;

θ_y is the contact angel without adding voltage;

ε_d is the dielectric constant of the insulator;

σ_{lv} is the liquid-vapor interfacial energy;

d is the thickness of the dielectric layer.

η is also named the electrowetting number.

The electrowetting number η is affected by the voltage and by the properties of the dielectric layer. In most DMF systems, a proper voltage enough to move the liquid droplet is applied. In our experiments a voltage of 30V DC was used to drive liquid droplets. Depending on the condition of the dielectric layer, the actual DC voltage applied was between 28-35V DC.

The selection of dielectric material is important for the fabrication of DMF chips since it will determine the parameters ε_d and d in Eq 3. In DMF-SAWN experiments, electrode patterns were deposited on the wafer following the same procedure used with the SAWN wafer (Figure 4.2, row 1). The wafer was then diced into proper size with a Disco saw dicing instrument and cleaned thoroughly. Any remaining impurities can cause cracks in the following high-temperature PECVD step (Figure 4.2, row 2). The diced chips were placed on a 4 inch diameter silicon carrier wafer. Silicon nitrate was deposited on the lithium niobate chip at 300 ℃ for 25 minutes to cover the entire surface of the chip. After the deposition of dielectric layer, the chip was removed from the instrument and the dielectric layer thickness measured. Since $LiNbO_3$ was

a transparent material that is challenging to measure, the thickness of the dielectric layer on the carrier silicon wafer was measure instead and found to be 400 ±10 nm.

Photolithography was performed again above the dielectric layer following the same operation parameters. The exposed patterns were the electrodes at the edge of the chip, which were connected to the electronic devices. Dry etching was used to remove the dielectric layer on the electrodes. After the dry etching the photoresist was washed off with acetone (Figure 4.2, row 3) and thoroughly cleaned. Teflon® AF 2400, a common material to provide hydrophobicity, was spun on the surface. The chip was heated on a hotplate to 160 ℃ for 10 minutes and then at 300 ℃ for 30 minutes to solidify the hydrophobic layer. The Teflon® layer on the undesired area was then gently removed to expose the metal electrodes. There are two types of cover plates used in the experiments, one is a commercially available indium-tin-oxide (ITO) glass, and the other is a cut silicon wafer coated with Teflon® AF and deposited with TiO_2[108].

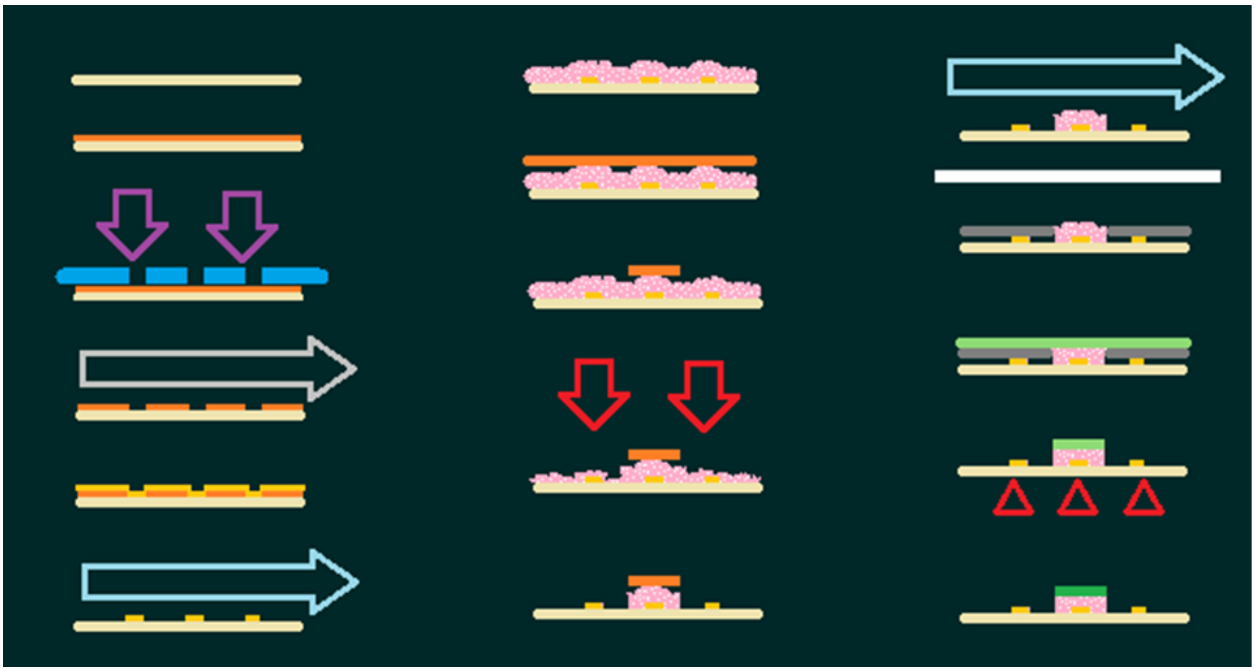

Figure 4.2 Fabrication of a DMF-SAWN chip. The $LiNbO_3$ chip goes through photolithography, metal evaporation, plasma enhanced chemical vapour deposition, photo lithography, dry etching, spin-coating and baking to get a DMF-SAWN chip.

An actual example for the fabrication of the DMF-SAWN chip is shown in Figure 4.3. There are two types of chip design. The design on the left with electrodes on two sides was the original prototype, which was replaced with the design on the right (Figure 4.3E). In the new design all the eletrodes were on one side. Therefore the other side can be used to conveniently add or remove the cover plate. The chip can also be placed in front of the mass spectrometer with a shorter distance. The enlarged circles showed details of the design including the SAWN interdigitated electrodes (Figure 4.3E, a) with 100 micron space in between the fingers, and DMF pads (Figure 4.3Eb) where liquid droplet was placed, the distance between the pads was 10 micron. The curveline was used to increase contact and help with the movement of the droplet.

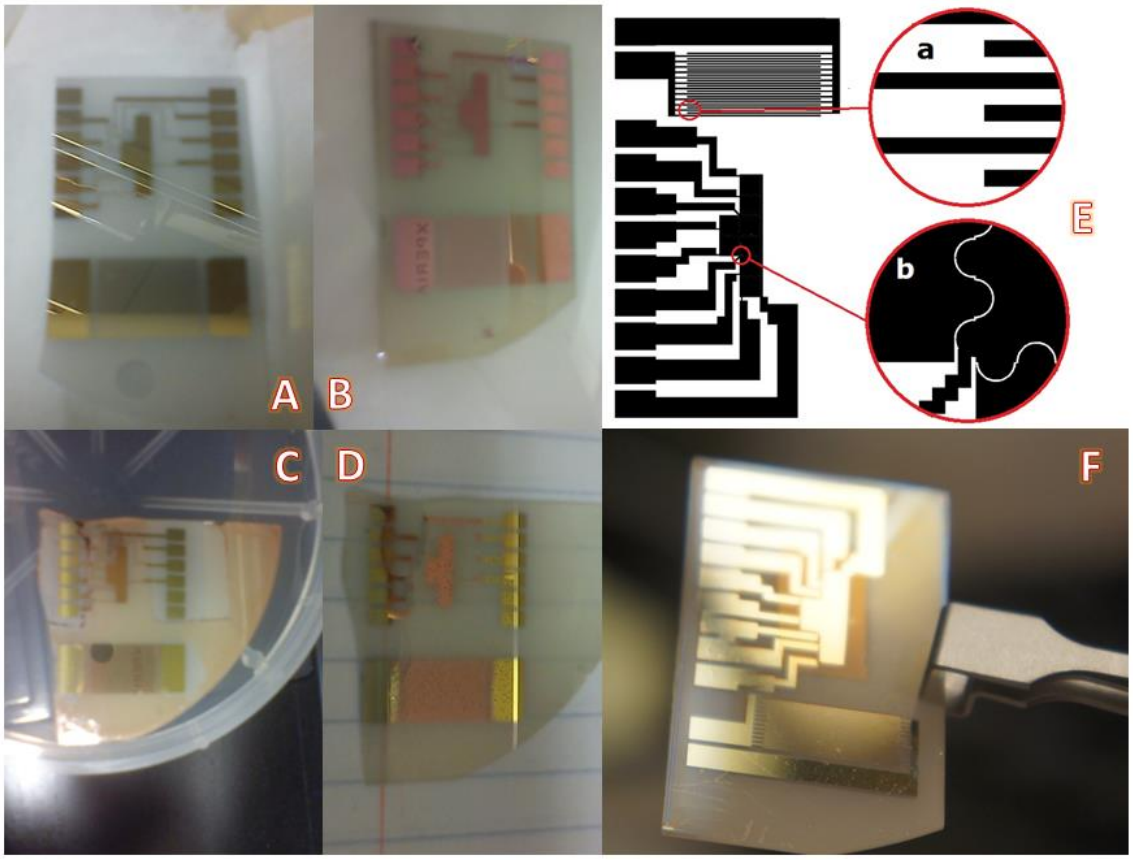

Figure 4.3 DMF-SAWN chip A) after metalizaion, B) after PECVD, pink layer is because of thin layer reflection of the light, C) after dry etching, the orange color is the color of photo resist D) after spin-coating and baking. Metal is exposed with the center covered with dielectric material and hydrophobic layer, E) CAD design of 2nd DMF-SAWN chip F) Actual piece of DMF-SAWN chip.

4.2.2 Movement of Droplet Utilizing EWOD

Based on the EWOD model above, there are several types of layout in applications of DMF. They can be divided into two main categories: with or without a cover plate[109].

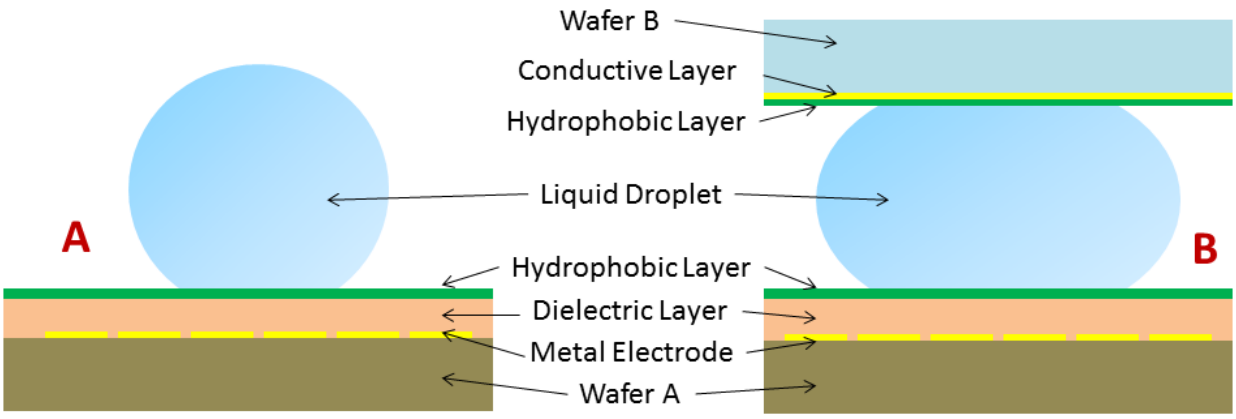

Figure 4.4 Single plate and double plate setup of DMF. A) in single-plate set up, the liquid droplet sits on the bottom plate. B) in double-plate setup the liquid droplet sits between two plates, with the top plate usually transparent to observe the movement.

As shown in Figure 4.4A, in one-plate setup the droplet sits on the plate and the voltage is applied on two electrodes on the plate, driving the liquid toward a certain position. This is a simple setup that is convenient to add in liquid droplets to the plate. However in this setup evaporation is a main concern in reactions that take longer time than a few minutes. In a two-plate configuration (Figure 4.4B), the cover plate is usually grounded and transparent. ITO glass coated with Teflon® is a commonly used top plate. In this design voltage is applied between the cover and bottom plates. Obviously, this design slows droplet evaporation, however, it is difficult to introduce liquid between the two plates, requiring a capillary be inserted between the plates to bring liquid to the designated position.

There are four fundamental droplet operations required for a basic DMF experiment, including: 1) creating liquid droplets from a reservoir, 2) splitting droplets, 3) merging droplets and 4) transporting droplets[68]. By various combinations of these four steps, sample processing and biochemical reactions can be carried out on chip. The DMF-SAWN setup is a simple one plate

setup that allows merging and transporting droplets. Additionally, it provides the ability to mix droplets and nebulize by action of the surface acoustic wave.

4.2.3 Bio-analytical Applications with DMF

Digital microfluidics was originally applied to electro-engineering fields, but has more recently been applied to a variety of biochemistry and bio-analytical areas[67, 105], including cell-based assays[110,111], DNA involved applications[69], protein chemistry[106], and other bioassays[112]. Due to interest in single cell analysis, cell based study has been a popular target for miniaturization[113]. In 2008, the Wheeler group applied DMF to a toxicity assay detecting the effect of adding different concentration of Tween 20 to cells[114]. Their DMF assay was more sensitive than a 384 well plate since it generated a better approximation of the empirical value. Fan et al used DMF to separate cells into different regions of a droplet[115]. Zhou et al. reported that application of an electric field to the liquid DMF produced few obvious effects on cells[116]. DMF has also been reported to perform on-chip PCR by Chang et al. who embedded the DMF chip with a micro-heater to control the reaction[117]. Later reports have improved the design and developed high-throughput multiplexed PCR applications. Immunoassays detect analytes in biological samples with high selectivity and have been combined with DMF. Sista et al. reported a droplet-based magnetic bead immunoassay for insulin and interleukin-6 detection[118]. Enzyme assays have long been a popular target for DMF. Enzymes used in DMF studies included luciferase, glucose oxidase and alkaline phosphatase. Proteomic and other research have also been conducted using DMF[119].

DMF platforms are capable of combining with several detection methods. Fluorescence detection is a common method since DMF devices usually have a clear cover plate that is convenient for the collection of optical signals. Imaging and microscopy methods are also often used especially for live cell related research. Electrochemical detectors are sometimes imbedded into the system. Mass spectrometry has also been applied to DMF detection[119,120]. When coupled with MALDI, the sample is usually mixed with matrix on chip and let dry. The DMF chip can then be mounted to a MALDI plate. When coupled with ESI, the situation becomes slightly more complicated but there have been several reports on DMF-ESI plates[112,119] . Common methods includes the insertion of a capillary into the droplet on a DMF chip and driving liquid constantly to the capillary end and moving the end of a capillary around to pick up reacted liquid droplet. Given our expertise in SAWN, we choose to couple DMF with SAWN for MS analysis after on-chip reaction.

4.3 Phosphorylated Peptide Enrichment with Metal Oxide

Protein phosphorylation is a post-translational modification (PTM) of proteins in which a serine, a threonine or a tyrosine residue is phosphorylated by a protein kinase through the addition of a covalently bound phosphate group. Phosphorylation of protein is one of the most common modifications of protein for the purpose of modifying function, and is sometimes termed phosphorylated regulation. In almost all cases of phosphorylated protein regulation, the protein switches between a phosphorylated and a non-phosphorylated form, with one of these two forms active while the other one is inactive, respectively.

Mass spectrometry has been widely used in proteomics and phosphoproteomic studies[121,122]. The ability to provide accurate mass information and fragment ion information made it suitable for protein and peptide analysis. Post-translational modifications like phosphorylation can also be studied by mass spectrometry too. However, there are several challenges when using mass spectrometry for phosphorylated proteins/peptides research. The first challenge is that phosphorylated peptides usually have a lower PI than their non-phosphorylated form because of the acidic phosphate group making them more challenging to ionize in positive ion mode[123]. The second challenge is that the amount of phosphorylated protein present is often a small percentage of the total amount of that protein. As such after proteolytic digestion of the phosphor-protein, the phosphorylated peptide is often difficult to detect. Last but not least, phosphorylated peptides need to be ionized with a soft ionization method to preserve the molecular ion. This is especially true for labile phosphohistidine. Considering these properties of phosphorylated peptides, a common procedure is to first enrich the phosphorylated peptides prior to MS analysis in order to increase detectability.

4.3.1 Phosphorylated Peptide Enrichment Methods

Phosphorylated peptide enrichment can take on various forms depending on the sample type and study aims. To summarize there are essentially three strategies[124].

1) Immuno affinity uses antibodies to enrich phosphorylated peptide/protein. Selection of an antibody is a major limitation of this strategy and often an antibody for the specific phosphorylated protein is not available. In this case more generic antibodies against phosphorylated amino acids in a protein may be used. Regardless, a typical experiment with

immuno affinity will need large amounts of protein starting material, which is impossible under certain conditions.

2) Chemical derivatisation is another strategy in which the phosphorylated peptides go through chemical reactions and resulting in a chemical tag on only phosphorylated amino acids. These peptides are then affinity purified using a reagent that recognized the tag. The shortcomings often observed with this method are the multi-step reactions and cross reactivity with non-phosphorylated amino acids.

3) Ion metal affinity chromatography[125,126,127] which often uses TiO_2 columns has been frequently used for phosphorylated peptide enrichment. IMAC uses chelated metal ions such as Fe^{3+}, Al^{3+}, Ga^{3+} or Co^{2+} to bind with negatively charged phosphorylated peptides in the mobile phase. In TiO_2 chromatography, TiO_2 was shown to have an affinity for phosphate ions in aqueous solutions and provided a high selectivity toward phosphorylated peptides. The offline setup is simple, fast, and does not require expensive equipment. Furthermore, TiO_2 has high salt tolerance to most biochemistry buffers. This has resulted in a robust method for enrichment of phosphorylated peptides, and has already become a highly popular method for large-scale phosphorylated proteomic studies.

4.3.2 Phosphorylated Peptide Enrichment with Metal Oxide Surface

While a metal oxide such as TiO_2 has been shown to bind phosphorylated peptides when stabilized in column form, it can also bind phosphorylated peptides when it is decorated on a surface[128]. When a metal-oxide-decorated surface is used to enrich phosphorylated peptides, it

can be combined easily with microfluidics methods[129]. It has also become a popular method since the captured peptide can be released, mixed with matrix and directly analyzed by MALDI[130], eliminating the sample loss during liquid transfer. Metal oxide coated wafers such as TiO_2[131,108,132], ZrO_2[133] and ITO coated glass[134] have been proved to be able to capture phosphorylated peptides specifically.

A common procedure of phosphorylated peptide enrichment with a metal oxide decorated surface can be divided into four steps:1) binding the phosphorylated peptide on to the surface metal oxide, 2) washing off the non-phosphorylated peptides, 3) releasing the phosphorylated peptides and 4) preparing for analysis. To elaborate, the metal oxide coated surface is acidified first. A solution containing peptides is acidified and deposited on the surface to dry. Then the dried spot is washed with weak acid solution (eq. TFA) several times to eliminate the non-phosphorylated peptides. Finally a basic solution (eq. NH_4OH) is used to incubate and release the phosphorylated peptides. Although no cleanup is performed in this procedure, MALDI's high salt tolerance makes it possible to observe peptides in the MS1 spectra. However if the released liquid was collected and infused with ESI, a strong salt signal would be detected, but fragmentation of the peptides suspected being in a given m/z channel will allow peptide identification[128]. From such a tandem MS signal one can acquire the sequence information of the target peptide.

4.4 DMF-SAWN Chip for Phosphorylated Protein Analysis

Here we present a new DMF-SAWN platform for sample preparation and detection of phosphorylated peptides. As a planar device SAWN was an obvious choice for coupling to DMF

for sample preparation. With such a setup protein samples can be digested on chip and as shown below phosphopeptides enriched on-chip for SAWN MS analysis.

The reagents used in this experiment included water, acetonitrile, ammonium 98%, trifluoroacetic acid and formic acid. All chemicals were purchased from Sigma Aldrich. Samples used in the experiments including β-casein, casein mixture and angiotensin II were also purchased from Sigma Aldrich. Phosphorylated peptide standard was provided by Dr. Tureček group.

4.4.1 Instrument Setup

DMF-SAWN chip control system. The DMF-SAWN design here was a one-plate design. The DMF-SAWN chip was fabricated as described in the previous section. It was mounted on a clamp holder (Figure 4.7). The control systems for this chip included the SAWN control and the DMF control. The SAWN device was controlled by a fabricated SAWN electronics box fabricated by University of Washington Department of Chemistry Electronic Shop. The DMF part was controlled by the computer through an arduino board and a homemade electronic box. As shown in Figure 4.5 B, from left to right there are the arduino board for generating digital signals, the homemade electronic box that controlled the DC voltage, and the end of the clamp with DMF-SAWN chip. The design of the electronic box is shown in Figure 4.5A. Each DMF electrode was connected to two optical couplers, which used a digital signal (on: 5V, off: 0V) from the arduino board (blue circlet) to control the red and green circlet. When a pad was activated, a signal of 5V was sent to the blue circlet for the DC voltage; the 30V DC signal

would be directed to the pad. When the process was finished, the ground circlet could be activated putting the pad in the ground state. Since the droplet movement was usually a quick process, voltage was applied for only a short period of time (less than 1 sec). When the reaction was in process the pads were usually in the ground state. The movement of droplet was controlled by the bottom plate, while the top plate was added or removed during the experiment. The ITO glass (purchased from Sigma Aldrich) was used to trap phosphorylated peptides. Before the start of phosphorylated peptide separation experiments, the ITO glass was acidified with a solution containing 6% TFA, 80% acetonitrile, and 14% water.

Mass spectrometer settings. The mass spectrometer used for these experiments was a Thermo-Finnegan LTQ stand-alone where the front ion gauge was replaced with a dual ion funnel inlet (Spectroglyph, Richland WA) to refine the movement of ions and reach a better signal intensity. To allow operation with the ion funnel in place an extra pump was connected and the transfer capillary diameter increased (ID: 0.8mm).

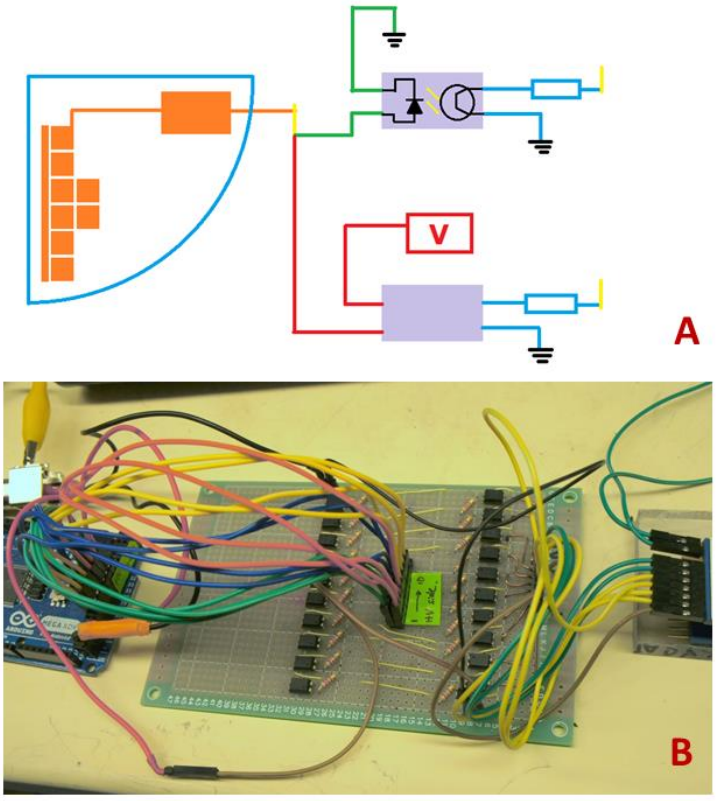

Figure 4.5 Control box for DMF part of the chip. A) the control of one pad is done through two opto-isolator. B) the actual electronic board for controlling multiple pads.

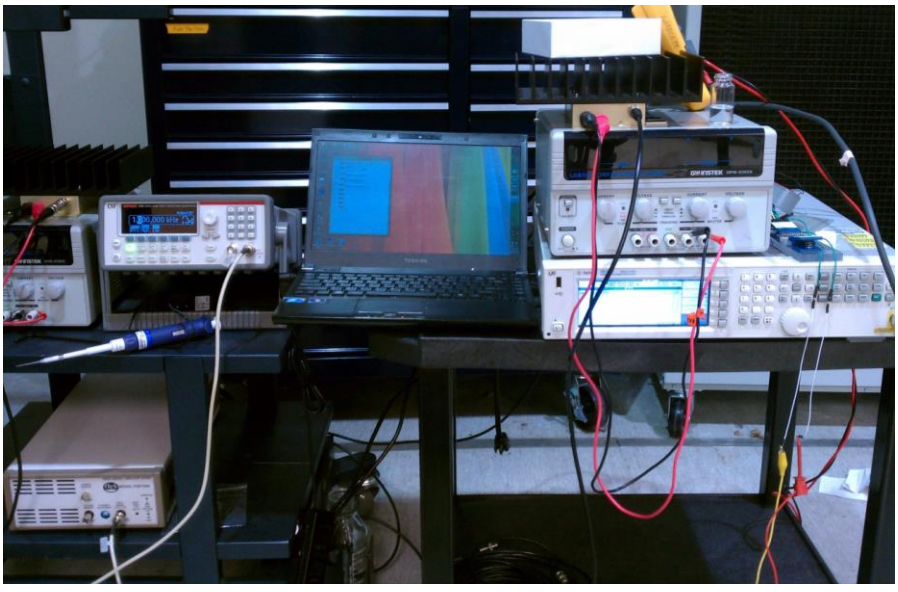

Figure 4.6 DMF-SAWN equipment.

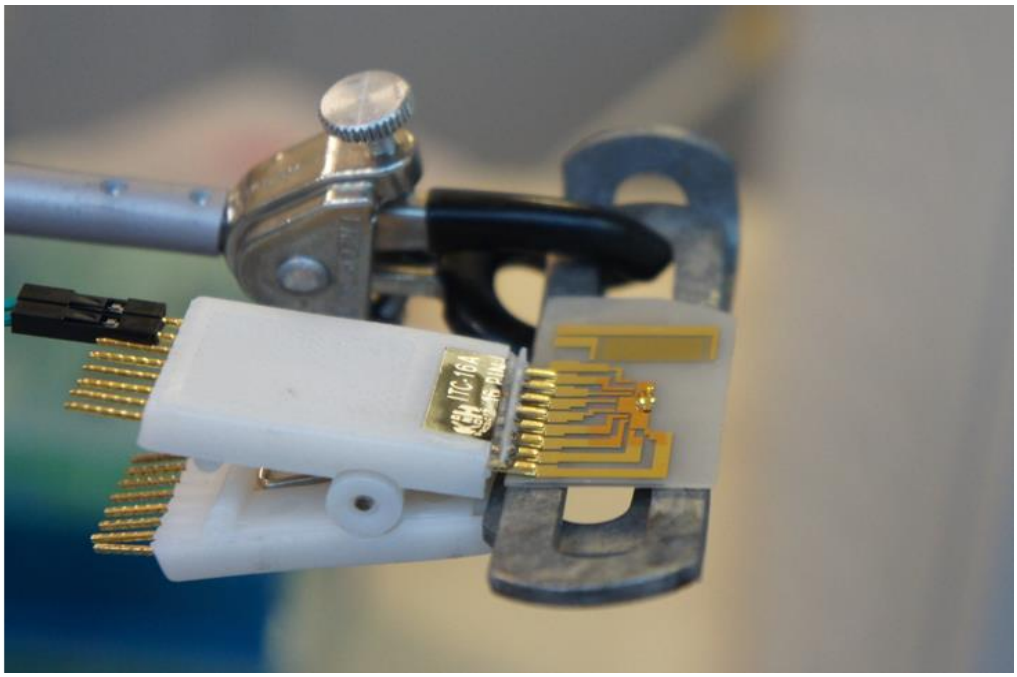

Figure 4.7 DMF-SAWN chip with a liquid droplet on.

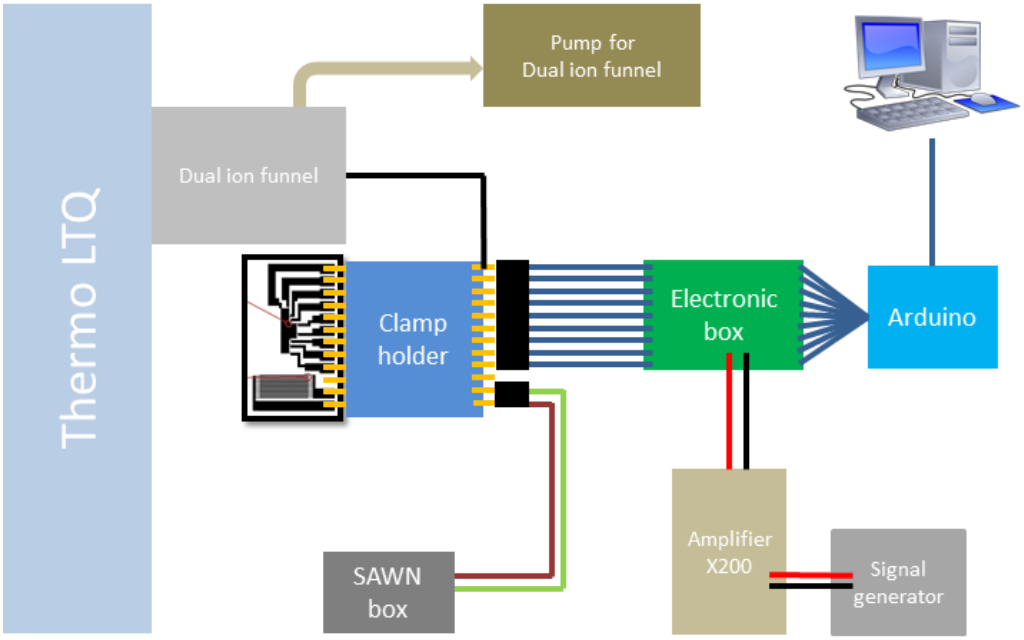

Figure 4.8 Schematic graph of DMF-SAWN chip setup.

4.4.2 On-chip Digestion of Phosphorylated Protein

A typical trypsin digestion procedure will usually take two days from start to finish, including denaturation, an overnight reaction with trypsin under 37 ℃, and desalting. Over the last 50 years a significant amount of research has been done to increase digestion efficiency, shorten digestion time, and simplify the process. For example, immobilized trypsin beads have been used to increase digest protein efficiency and can be reused. Additionally, external methods such as a microwave have also been applied to decrease digestion time. SAWN have been reported to be able to enhance the digestion process of protein present in an SDS-PAGE gel slice by the Yeo and Friend group[135]. In Yeo's paper, the digestion time was shortened from eight hours to several minutes. Since the use of SAW has the ability to enhance mass transfer in a liquid droplet and has proved to keep the reactivity of an enzyme, we chose to use SAW on our SAWN chip to help with the digestion of protein samples in liquid droplets on chip.

Beta casein (Sigma Aldrich, Bovine) was prepared at 10 ng/mL in water. The solution was placed in a 60 ℃ water bath for 30 minutes to mildly denature it and used directly for the experiment after it was cooled down to room temperature. A 1.8 μL droplet of this denatured solution was placed on the DMF-SAWN chip by pipet. It was then by action of the DMF device transferred to the designated position and merged with a 1.8 μL trypsin droplet (0.5 ng/mL). A surface acoustic wave was then activated at a low amplitude, around -20dBm to shake the liquid droplet. During this action the DMF-SAWN chip was covered with a petri dish to help prevent liquid evaporation. More droplets were transferred to the position during the incubation process depending on the condition to prevent the droplet from drying completely. After five minutes,

the liquid was allowed to shrink back its starting size (1.8μL) and the SAW was turned off. The remaining droplet was then merged with a concentrated formic acid droplet (1.8 μL 10% in water vol: vol) and moved close to the SAWN interdigitated electrodes. After it was acidified the SAW was turned on again to nebulize the droplet. This over all procedure was refined after changing a variety of parameters shown in the table below.

Parameter	Conditions	Effect
Denature temperature	No denature	Denature eliminated miscleavages. 60 ℃ and 95 ℃ gave similar results.
	60 ℃	
	95 ℃	
Denature time	30min	Denature time gave similar results in spectra.
	10min	
Trypsin : Protein amount	1:20	More miscleavages were observed in 1:50.
	1:50	
Surface Acoustic Wave mode	Continuous wave	Pulsed wave have the possibility of driving droplet to move on the surface. No difference in spectra.
	Pulsed wave	
SAW amplitude	-25dBm to -15dBm	The liquid shaking was observed in all amplitudes. A median is chosen.
Incubation time	5min	The incubation time must be at least five minutes. Longer time does not increase the digestion too much, and will require more DMF operations.
	10min	
Liquid pH	NH_4OH added	NH_4OH added liquid droplet showed much less signal intensity in spectrum, partially because the other substrate brought in with the base and because the acidifying isn't as complete.
	Neutral	

Table 4.1. On-chip digestion control parameters.

In order to verify the digestion process of DMF-SAWN chip, fully digested beta casein was ionized with ESI and was used for comparison. Most peptide peaks were observed in both DMF-SAWN digestion and traditional overnight digestion. However, DMF-SAWN on-chip digestion took less than 15 minutes including merging the liquid, SAW shaking and nebulization, compared to overnight digestion and multiple steps of reducing and denaturing. The identified peptides in MS1 are the same for both ESI and SAWN, although SAWN has a lower signal intensity. While SAWN digestion on chip is fast and could generate comparable peptides there are two obvious shortcomings. One is that the amount of trypsin used in this design is five times as much as in traditional digestion. The other is that there are more miscleavages. However, this could be refined using trypsin coated magnetic beads and the missed cleavages could probably be reduced by incorporating a more thorough denaturation.

Peptide MW and Sequence	MS1 peak in ESI Spectra	MS1 peak in SAWN Spectra
6359.3 YPVEPFTESQSLTLTDVENLHLPLPLLQSW MHQPHQPLPPTVMFPPQSYLSLSQSK	1590.6 (+4), 1272.7(+5), 1060.9 (+6), 909.5 (+7)	2120.4 (+3)
5316.9 IHPFAQTQSLVYPFPGPIPNSLPQNIPPLTQT PVVVPPFLQPEVMGVSK	Not found	Not found
2966.2 (-4p: 2646.3) ELEELNVPGEIVEpSLpSpSpSEESITR	1483.6 (+2), 989.3 (+3), 742.3 (+4). Non phosphate ion not seen / too weak	742.3 (+4), 594.0 (+5) Non phosphate ion not found / too weak
2186.2 DMPIQAFLLYQEPVLGPVR	1093.6 (+2), 729.4(+3)	2186.2 (+1), 1093.6 (+2)
2160.8 (-1p: 1981.9) FQpSEEQQQTEDELQDK	516.2 (+4), Non-phosphate: 1981.9 (+1), 991.4(+2)	1031.4 (+2), 687.9(+3) Non-phosphate: 991.4(+2)

830.4 AVPYPQR	830.4(+1)	830.4(+1)
780.5 VLPVPQK	780.5(+1)	780.5(+1)
748.4 EMPFPK	748.4(+1)	748.4(+1)
742.5 GPFPIIV	742.5(+1)	742.5(+1)
646.3 EAMAPK	646.3(+1)	646.3(+1)
2911.6(1 miscleavages) DMPIQAFLLYQEPVLGPVR & GPFPIIV	Not found	2911.5(+1)
1014.5(1 miscleavages) EMPFPK & HK	Not found	1014.5(+1)

.

Table 4.2. Identified MS1 peaks of Standard digestion with ESI and DMF-SAWN on-chip digestion. Although more miscleavages were found in SAWN compared to ESI, the main peaks were identical in both method.

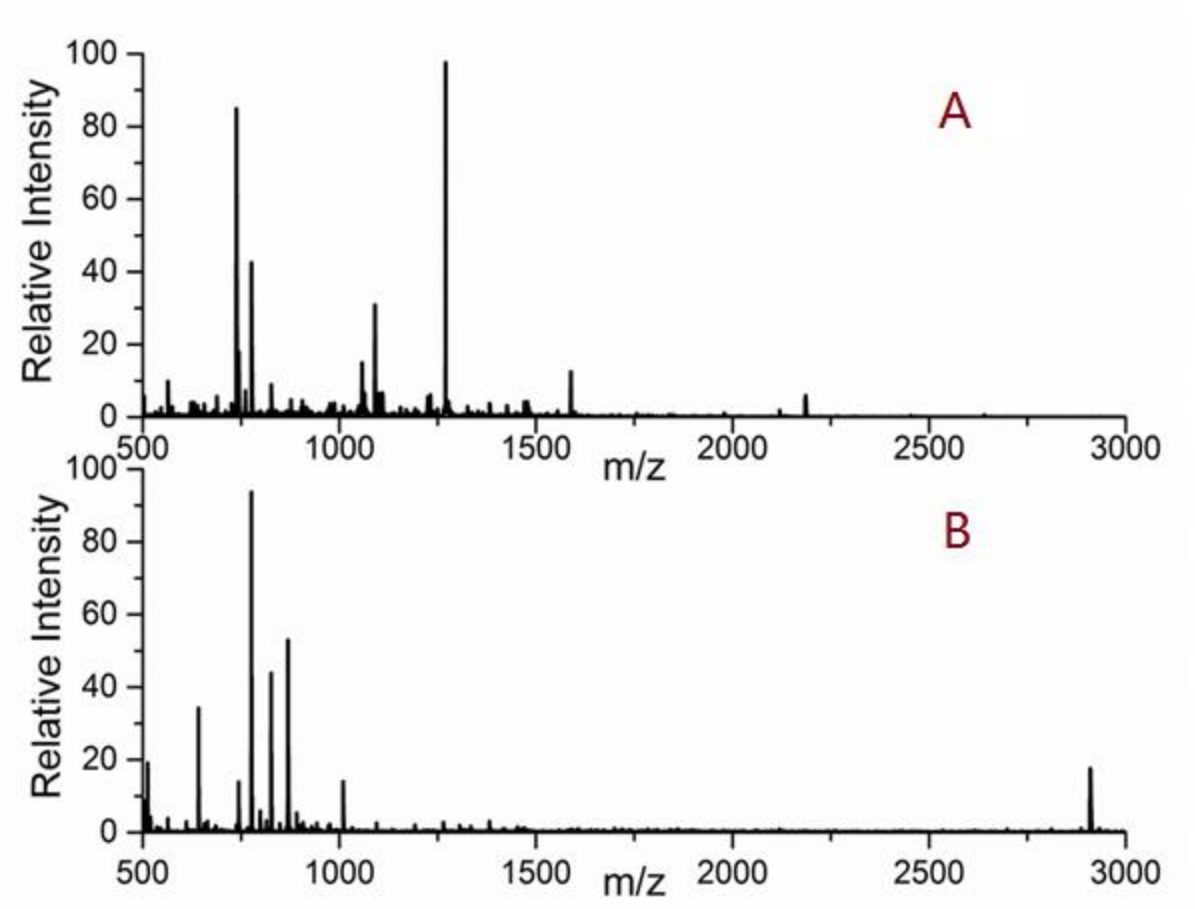

Figure 4.9 Beta casein digestion. A) Standard digestion with ESI. B) On-chip quick digesiton with SAWN. Although similar peaks were identified in both spectra. The miscleavages and varying charge state distribution of ions affected the MS1 spectra.

4.4.3 Phosphorylated Peptide Separation with DMF-SAWN and ITO chip

In this experiment, the bottom plate was used to control the movement of droplets and the top plate is used for binding phosphorylated peptides. As mentioned before, several materials, such as TiO_2, ZrO_2 coated surface and ITO glass could be used as the top plate to capture phosphopeptides. In our experiments two different top plates were prepared. One was ITO glass purchased from Sigma Aldrich. The other was a silicon chip coated with Teflon® and a spot of

TiO_2. After preliminary experiments, ITO glass was selected for the experiment due to the fact that it was clear and the position of the droplet could be easily controlled when covered with ITO glass. To bind phosphorylated peptides on ITO glass, there are several solvents needed, (A) the loading solvent, (B) the washing solvent (C) the releasing solvent and (D) the acidifying solvent with the following compositions:

Solvent A: 6% TFA, 80% ACN, 14% H_2O, also called binding solvent in some literature;

Solvent B: 0.5% TFA, 10% ACN, 89.5% H_2O, washing solvent;

Solvent C: NH_4OH PH > 11, release solvent;

Solvent D: 10% Formic Acid in H_2O, acidifying solvent.

ITO glass was first acidified by allowing a droplet of solution (A) to dry on the surface. In our experiment, this step was performed to the entire surface of ITO glass. The peptide solution was mixed with solution (A) at a 1:1 ratio on the chip and the ITO glass was added to the spot until the liquid dried. Then the ITO glass was removed to allow the movement of wash solution droplets and placed back after the droplet was in place. The spot on ITO glass was washed with solution (B) four to six times after which each time the solvent was gently shaken and nebulized by SAWN without MS detection to remove the liquid rapidly. After that solution (C) was brought into the position and phosphopeptides recovered by wicking into the liquid droplet from the surface. After the ITO glass was removed, solution (D) was added to the remaining basic solution. The droplet was nebulized and the contents analyzed by MS. Since ITO glass was not covered by Teflon, in this setup it needed to be removed after each nebulization to allow the new

droplet to move to the position. SAWN was used as both the nebulization method for MS analysis and as a method to remove liquid waste from the chip without MS analysis.

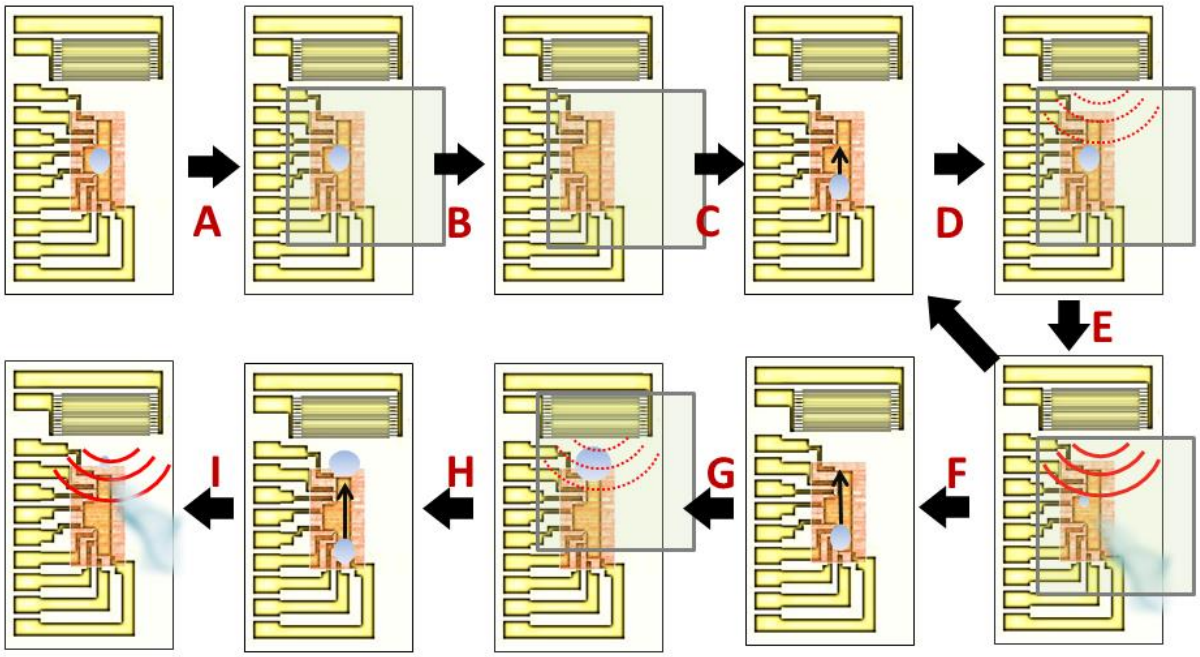

Figure 4.10 On-chip separation of phosphorylated peptide procedure.

To investigate the ability of DMF-SAWN chip to separate phosphorylated peptides peptides from a solution containing predominantly nonphosphorylated peptides, a 1:1 mixture of two standard peptides was used first. Angiotensin II, a commonly used non-phosphorylated peptide with sequence Asp-Arg-Val-Tyr-Ile-His-Pro-Phe (DRVYIHPF, m/z=1046), was mixed with a phosphorylated peptide standard of the sequence Ala-Ala-pSer-Ala-Arg (AApSAR, m/z=554), where pSer and pS represent phosphorylated serine. The non-phosphorylated form of this same peptide has a MW=474. The peptide mixture was made with an aqueous solution at a concentration of 1ng/mL for both substrates. Tandem MS spectra were acquired to identify that the phosphopeptide had been separated from the nonphosphorylated peptide. Prior DMF-SAWN

separation, both angiotensin II and phosphorylated peptide standard AApSAR were detected (Figure 4.11, top left and top right). However after DMF action only the phosphorylated peptide ions (Figure 4.11, middle left) was detected. The non-phosphorylated peptide was not present (Figure 4.11, middle right) at the m/z channel representing its protonated m/z value. In the spectrum for phosphorylated peptide tandem MS, the base peak was an ion representing loss of 98 [H_3PO_4] (m/z=555 - 457) and MS3 of this fragment ion at m/z=457 was acquired from which the annotations in Figure 4.11 lower left, are derived. These results proved that DMF-SAWN separation of phosphorylated and non-phosphorylated peptides on a simple mixture could be successful. The main limitation of this approach is that SAWN does not have comparable salt tolerance as MALDI and required tandem MS data on a specific m/z channel to identify peptides.

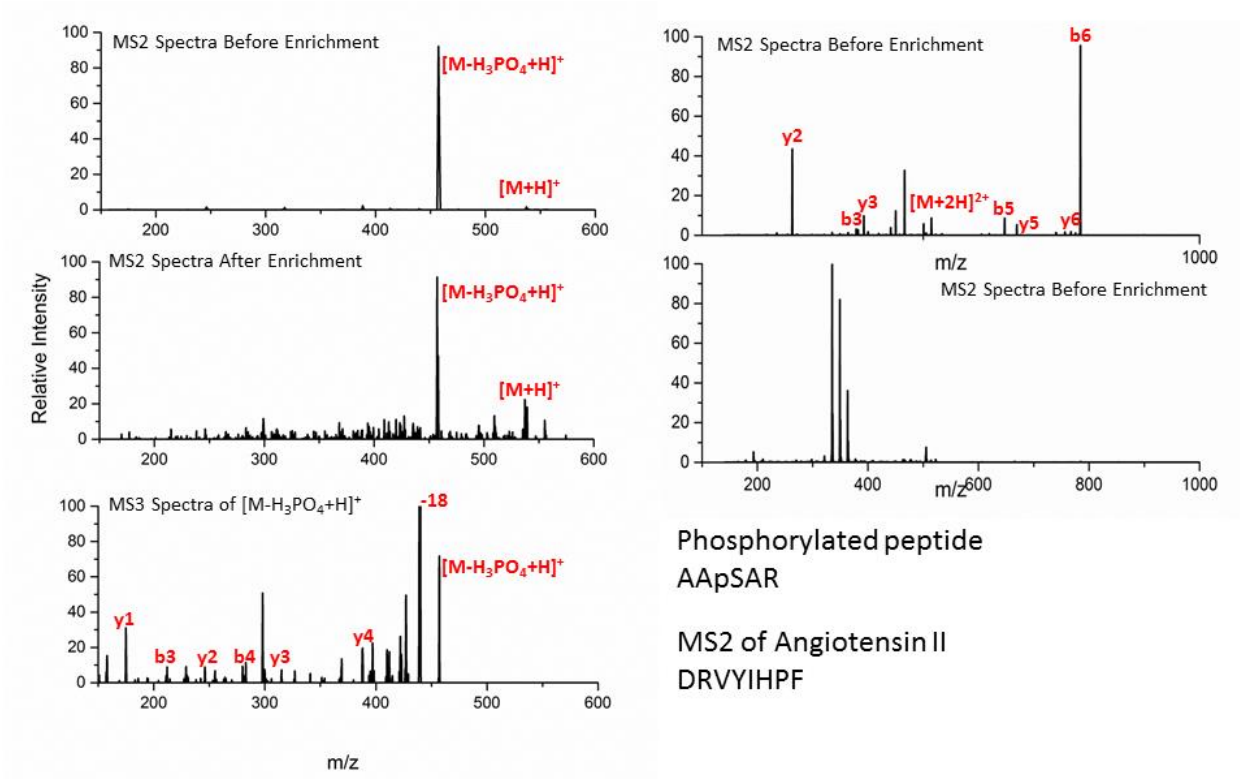

Figure 4.11 Seperation of phosphorylated paptide standard and angiotensin II. MS2 and MS3 spectra of phosphorylated peptide standard are acquired to identify the peptide.

4.4.4 Phosphorylated Protein On-chip Digestion and Enrichment

The above sections describe a DMF-SAWN chip that was built and applied to the digestion of protein on chip and the separation of a phosphorylated peptide from a nonphosphorylated peptide on chip. It should be noted that the DMF-SAWN digested protein produced identical peptide ions as produced by the standard digestion protocol and ESI-MS analysis. Although there were a few miscleaved peptides present, digestion of the protein was relatively complete. SAW activation was used to shake the liquid droplet to enhance mass transfer and increase the digestion efficiency, while DMF was used to resupply the liquid droplets to prevent evaporation. For the on-chip phosphorylated peptide separation, a standard peptide mixture was separated and collision induced dissociation used to confirm the existence of phosphorylated peptide from the ITO surface while the non-phosphorylated peptide was shown to be washed away.

Since the on-chip digestion and phosphorylated peptide separation both generated promising results, a sample preparation procedure for a denatured protein mixture in aqueous solution was performed solely on chip. This allowed SAWN to be used again immediately for MS analysis directly on-chip.

To examine the performance of the DMF-SAWN sample preparation platform in this process, a casein mixture (Sigma Aldrich, bovine) was used as the sample, which was known to contain mainly β-casein, α-s1 casein and α-s2 casein[136]. The casein mixture was prepared at a concentration of 100ng/mL in water and the digestion process performed as in the previous section. After digestion, a droplet of solvent (A) was moved to the peptide droplet to acidify the

peptide solution. When the ITO glass cover slip was placed on the chip the liquid was wicked to the ITO surface due to a difference in hydrophobicity between the two surfaces. The acidified solution was then dried on the pre-acidified ITO glass. The phosphopeptide separation process was as described in the previous section. After the sample preparation, the droplet was nebulized and the peptides were analyzed by mass spectrometer. The mass spectrometer was preset to collect tandem MS spectra of known m/z values from the mass list. The mass list included the doubly and triply charged ions of possible peptide mass from the digestion of casein mixture including α-S2-casein, α-S1-casein and β-casein. The mass window for fragmentation was 1.5 Da. The singly charged ions, although also observed from trypsin digest on chip, were not selected due to the difficulty in interoperating the subsequent fragmentation patterns. Compared to ESI data, the SAWN tandem MS data showed low signal intensity, yet presented a high S/N ratio. Due to the low signal intensity, common sequence identification software cannot identify the peaks. Therefore, the acquired tandem MS spectra were analyzed manually. For a phosphorylated peptide, there is also a possibility of losing a $[H_3PO_4]$ (m/z=98) or a $[HPO_3]$ (80). These fragmentations were also taken into consideration. The identified peptides were from all three proteins. The information of these peptides is listed in Table 4.3.

Protein	Sequence	[M+H]+	No. of phosphorylation	pI
α-S2-casein	TVDMESTEVFTK	1466.8	1	2.99
α-S2-casein	TVDMESTEVFTK*	1482.8	1	2.99
α-S2-casein	EQLSTSEENSKK	1539.8	2	3.1
α-S2-casein	TVDMESTEVFTKK	1595.8	1	4.02
α-S1-casein	VPQLEIVPNSAEER	1661.0	1	3.07
α-S1-casein	YLGEYLIVPNSAEER	1833.1	1	3.07
α-S1-casein	DIGSESTEDQAMEDIK-80	1847.9	1	1.86
α-S1-casein	DIGSESTEDQAMEDIK	1927.9	2	1.86
α-S1-casein	YKVPQLEIVPNSAEER	1954.2	1	4.15
β-casein	FQSEEQQQTEDELQDK	2062.0	1	2.83
α-S2-casein	NANEEEYSIGSSSEESAEVATEEVK-80	3008.0	4	1.16

*Table 4.3. Identified peptides of casein mixture with DMF-SAWN on-chip quick digestion and phosphorylated peptide separation. (-80 phosphate loss; * methionine oxidation)*

From the list we can see for all three casein proteins, at least one of the phosphorylated peptides was identified. This indicated the digestion process was successful even with a three protein mixture. β-casein is a 224 amino acid (AA) protein containing five phosphorylated residues and two phosphorylated tryptic peptides. One peptide has four phosphorylated site (MW=2,966) and the other has only one phosphorylated site (MW=2,061) (Figure 4.12). Although in the on-chip digestion experiments, β-casein was digested and analyzed, and both phosphorylated peptides were observed in the MS1 spectrum, the peptide with four phosphorylated site was not identified. α-S1-casein is a 214 AA protein with nine phosphorylated residues and four phosphorylated peptides. The phosphopeptide with three and five phosphorylated residues was not identified. α-S2-casein is a 222 AA protein with twelve phosphorylated site and five phosphorylated peptides. Only one of the two phosphopeptides with four phosphorylation site were identified. However, all of the phosphopeptides with two or one phosphorylation site were successfully identified.

Due to different variations of peptides such as miscleavages, loss of the phosphite (–80) or methionine oxidation, the same peptide might be identified for multiple times.

Failure to identify peptides with a large number of phosphorylated residues may be due to a decrease pI making them more difficult to nebulize. For the casein mixture, these peptides were also of a larger mass. Although the mass range of peptides identified goes up to 3000 Da, most of the identified peptides were less than 2000 Da. While SAWN to date has been used to detect proteins up to about 20kDa, there may also be some as yet unexplained bias against the larger phosphorylated peptides not detected here. Additionally, the lack of an applied DC voltage as with ESI might decrease the possibility to ionize such peptides with a lower pI as efficiently as ESI. Selected spectra for identified peptides are provided in the Figures 4.12-4.16.

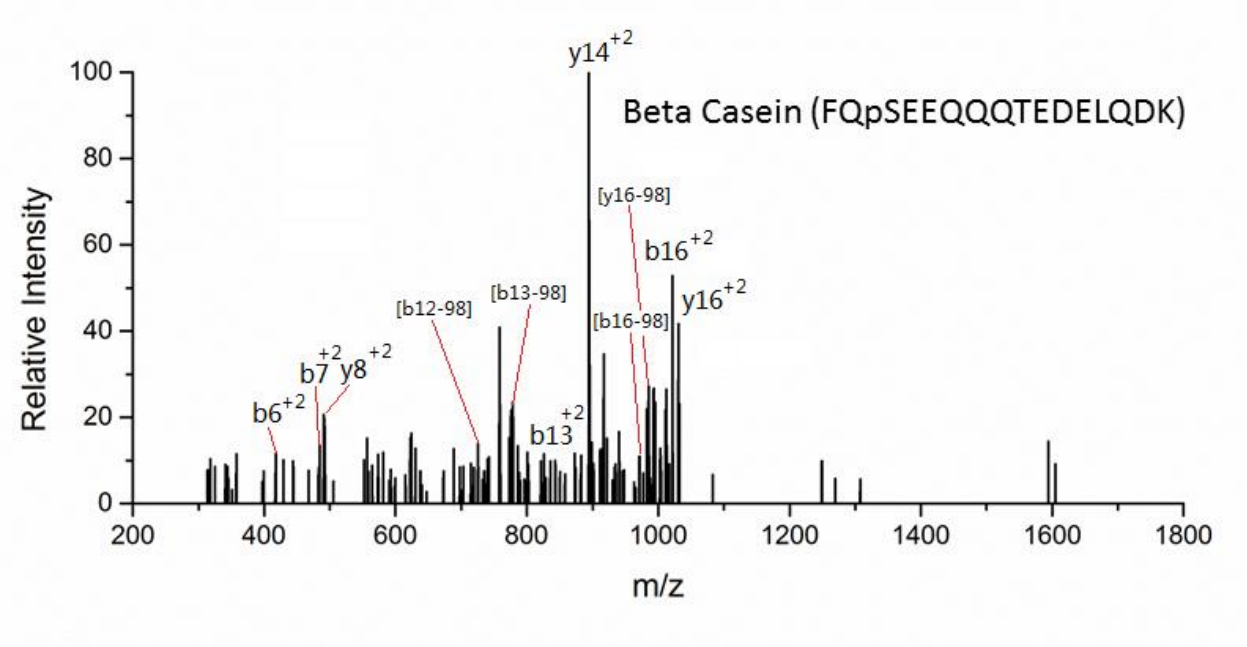

Figure 4.12 Fragmentation of peptide FQSEEQQQTEDELQDK (β-casein).

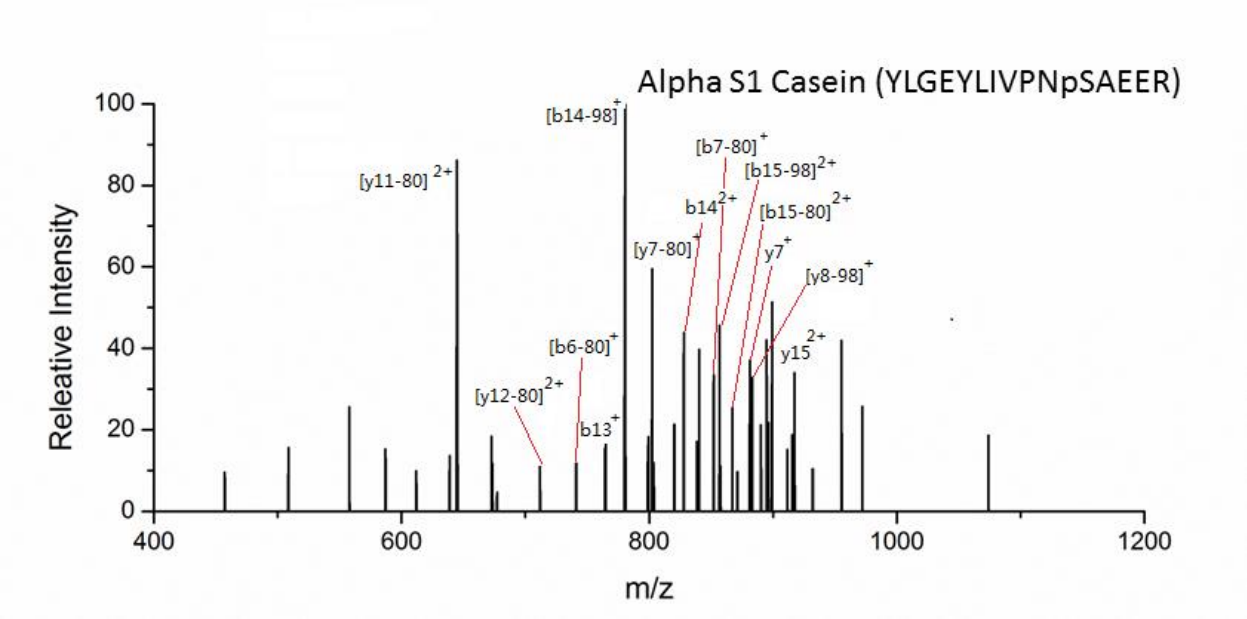

Figure 4.13 Fragmentation of peptide YLGEYLIVPNSAEER (α-s1-casein).

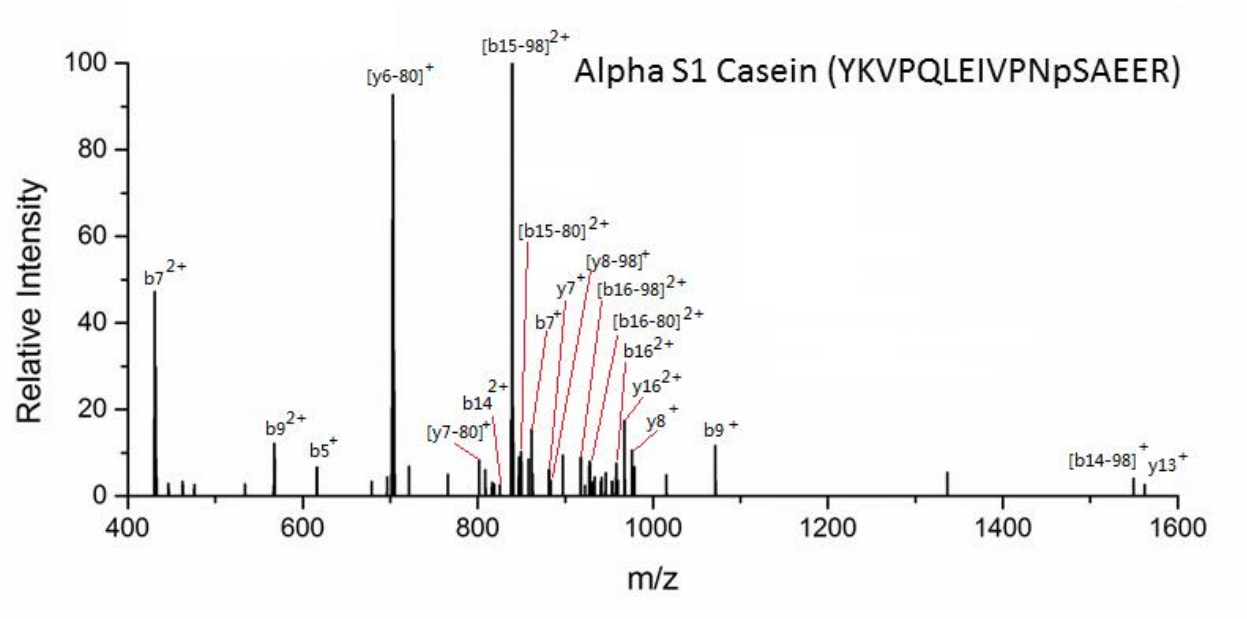

Figure 4.14 Fragmentation of peptide YKVPQLEIVPNSAEER (α-S1-casein).

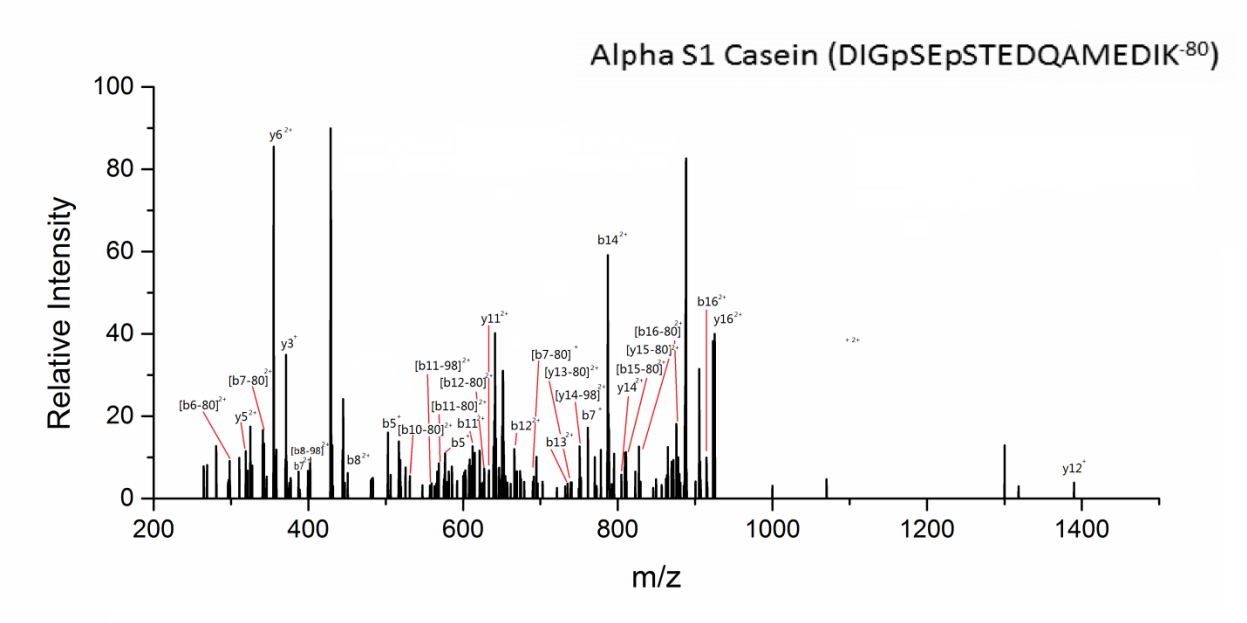

Figure 4.15 Fragmentation of peptide DIGSESTEDQAMEDIK-80 (α-S1-casein). The parent ion has a phosphate loss that can be on either position 4 or 6. Both condition were included when analyzing the spectra.

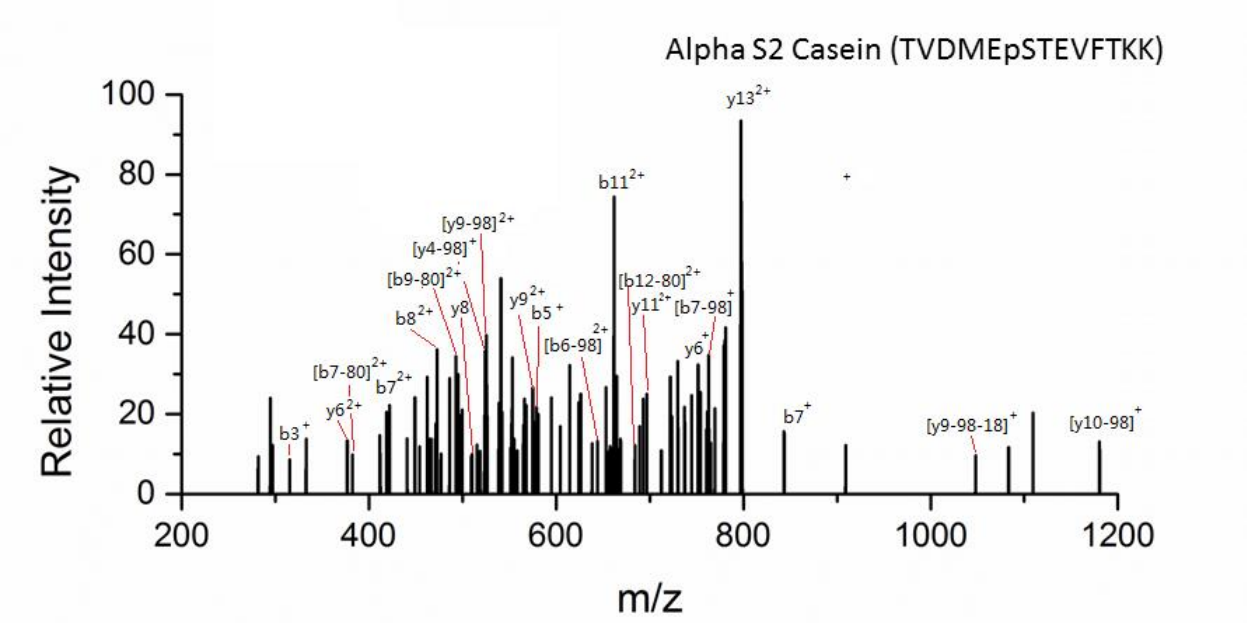

Figure 4.16 Fragmentation of peptide TVDMESTEVFTKK (α-S2-casein).

4.4.5 Technical Considerations in the DMF SAWN Platform

The DMF-SAWN platform proved capable of digesting protein mixtures on chip, enriching phosphorylated peptides, and identifying peptides through SAWN-MS and SAWN-MS/MS. However, as a homemade platform, the DMF-SAWN platform has several limitations that could be further improved. Following are some of the obvious limitations and possible improvements to the methods.

1) The on-chip trypsin digestion. In the above method, the amount of trypsin consumed was five times higher compared to the traditional digestion process. Under the assumption that 200 seconds of plume is needed to completely analyze one complex mixture, about 15 liquid droplets of digested peptide solution are required. The total amount of protein sample will be around 10 ng. Therefore the use of trypsin will be 5-10 times that used in a normal digestion process for the same amount of protein. For a more complicated sample, the amount will increase accordingly with the amount of protein. On the other hand, trypsin self-digestion brought in peptides that were not the target of the research. While in these experiments the trypsin self-digestion peptides were mostly washed off in the separation step, it might be present in certain research that does not include separation.

2) Low signal intensity. Although SAWN was modified in the previous chapter for higher efficiency and higher signal intensity, in the DMF-SAWN design the SAWN part was the original progressive wave design without DC voltage. The signal intensity of DMF-SAWN chip was still low even from the tandem mass spectra of some peptides and in general lower than ESI. A simple solution involves incorporating the SW concept into future DMF-SAWN chips.

3) One-plate system with ITO glass. The system used in this experiment was a one-plate DMF with SAWN on the same plate. ITO glass was moved up and down due to different needs. PDMS spacers were used to control the distance between the ITO glass and the bottom wafer. As a prototype, it proved the concept of DMF-SAWN was useful in sample preparation before mass spectrometry analysis. However, it was not a stable system that was easy to use.

4) Single reaction channel. The DMF-SAWN chip was a single channel chip. If the design was improved multiple reactions would be carried out on chip simultaneously. This would decrease the average time per sample and increase the throughput.

Over all, the above problems had limited the present DMF-SAWN platform to be a better complex sample preparation process or to be a high throughput analysis. The fabrication cost and consumption of the enzyme also make it economically unfeasible. However, there are several changes we can make to the present DMF-SAWN device to improve the overall performance and reduce the cost such as following.

1) Use a two-plate system instead of the present one-plate system. Fabrication of lithium niobate is challenging due to its piezoelectric properties, especially the deformation caused by temperature change. It is also more expensive compared to silicon wafers or glass wafers. Therefore fabricating the main components on a lithium niobate wafer is not a cost-friendly method.

Since lithium niobate is transparent, it is possible to be used as the top plate, while the bottom plate is a silicon wafer with DMF design. The sample can be nebulized from the top plate. Absorption material for phosphorylated peptide, usually metal oxide such as TiO_2 can be deposited on a specific area on the bottom plate, or be replaced with TiO_2 coated magnetic beads[133,137]. The new design will not need removing and replacing the top plate for multiple times during the process. The DMF plate, which is less durable, could be replaced easily. The top plate can also eliminate evaporation during the incubation.

2) Use SW SAWN or electro-SAWN to enhance the signal intensity of SAWN MS spectra. The performance of SW SAWN was described in Chapter 3. SW SAWN decreased average aerosol droplet size and increased signal intensity. With a two plate system, more space could be used in the fabrication of SW SAWN as a cover plate.

3) Use electromagnetic field and magnetic beads to reduce the use of trypsin. Trypsin-coated magnetic beads have been used for fast and efficient digestion. It could also be applied to DMF-SAWN setup for convenient on chip digestion and the consumption of trypsin can be reduced by repeated use of trypsin coated beads. This would also help clearing the spectra since it would eliminate trypsin self-digestion can be eliminated.

4.5 Conclusion

In this chapter SAWN has been modified to connect with a DMF platform to create a novel platform capable of moving, merging, mixing and nebulizing liquid samples. With this platform, simple sample preparation utilizing biochemical reactions and surface absorption were carried

out prior to MS analysis. The DMF-SAWN on-chip digestion took less than ten minutes to digest the protein and to nebulize it directly from the chip surface. Compared to eight hour traditional digestion, on-chip digestion spectrum presented most of the digested peptides with some miscleavages. The on-chip phosphopeptide separation successfully retained the phosphorylated peptide standard while the non-phosphorylated peptide was washed off. Phosphorylated protein analysis was performed on a DMF-SAWN chip. A mixture of phosphorylated proteins was digested with trypsin on-chip. Peptides from the digestion were separated with absorbance to ITO glass through the DMF controlled movements on-chip. After washing off the non-phosphorylated peptides, the remaining peptides were nebulized and detected with tandem MS. The phosphorylated peptides were identified from all three phosphoprotein. The platform used here for phosphoprotein characterization could potentially be applied to other bio-analytical sample preparations. Finally several technical aspects that can further improve the performance of the DMF-SAWN chip were discussed.

Chapter 5 Conclusions and Perspective

5.1 Conclusions

Following the first paper on SAWN-MS by Heron et al published in 2010, SAWN-MS has received wide notice. The softness of SAWN made it possible to analyze fragile compounds or non-covalent complexes. The simple setup and easy operation made it ideal for SAWN to be combined with miniaturized microfluidic devices for high throughput analysis. There have been multiple research papers published on SAWN since then. It has also been introduced to both the analytical community and the micro fabrication journals. The technique was introduced in review papers on journals such as Lab on a Chip, Analytical Chemistry and Annual Review in Fluid Mech.

The various modifications and refinements made to the original progressive wave SAWN improved the signal intensity while providing some non-direct evidence of the ion generation during SAWN process. Electro-SAWN, SW SAWN as well as other designs not introduced here such as the SAWN probe and ring electrode SAWN was developed. Various coatings such as Teflon® that change the surface properties of SAWN were investigated. SAWN was generated in pulsed mode and continuous mode. Sample injection of SAWN could be either a capillary tube injection that support continuous flow, or a droplet style injection directly from the pipette. The multiple choices of SAWN operation are available for different research or application.

As an on-chip nebulization method, SAWN is naturally compatible with microfluidic methods. DMF-SAWN is an attempt to simplify the sample preparation process before MS analysis. In the

DMF-SAWN setup, biological reactions were performed within several hours, followed by direct mass spectrometry analysis. DMF-SAWN setup also reduced the complexity of the procedures which in turn reduced the possibility of sample losses during transfer processes.

5.2 Perspective

5.2.1 Miniaturization of SAWN device

The SAWN devices were built on a piezoelectric material with gold electrodes. The cost of could be reduced through decreasing the chip size and using a cheaper metal such as Aluminum for the ITD electrode. While some mass spectrometers such as Thermo LTQ has an open source which is easy to modify, other mass spectrometers might have limited space for ionization source. Reduced size SAWN chips can also be mounted easier with multiple mass spectrometers, especially ones with limited area for ion source.

5.2.2 Mechanism study of SAWN

Although the mechanism of SAWN is not yet fully elucidated, the study on native SAWN current and nebulized aerosol droplet size distribution provided some indirect evidence that might be helpful for mechanistic studies. Following the previous studies, a higher frequency SAWN chip can be fabricated and used to control the droplet size through chip design. Different piezoelectric materials and variable surface coatings can also be used to study the origin of the charges.

5.2.3 DMF-SAWN chip for high throughput analysis

DMF-SAWN was able to perform simple biological reactions on chip prior to nebulization. However the present design is a single channel system that could not be applied to high throughput analysis. The future development of DMF-SAWN will be the fabrication of a two-plate system combined with modified magnetic beads for repeated use and high throughput analysis. Transparent SAWN wafers can be used as the cover plate while silicon wafers containing DMF patterns. This will reduce the cost and simplify the chip fabrication.

References

1. Thomson, J. J., LVIII. On the masses of the ions in gases at low pressures. *Philosophical Magazine Series 5* **1899,** *48* (295), 547-567.

2. Thomson, J. J., LIV. Positive rays. *Philosophical Magazine Series 6* **1908,** *16* (94), 657-691.

3. Aston, F. W., LIX. The mass-spectra of chemical elements. *Philosophical Magazine Series 6* **1920,** *39* (233), 611-625.

4. McLafferty, F. W.; Tureček, F., *Interpretation of Mass Spectra*. 4 ed.; University Science Books: Sausalito, California, 1993.

5. Tito, M. A.; Tars, K.; Valegard, K.; Hajdu, J.; Robinson, C. V., Electrospray Time-of-Flight Mass Spectrometry of the Intact MS2 Virus Capsid. *Journal of the American Chemical Society* **2000,** *122* (14), 3550-3551.

6. Gelb, M. H.; Turecek, F.; Scott, C. R.; Chamoles, N. A., Direct multiplex assay of enzymes in dried blood spots by tandem mass spectrometry for the newborn screening of lysosomal storage disorders. *J Inherit Metab Dis* **2006,** *29* (2-3), 397-404.

7. Gary, S., *The Expanding Role of Mass Spectrometry in Biotechnology*. 2 ed.; MCC Press: San Diego, California, 2006.

8. Loo, J. A., Studying noncovalent protein complexes by electrospray ionization mass spectrometry. *Mass Spectrometry Reviews* **1997,** *16* (1), 1-23.

9. Arnold, S. L. M.; Amory, J. K.; Walsh, T. J.; Isoherranen, N., A sensitive and specific method for measurement of multiple retinoids in human serum with UHPLC-MS/MS. *Journal of Lipid Research* **2012,** *53* (3), 587-598.

10. Hiraoka, K.; Kudaka, I., Electrospray interface for liquid chromatography/mass spectrometry. *Rapid Communications in Mass Spectrometry* **1990,** *4* (12), 519-526.

11. Aebersold, R.; Mann, M., Mass spectrometry-based proteomics. *Nature* **2003,** *422* (6928), 198-207.

12. Petrotchenko, E. V.; Borchers, C. H., Crosslinking combined with mass spectrometry for structural proteomics. *Mass Spectrom Rev* **2010,** *29* (6), 862-76.

13. Percy, A. J.; Rey, M.; Burns, K. M.; Schriemer, D. C., Probing protein interactions with hydrogen/deuterium exchange and mass spectrometry-a review. *Anal Chim Acta* **2012,** *721*, 7-21.

14. Jones, J. W.; Cohen, I. E.; Turecek, F.; Goodlett, D. R.; Ernst, R. K., Comprehensive structure characterization of lipid A extracted from Yersinia pestis for determination of its phosphorylation configuration. *J Am Soc Mass Spectrom* **2010,** *21* (5), 785-99.

15. Schone, C.; Hofler, H.; Walch, A., MALDI imaging mass spectrometry in cancer research: combining proteomic profiling and histological evaluation. *Clin Biochem* **2013,** *46* (6), 539-45.

16. Tanaka, K.; Waki, H.; Ido, Y.; Akita, S.; Yoshida, Y.; Yoshida, T.; Matsuo, T., Protein and polymer analyses up to *m/z* 100 000 by laser ionization time-of-flight mass spectrometry. *Rapid Communications in Mass Spectrometry* **1988,** *2* (8), 151-153.

17. Fenn, J. B.; Mann, M.; Meng, C. K.; Wong, S. F.; Whitehouse, C. M., Electrospray ionization for mass spectrometry of large biomolecules. *Science* **1989,** *246* (4926), 64-71.

18. Juraschek, R.; Dulcks, T.; Karas, M., Nanoelectrospray - More Than Just a Minimized-Flow Electrospray Ionization Source. *Journal of the American Society for Mass Spectrometry* **1999,** *10* (4), 300-308.

19. Huang, M.-Z.; Cheng, S.-C.; Cho, Y.-T.; Shiea, J., Ambient ionization mass spectrometry: A tutorial. *Analytica Chimica Acta* **2011,** *702* (1), 1-15.

20. Weston, D. J., Ambient ionization mass spectrometry: current understanding of mechanistic theory; analytical performance and application areas. *Analyst* **2010,** *135* (4), 661-668; Nemes, P.; Vertes, A., Laser ablation electrospray ionization for atmospheric pressure, in vivo, and imaging mass spectrometry. *Anal Chem* **2007,** *79* (21), 8098-106.

21. Harper, J. D.; Charipar, N. A.; Mulligan, C. C.; Zhang, X.; Cooks, R. G.; Ouyang, Z., Low-temperature plasma probe for ambient desorption ionization. *Anal Chem* **2008,** *80* (23), 9097-104.

22. Takáts, Z.; Wiseman, J. M.; Gologan, B.; Cooks, R. G., Mass spectrometry sampling under ambient conditions with desorption electrospray ionization. *Science* **2004,** *306* (5695), 471-3.

23. Takáts, Z.; Wiseman, J. M.; Cooks, R. G., Ambient mass spectrometry using desorption electrospray ionization (DESI): instrumentation, mechanisms and applications in forensics, chemistry, and biology. *J Mass Spectrom* **2005,** *40* (10), 1261-75.

24. Takats, Z.; Cotte-Rodriguez, I.; Talaty, N.; Chen, H.; Cooks, R. G., Direct, trace level detection of explosives on ambient surfaces by desorption electrospray ionization mass spectrometry. *Chemical Communications* **2005,** (15), 1950-1952.

25. McEwen, C. N.; McKay, R. G.; Larsen, B. S., Analysis of solids, liquids, and biological tissues using solids probe introduction at atmospheric pressure on commercial LC/MS instruments. *Anal Chem* **2005,** *77* (23), 7826-31.

26. Wu, J.; Hughes, C. S.; Picard, P.; Letarte, S.; Gaudreault, M.; Levesque, J. F.; Nicoll-Griffith, D. A.; Bateman, K. P., High-throughput cytochrome P450 inhibition assays using laser diode thermal desorption-atmospheric pressure chemical ionization-tandem mass spectrometry. *Anal Chem* **2007,** *79* (12), 4657-65.

27. Cody, R. B.; Laramée, J. A.; Durst, H. D., Versatile new ion source for the analysis of materials in open air under ambient conditions. *Anal Chem* **2005,** *77* (8), 2297-302.

28. Huang, M. Z.; Hsu, H. J.; Wu, C. I.; Lin, S. Y.; Ma, Y. L.; Cheng, T. L.; Shiea, J., Characterization of the chemical components on the surface of different solids with electrospray-assisted laser desorption ionization mass spectrometry. *Rapid Commun Mass Spectrom* **2007,** *21* (11), 1767-75.

29. Chen, H.; Venter, A.; Cooks, R. G., Extractive electrospray ionization for direct analysis of undiluted urine, milk and other complex mixtures without sample preparation. *Chemical Communications* **2006,** (19), 2042-2044.

30. Gilbert-López, B.; Schilling, M.; Ahlmann, N.; Michels, A.; Hayen, H.; Molina-Díaz, A.; García-Reyes, J. F.; Franzke, J., Ambient diode laser desorption dielectric barrier discharge ionization mass spectrometry of nonvolatile chemicals. *Anal Chem* **2013,** *85* (6), 3174-82.

31. Haapala, M.; Pól, J.; Saarela, V.; Arvola, V.; Kotiaho, T.; Ketola, R. A.; Franssila, S.; Kauppila, T. J.; Kostiainen, R., Desorption atmospheric pressure photoionization. *Anal Chem* **2007,** *79* (20), 7867-72.

32. Na, N.; Zhao, M.; Zhang, S.; Yang, C.; Zhang, X., Development of a dielectric barrier discharge ion source for ambient mass spectrometry. *J Am Soc Mass Spectrom* **2007,** *18* (10), 1859-62.

33. Sampson, J. S.; Hawkridge, A. M.; Muddiman, D. C., Generation and detection of multiply-charged peptides and proteins by matrix-assisted laser desorption electrospray ionization (MALDESI) Fourier transform ion cyclotron resonance mass spectrometry. *J Am Soc Mass Spectrom* **2006,** *17* (12), 1712-6.

34. Ratcliffe, L. V.; Rutten, F. J.; Barrett, D. A.; Whitmore, T.; Seymour, D.; Greenwood, C.; Aranda-Gonzalvo, Y.; Robinson, S.; McCoustra, M., Surface analysis under ambient conditions using plasma-assisted desorption/ionization mass spectrometry. *Anal Chem* **2007,** *79* (16), 6094-101.

35. Shelley, J. T.; Ray, S. J.; Hieftje, G. M., Laser ablation coupled to a flowing atmospheric pressure afterglow for ambient mass spectral imaging. *Anal Chem* **2008,** *80* (21), 8308-13.

36. Haddad, R.; Sparrapan, R.; Kotiaho, T.; Eberlin, M. N., Easy ambient sonic-spray ionization-membrane interface mass spectrometry for direct analysis of solution constituents. *Anal Chem* **2008,** *80* (3), 898-903.

37. Rezenom, Y. H.; Dong, J.; Murray, K. K., Infrared laser-assisted desorption electrospray ionization mass spectrometry. *Analyst* **2008,** *133* (2), 226-232.

38. Nyadong, L.; Galhena, A. S.; Fernandez, F. M., Desorption electrospray/metastable-induced ionization: a flexible multimode ambient ion generation technique. *Anal Chem* **2009,** *81* (18), 7788-94.

39. Ren, Y.; Wang, H.; Liu, J.; Zhang, Z.; McLuckey, M. N.; Ouyang, Z., Analysis of Biological Samples Using Paper Spray Mass Spectrometry: An Investigation of Impacts by the Substrates, Solvents and Elution Methods. *Chromatographia* **2013,** *76* (19-20), 1339-1346.

40. Wang, H.; Wu, Y.; Guo, B.; Sun, W.; Ding, L.; Chen, B., Quantification of low-polar small molecules using room temperature ionic liquids matrix-assisted desorption corona beam ionization. *Analyst* **2012,** *137* (17), 3982-8.

41. Ko, J. Y.; Choi, S. M.; Rhee, Y. M.; Beauchamp, J. L.; Kim, H. I., Studying interfacial reactions of cholesterol sulfate in an unsaturated phosphatidylglycerol layer with ozone using field induced droplet ionization mass spectrometry. *J Am Soc Mass Spectrom* **2012,** *23* (1), 141-52.

42. Liu, J.; Zhang, C.; Sun, J.; Ren, X.; Luo, H., Laser desorption dual spray post-ionization mass spectrometry for direct analysis of samples via two informative channels. *J Mass Spectrom* **2013,** *48* (2), 250-4.

43. Lin, J. Y.; Chen, T. Y.; Chen, J. Y.; Chen, Y. C., Multilayer gold nanoparticle-assisted thermal desorption ambient mass spectrometry for the analysis of small organics. *Analyst* **2010,** *135* (10), 2668-75.

44. Wu, C. I.; Wang, Y. S.; Chen, N. G.; Wu, C. Y.; Chen, C. H., Ultrasound ionization of biomolecules. *Rapid Commun Mass Spectrom* **2010,** *24* (17), 2569-74.

45. Cooks, R. G.; Ouyang, Z.; Takats, Z.; Wiseman, J. M., Detection Technologies. Ambient mass spectrometry. *Science* **2006,** *311* (5767), 1566-70.

46. Rezk, A. R.; Qi, A.; Friend, J. R.; Li, W. H.; Yeo, L. Y., Uniform mixing in paper-based microfluidic systems using surface acoustic waves. *Lab Chip* **2012,** *12* (4), 773-9.

47. Collins, D. J.; Manor, O.; Winkler, A.; Schmidt, H.; Friend, J. R.; Yeo, L. Y., Atomization off thin water films generated by high-frequency substrate wave vibrations. *Physical Review E* **2012,** *86* (5), 056312.

48. Heron, S. R.; Wilson, R.; Shaffer, S. A.; Goodlett, D. R.; Cooper, J. M., Surface Acoustic Wave Nebulization of Peptides As a Microfluidic Interface for Mass Spectrometry. *Analytical Chemistry* **2010,** *82* (10), 3985-3989.

49. Bourquin, Y.; Reboud, J.; Wilson, R.; Zhang, Y.; Cooper, J. M., Integrated immunoassay using tuneable surface acoustic waves and lensfree detection. *Lab on a Chip* **2011,** *11* (16), 2725-2730.

50. Shilton, R. J.; Yeo, L. Y.; Friend, J. R., Quantification of surface acoustic wave induced chaotic mixing-flows in microfluidic wells. *Sensors and Actuators B: Chemical* **2011,** *160* (1), 1565-1572.

51. Tarasow, T. M.; Penny, L.; Patwardhan, A.; Hamren, S.; McKenna, M. P.; Urdea, M. S., Microfluidic strategies applied to biomarker discovery and validation for multivariate diagnostics. *Bioanalysis* **2011,** *3* (19), 2233-2251.

52. Ding, X.; Li, P.; Lin, S.-C. S.; Stratton, Z. S.; Nama, N.; Guo, F.; Slotcavage, D.; Mao, X.; Shi, J.; Costanzo, F.; Huang, T. J., Surface acoustic wave microfluidics. *Lab on a Chip* **2013,** *13* (18), 3626-3649.

53. Kulkarni, K.; Friend, J.; Yeo, L.; Perlmutter, P., Surface acoustic waves as an energy source for drop scale synthetic chemistry. *Lab on a Chip* **2009,** *9* (6), 754-755.

54. Alvarez, M.; Friend, J.; Yeo, L. Y., Rapid generation of protein aerosols and nanoparticles via surface acoustic wave atomization. *Nanotechnology* **2008,** *19* (45), 455103.

55. Vuong, T.; Qi, A.; Muradoglu, M.; Cheong, B. H.-P.; Liew, O. W.; Ang, C. X.; Fu, J.; Yeo, L.; Friend, J.; Ng, T. W., Precise drop dispensation on superhydrophobic surfaces using acoustic nebulization. *Soft Matter* **2013,** *9* (13), 3631-3639.

56. Qi, A.; Friend, J. R.; Yeo, L. Y.; Morton, D. A. V.; McIntosh, M. P.; Spiccia, L., Miniature Inhalation Therapy Platform Using Surface Acoustic Wave Microfluidic Atomization. *Lab Chip* **2009,** *9* (15), 2184-2193.

57. Qi, A.; Yeo, L.; Friend, J.; Ho, J., The extraction of liquid, protein molecules and yeast cells from paper through surface acoustic wave atomization. *Lab Chip* **2010,** *10* (4), 470-6.

58. Yeo, L. Y.; Friend, J. R.; McIntosh, M. P.; Meeusen, E. N.; Morton, D. A., Ultrasonic nebulization platforms for pulmonary drug delivery. *Expert Opin Drug Deliv* **2010,** *7* (6), 663-79.

59. Raghavan, R.; Friend, J.; Yeo, L., Particle concentration via acoustically driven microcentrifugation: microPIV flow visualization and numerical modelling studies. *Microfluidics and Nanofluidics* **2010,** *8* (1), 73-84.

60. Gao, D.; Liu, H.; Jiang, Y.; Lin, J. M., Recent advances in microfluidics combined with mass spectrometry: technologies and applications. *Lab Chip* **2013,** *13* (17), 3309-22.

61. Huang, Y.; Yoon, S. H.; Heron, S. R.; Masselon, C. D.; Edgar, J. S.; Tureček, F.; Goodlett, D. R., Surface acoustic wave nebulization produces ions with lower internal energy than electrospray ionization. *J Am Soc Mass Spectrom* **2012,** *23* (6), 1062-70.

62. Ho, J.; Tan, M. K.; Go, D. B.; Yeo, L. Y.; Friend, J. R.; Chang, H. C., Paper-Based Microfluidic Surface Acoustic Wave Sample Delivery and Ionization Source for Rapid and Sensitive Ambient Mass Spectrometry. *Analytical Chemistry* **2011,** *83* (9), 3260-3266.

63. Yoon, S. H.; Huang, Y.; Edgar, J. S.; Ting, Y. S.; Heron, S. R.; Kao, Y.; Li, Y.; Masselon, C. D.; Ernst, R. K.; Goodlett, D. R., Surface acoustic wave nebulization facilitating lipid mass spectrometric analysis. *Anal Chem* **2012,** *84* (15), 6530-7.

64. Frieder Mugele and Jean-Christophe, B., Electrowetting: from basics to applications. *Journal of Physics: Condensed Matter* **2005,** *17* (28), R705.

65. Pollack, M. G.; Fair, R. B.; Shenderov, A. D., Electrowetting-based actuation of liquid droplets for microfluidic applications. *Applied Physics Letters* **2000,** *77* (11), 1725-1726.

66. Miller, E. M.; Ng, A. H.; Uddayasankar, U.; Wheeler, A. R., A digital microfluidic approach to heterogeneous immunoassays. *Anal Bioanal Chem* **2011,** *399* (1), 337-45.

67. Wheeler, A. R., Chemistry. Putting electrowetting to work. *Science* **2008,** *322* (5901), 539-40.

68. Kim, H.; Jebrail, M. J.; Sinha, A.; Bent, Z. W.; Solberg, O. D.; Williams, K. P.; Langevin, S. A.; Renzi, R. F.; Van De Vreugde, J. L.; Meagher, R. J.; Schoeniger, J. S.; Lane, T. W.; Branda, S. S.; Bartsch, M. S.; Patel, K. D., A Microfluidic DNA Library Preparation Platform for Next-Generation Sequencing. *PLoS ONE* **2013,** *8* (7), e68988.

69. Kreutz, J. E.; Munson, T.; Huynh, T.; Shen, F.; Du, W.; Ismagilov, R. F., Theoretical Design and Analysis of Multivolume Digital Assays with Wide Dynamic Range Validated Experimentally with Microfluidic Digital PCR. *Analytical Chemistry* **2011,** *83* (21), 8158-8168.

70. Shen, F.; Du, W.; Kreutz, J. E.; Fok, A.; Ismagilov, R. F., Digital PCR on a SlipChip. *Lab on a Chip* **2010,** *10* (20), 2666-2672.

71. Barbulovic-Nad, I.; Yang, H.; Park, P. S.; Wheeler, A. R., Digital microfluidics for cell-based assays. *Lab Chip* **2008,** *8* (4), 519-26.

72. Kirby, A. E.; Wheeler, A. R., Digital Microfluidics: An Emerging Sample Preparation Platform for Mass Spectrometry. *Analytical Chemistry* **2013,** *85* (13), 6178-6184.

73. Collette, C.; De Pauw, E., Calibration of the internal energy distribution of ions produced by electrospray. *Rapid Communications in Mass Spectrometry* **1998,** *12* (4), 165-170.

74. Naban-Maillet, J.; Lesage, D.; Bossee, A.; Gimbert, Y.; Sztaray, J.; Vekey, K.; Tabet, J. C., Internal energy distribution in electrospray ionization. *Journal of Mass Spectrometry* **2005,** *40* (1), 1-8.

75. Greisch, J. F.; Gabelica, V.; Remacle, F.; De Pauw, E., Thermometer ions for matrix-enhanced laser desorption/ionization internal energy calibration. *Rapid Communications in Mass Spectrometry* **2003,** *17* (16), 1847-1854.

76. Luo, G. H.; Marginean, I.; Vertes, A., Internal energy of ions generated by matrix-assisted laser desorption/ionization. *Analytical Chemistry* **2002,** *74* (24), 6185-6190.

77. Nefliu, M.; Smith, J. N.; Venter, A.; Cooks, R. G., Internal energy distributions in desorption electrospray ionization (DESI). *J Am Soc Mass Spectrom* **2008,** *19* (3), 420-7.

78. Touboul, D.; Jecklin, M. C.; Zenobi, R., Ion internal energy distributions validate the charge residue model for small molecule ion formation by spray methods. *Rapid Commun Mass Spectrom* **2008,** *22* (7), 1062-8.

79. Dagan, S.; Hua, Y. M.; Boday, D. J.; Somogyi, A.; Wysocki, R. J.; Wysocki, V. H., Internal energy deposition with silicon nanoparticle-assisted laser desorption/ionization (SPALDI) mass spectrometry. *International Journal of Mass Spectrometry* **2009,** *283* (1-3), 200-205.

80. Harris, G. A.; Hostetler, D. M.; Hampton, C. Y.; Fernandez, F. M., Comparison of the internal energy deposition of direct analysis in real time and electrospray ionization time-of-flight mass spectrometry. *J Am Soc Mass Spectrom* **2010,** *21* (5), 855-63.

81. Zins, E. L.; Pepe, C.; Schroder, D., Energy-dependent dissociation of benzylpyridinium ions in an ion-trap mass spectrometer. *Journal of Mass Spectrometry* **2010,** *45* (11), 1253-1260.

82. Zins, E. L.; Pepe, C.; Rondeau, D.; Rochut, S.; Galland, N.; Tabet, J. C., Theoretical and experimental study of tropylium formation from substituted benzylpyridinium species. *Journal of Mass Spectrometry* **2009,** *44* (1), 12-17.

83. Zins, E. L.; Rondeau, D.; Karoyan, P.; Fosse, C.; Rochut, S.; Pepe, C., Investigations of the fragmentation pathways of benzylpyridinium ions under ESI/MS conditions. *Journal of Mass Spectrometry* **2009,** *44* (12), 1668-1675.

84. Barylyuk, K. V.; Chingin, K.; Balabin, R. M.; Zenobi, R., Fragmentation of benzylpyridinium "thermometer" ions and its effect on the accuracy of internal energy calibration. *J Am Soc Mass Spectrom* **2010,** *21* (1), 172-7.

85. Curtiss, L. A.; Raghavachari, K.; Trucks, G. W.; Pople, J. A., Gaussain-2 theory for molecular energies of foirst and second-row compounds. *J. Chem. Phys.* **1991,** *94*, 7221-7230.

86. Frisch, M. J.; Trucks, G. W.; Schlegel, H. B.; Scuseria, G. E.; Robb, M. A.; Cheeseman, J. R.; Montgomery, J. A.; Jr., T. V.; Kudin, K. N.; Burant, J. C.; Millam, J. M.; Iyengar, S. S.; Tomasi, J.; Barone, V.; Mennucci, B.; Cossi, M.; Scalmani, G.; Rega, N.; Petersson, G. A.; Nakatsuji, H.; Hada, M.; Ehara, M.; Toyota, K.; Fukuda, R.; Hasegawa, J.; Ishida, M.; Nakajima, T.; Honda, Y.; Kitao, O.; Nakai, H.; Klene, M.; Li, X.; Knox, J. E.; Hratchian, H. P.; Cross, J. B.; Bakken, V.; Adamo, C.; Jaramillo, J.; Gomperts, R.; Stratmann, R. E.; Yazyev, O.; Austin, A. J.; Cammi, R.; Pomelli, C.; Ochterski, J. W.; Ayala, P. Y.; Morokuma, K.; Voth, G. A.; Salvador, P.; Dannenberg, J. J.; Zakrzewski, V. G.; Dapprich, S.; Daniels, A. D.; Strain, M. C.; Farkas, O.; Malick, D. K.; Rabuck, A. D.; Raghavachari, K.; Foresman, J. B.; Ortiz, J. V.; Cui, Q.; Baboul, A. G.; Clifford, S.; Cioslowski, J.; Stefanov, B. B.; Liu, G.; Liashenko, A.; Piskorz, P.; Komaromi, I.; Martin, R. L.; Fox, D. J.; Keith, T.; Al-Laham, M. A.; Peng, C. Y.; Nanayakkara, A.; Challacombe, M.; Gill, P. M. W.; Johnson, B.; Chen, W.; Wong, M. W.; Gonzalez, C.; Pople, J. A., *Gaussian 03, Revision B. 05*. Gaussian, Inc.: Pittsburgh PA, , 2003.

87. Becke, A. D., A New Mixing of Hartree-Fock and Local Density-Functional Theories. *Journal of Chemical Physics* **1993,** *98* (2), 1372-1377.

88. Becke, A. D., Density-Functional Thermochemistry .3. The Role of Exact Exchange. *Journal of Chemical Physics* **1993,** *98* (7), 5648-5652; Stephens, P. J.; Devlin, F. J.; Chabalowski, C. F.; Frisch, M. J., Ab-Initio Calculation of Vibrational Absorption and Circular-Dichroism Spectra Using Density-Functional Force-Fields. *Journal of Physical Chemistry* **1994,** ***98*** (45), 11623-11627.

89. Čížek, J.; Paldus, J.; Šroubková, L., Cluster Expansion Analysis for Delocalized Systems. *International Journal of Quantum Chemistry* **1969,** *3* (2), 149-167.

90. Purvis, G. D.; Bartlett, R. J., A Full Coupled-Cluster Singles and Doubles Model - the Inclusion of Disconnected Triples. *Journal of Chemical Physics* **1982,** *76* (4), 1910-1918.

91. Smith, J. N.; Flagan, R. C.; Beauchamp, J. L., Droplet Evaporation and Discharge Dynamics in Electrospray Ionization. *The Journal of Physical Chemistry A* **2002,** *106* (42), 9957-9967.

92. Wortmann, A.; Kistler-Momotova, A.; Zenobi, R.; Heine, M.; Wilhelm, O.; Pratsinis, S., Shrinking Droplets in Electrospray Ionization and their Influence on Chemical Equilibria. *Journal of the American Society for Mass Spectrometry* **2007,** *18* (3), 385-393.

93. Kebarle, P., A brief overview of the present status of the mechanisms involved in electrospray mass spectrometry. *Journal of Mass Spectrometry* **2000,** *35* (7), 804-817.

94. Kebarle, P.; Tang, L., From ions in solution to ions in the gas phase - the mechanism of electrospray mass spectrometry. *Analytical Chemistry* **1993,** *65* (22), 972A-986A.

95. Kasimanickam, V. R.; Kasimanickam, R. K., Retinoic acid signaling biomarkers after treatment with retinoic acid and retinoic acid receptor alpha antagonist (Ro 41-5253) in canine testis: an in vitro organ culture study. *Theriogenology* **2013,** *79* (1), 10-6.

96. Bushue, N.; Wan, Y. J., Retinoid pathway and cancer therapeutics. *Adv Drug Deliv Rev* **2010,** *62* (13), 1285-98.

97. Jones, J. W.; Shaffer, S. A.; Ernst, R. K.; Goodlett, D. R.; Turecek, F., Determination of pyrophosphorylated forms of lipid A in Gram-negative bacteria using a multivaried mass spectrometric approach. *Proc Natl Acad Sci U S A* **2008,** *105* (35), 12742-7.

98. Ting, Y. S.; Shaffer, S. A.; Jones, J. W.; Ng, W. V.; Ernst, R. K.; Goodlett, D. R., Automated lipid A structure assignment from hierarchical tandem mass spectrometry data. *J Am Soc Mass Spectrom* **2011,** *22* (5), 856-66.

99. Domingues, M. R. M.; Reis, A.; Domingues, P., Mass spectrometry analysis of oxidized phospholipids. *Chemistry and Physics of Lipids* **2008,** *156* (1–2), 1-12.

100. Ivanova, P. T.; Cerda, B. A.; Horn, D. M.; Cohen, J. S.; McLafferty, F. W.; Brown, H. A., Electrospray ionization mass spectrometry analysis of changes in phospholipids in RBL-2H3 mastocytoma cells during degranulation. *Proceedings of the National Academy of Sciences* **2001,** *98* (13), 7152-7157.

101. Pulfer M Fau - Murphy, R. C.; Murphy, R. C., Electrospray mass spectrometry of phospholipids. **2003,** (0277-7037 (Print)).

102. Garc á-Reyes, J. F.; Mazzoti, F.; Harper, J. D.; Charipar, N. A.; Oradu, S.; Ouyang, Z.; Sindona, G.; Cooks, R. G., Direct olive oil analysis by low-temperature plasma (LTP) ambient ionization mass spectrometry. *Rapid Commun Mass Spectrom* **2009,** *23* (19), 3057-62.

103. Ju, J.; Yamagata, Y.; Ohmori, H.; Higuchi, T., Standing wave type surface acoustic wave atomizer. *Sensors and Actuators A: Physical* **2008,** *147* (2), 570-575.

104. Jurchen, J. C.; Garcia, D. E.; Williams, E. R., Further studies on the origins of asymmetric charge partitioning in protein homodimers. *J Am Soc Mass Spectrom* **2004,** *15* (10), 1408-15.

105. Jebrail, M. J.; Wheeler, A. R., Let's get digital: digitizing chemical biology with microfluidics. *Current Opinion in Chemical Biology* **2010,** *14* (5), 574-581.

106. Luk, V. N.; Wheeler, A. R., A Digital Microfluidic Approach to Proteomic Sample Processing. *Analytical Chemistry* **2009,** *81* (11), 4524-4530.

107. Klarman, D.; Andelman, D.; Urbakh, M., A Model of Electrowetting, Reversed Electrowetting, and Contact Angle Saturation. *Langmuir* **2011,** *27* (10), 6031-6041.

108. Blacken, G. R.; Volny, M.; Diener, M.; Jackson, K. E.; Ranjitkar, P.; Maly, D. J.; Turecek, F., Reactive landing of gas-phase ions as a tool for the fabrication of metal oxide surfaces for in situ phosphopeptide enrichment. *J Am Soc Mass Spectrom* **2009,** *20* (6), 915-26.

109. Abdelgawad, M.; Park, P.; Wheeler, A. R., Optimization of device geometry in single-plate digital microfluidics. *Journal of Applied Physics* **2009,** *105* (9), 094506-7.

110. Shih, S. C.; Barbulovic-Nad, I.; Yang, X.; Fobel, R.; Wheeler, A. R., Digital microfluidics with impedance sensing for integrated cell culture and analysis. *Biosens Bioelectron* **2013,** *42*, 314-20.

111. Rane, T. D.; Zec, H. C.; Puleo, C.; Lee, A. P.; Wang, T.-H., Droplet microfluidics for amplification-free genetic detection of single cells. *Lab on a Chip* **2012,** *12* (18), 3341-3347.

112. Shih, S. C.; Yang, H.; Jebrail, M. J.; Fobel, R.; McIntosh, N.; Al-Dirbashi, O. Y.; Chakraborty, P.; Wheeler, A. R., Dried blood spot analysis by digital microfluidics coupled to nanoelectrospray ionization mass spectrometry. *Anal Chem* **2012,** *84* (8), 3731-8.

113. Choi, K.; Ng, A. H. C.; Fobel, R.; Wheeler, A. R., Digital Microfluidics. *Annual Review of Analytical Chemistry* **2012,** *5* (1), 413-440.

114. Barbulovic-Nad, I.; Yang, H.; Park, P. S.; Wheeler, A. R., Digital microfluidics for cell-based assays. *Lab on a Chip* **2008,** *8* (4), 519-526.

115. Fan, S.-K.; Huang, P.-W.; Wang, T.-T.; Peng, Y.-H., Cross-scale electric manipulations of cells and droplets by frequency-modulated dielectrophoresis and electrowetting. *Lab on a Chip* **2008,** *8* (8), 1325-1331.

116. Zhou, J.; Lu, L.; Byrapogu, K.; Wootton, D. M.; Lelkes, P. I.; Fair, R., Electrowetting-based multi-microfluidics array printing of high resolution tissue construct with embedded cells and growth factors. *Virtual and Physical Prototyping* **2007,** *2* (4), 217-223.

117. Chang, Y.-H.; Lee, G.-B.; Huang, F.-C.; Chen, Y.-Y.; Lin, J.-L., Integrated polymerase chain reaction chips utilizing digital microfluidics. *Biomedical Microdevices* **2006,** *8* (3), 215-225.

118. Sista, R. S.; Eckhardt, A. E.; Srinivasan, V.; Pollack, M. G.; Palanki, S.; Pamula, V. K., Heterogeneous immunoassays using magnetic beads on a digital microfluidic platform. *Lab on a Chip* **2008,** *8* (12), 2188-2196.

119. Kirby, A. E.; Wheeler, A. R., Microfluidic origami: a new device format for in-line reaction monitoring by nanoelectrospray ionization mass spectrometry. *Lab on a Chip* **2013,** *13* (13), 2533-2540.

120. Freire, S. L.; Wheeler, A. R., Proteome-on-a-chip: mirage, or on the horizon? *Lab Chip* **2006,** *6* (11), 1415-23.

121. Salih, E., Phosphoproteomics by mass spectrometry and classical protein chemistry approaches. *Mass Spectrom Rev* **2005,** *24* (6), 828-46.

122. Singh, P.; Shaffer, S. A.; Scherl, A.; Holman, C.; Pfuetzner, R. A.; Freeman, T. J. L.; Miller, S. I.; Hernandez, P.; Appel, R. D.; Goodlett, D. R., Characterization of Protein Cross-Links via Mass Spectrometry and an Open-Modification Search Strategy. *Analytical Chemistry* **2008,** *80* (22), 8799-8806.

123. Kjellstrom, S.; Jensen, O. N., Phosphoric acid as a matrix additive for MALDI MS analysis of phosphopeptides and phosphoproteins. *Anal Chem* **2004,** *76* (17), 5109-17.

124. Dunn, J. D.; Reid, G. E.; Bruening, M. L., Techniques for phosphopeptide enrichment prior to analysis by mass spectrometry. *Mass Spectrom Rev* **2010,** *29* (1), 29-54.

125. Thingholm, T. E.; Jensen, O. N., Enrichment and characterization of phosphopeptides by immobilized metal affinity chromatography (IMAC) and mass spectrometry. *Methods Mol Biol* **2009,** *527*, 47-56, xi.

126. Thingholm, T. E.; Jensen, O. N.; Larsen, M. R., Enrichment and separation of mono- and multiply phosphorylated peptides using sequential elution from IMAC prior to mass spectrometric analysis. *Methods Mol Biol* **2009,** *527*, 67-78, xi.

127. Wu, H. T.; Hsu, C. C.; Tsai, C. F.; Lin, P. C.; Lin, C. C.; Chen, Y. J., Nanoprobe-based immobilized metal affinity chromatography for sensitive and complementary enrichment of multiply phosphorylated peptides. *Proteomics* **2011,** *11* (13), 2639-53.

128. Cuccurullo, M.; Schlosser, G.; Cacace, G.; Malorni, L.; Pocsfalvi, G., Identification of phosphoproteins and determination of phosphorylation sites by zirconium dioxide enrichment and SELDI-MS/MS. *J Mass Spectrom* **2007,** *42* (8), 1069-78.

129. Chen, C. J.; Lai, C. C.; Tseng, M. C.; Liu, Y. C.; Lin, S. Y.; Tsai, F. J., Simple fabrication of hydrophobic surface target for increased sensitivity and homogeneity in matrix-assisted laser desorption/ionization time-of-flight mass spectrometry analysis of peptides, phosphopeptides, carbohydrates and proteins. *Anal Chim Acta* **2013,** *783*, 31-8.

130. Eriksson, A.; Bergquist, J.; Edwards, K.; Hagfeldt, A.; Malmstrom, D.; Agmo Hernandez, V., Optimized protocol for on-target phosphopeptide enrichment prior to matrix-assisted laser desorption-ionization mass spectrometry using mesoporous titanium dioxide. *Anal Chem* **2010,** *82* (11), 4577-83.

131. Krasny, L.; Pompach, P.; Strohalm, M.; Obsilova, V.; Strnadova, M.; Novak, P.; Volny, M., In-situ enrichment of phosphopeptides on MALDI plates modified by ambient ion landing. *J Mass Spectrom* **2012,** *47* (10), 1294-302.

132. Blacken, G. R.; Volny, M.; Vaisar, T.; Sadilek, M.; Turecek, F., In situ enrichment of phosphopeptides on MALDI plates functionalized by reactive landing of zirconium(IV)-n-propoxide ions. *Anal Chem* **2007,** *79* (14), 5449-56.

133. Lo, C.-Y.; Chen, W.-Y.; Chen, C.-T.; Chen, Y.-C., Rapid Enrichment of Phosphopeptides from Tryptic Digests of Proteins Using Iron Oxide Nanocomposites of Magnetic Particles Coated with Zirconia as the Concentrating Probes. *Journal of Proteome Research* **2006,** *6* (2), 887-893.

134. Kouvonen, P.; Rainio, E. M.; Suni, V.; Koskinen, P.; Corthals, G. L., Enrichment and sequencing of phosphopeptides on indium tin oxide coated glass slides. *Mol Biosyst* **2011,** *7* (6), 1828-37.

135. Kulkarni, K. P.; Ramarathinam, S. H.; Friend, J.; Yeo, L.; Purcell, A. W.; Perlmutter, P., Rapid microscale in-gel processing and digestion of proteins using surface acoustic waves. *Lab Chip* **2010,** *10* (12), 1518-20.

136. Baum, F.; Ebner, J.; Pischetsrieder, M., Identification of Multiphosphorylated Peptides in Milk. *J Agric Food Chem* **2013**.

137. Huang, Y.; Shi, Q.; Tsung, C. K.; Gunawardena, H. P.; Xie, L.; Yu, Y.; Liang, H.; Yang, P.; Stucky, G. D.; Chen, X., An optimized magnetite microparticle-based phosphopeptide enrichment strategy for identifying multiple phosphorylation sites in an immunoprecipitated protein. *Anal Biochem* **2011,** *408* (1), 19-31.

Vita

2008-2013 Graduate Student
Department of Chemistry, University of Washington, Seattle
2004-2008 B. Eng.
Department of Chemistry, Beijing Institute of Technology, Beijing

Publication since 2008

[1] **Huang, Y.,** Yoon, S. H., Heron, S. R., Masselon, C. D., Edgar, J. S., Tureček, F., Goodlett, D. R., *J Am Soc Mass Spectrom.* 2012, *23*. 1062-1070.

[2] Yoon, S. H., **Huang, Y.**, Edgar, J. S., Ting, Y. S., Heron, S. R., Kao, Y., Li, Y., Masselon, C. D., Ernst, R. K., Goodlett, D. R., *Anal Chem.* 2012, *84*.6530-6537.